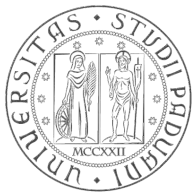

Università degli Studi di Padova

Facoltà di Ingegneria Meccatronica

Corso di Laurea Magistrale in Ingegneria Meccatronica

Adaptive Control for Rehabilitation Systems

Laureando

Luca Corrà

Relatore

Roberto Oboe

Co-relatore

Tomoyuki Shimono

Anno Accademico 2016/2017

Acknowledgement

Vorrei dedicare un momento per ringraziare tutti coloro che mi hanno sostenuto e permesso di raggiungere questo importante traguardo.

Ringrazio anzitutto il mio relatore, il professor Roberto Oboe, grazie al quale ho potuto apprendere moltissimo ed ho avuto l'opportunità di lavorare in Giappone. La ringrazio per la fiducia dimostratami.

I want to thank to my co-supervisor Tomoyuki Shimono sensei for welcoming me to the Shimono lab at YNU in Japan. Thank you for your support.

Un grandissimo ringraziamento va alla mia famiglia per aver sempre creduto in me. Vi ringrazio per ogni singolo sacrificio che avete fatto, permettendomi di arrivare fino alla realizzazione di questo grande sogno.

Ovviamente ringrazio tutti i miei amici italiani, in particolare Andrea, Pierpaolo e Tammy per le serate passate a giocare a briscola o a perdere tempo in generale. Ringrazio tutta la compagnia di Castegnero, in quanto non sarei quel che sono senza di voi.

Another special thanks goes to my Japanese friends, especially to Kouta for having shown himself a great friend immediately and who supported me in the 6 months of thesis.

Per finire, il ringraziamento più importante va alla mia fidanzata Lorenza che ha condiviso con me tutte le gioie ed i dolori di questo percorso, dandomi la forza di arrivare fino al traguardo.

Contents

Abstract

This master thesis describes the design of control strategies for the recovery of motor skills of patients affected by particular diseases that damage the neuromuscular apparatus of the human body, such as stroke. There are two different but related activities in this project. At first, a non linear parameter identification procedure has been used to identify the impedance at the end-point of the human arm, represented by a mass attached to a spring and a damper. By this choice, the action of all muscle bundles is summarized by three parameters. The identification of such parameters is based on the Recursive Least Square (RLS) method. To obtain more accurate estimation values, the RLS algorithm uses the state values (position and velocity) provided by a state observer based on Kalman Filter (KF). This observer is a sensor fusion algorithm that uses measurements provided by a low-cost accelerometer and encoder to obtain more accurate state estimates, reducing the measurement and process noises. The estimates of the impedance at the end-point of the human arm can be used by physiotherapists to obtain a quantitative evaluation of patient's improvements. So, comparing the impedance values obtained before starting the therapy with the values after the exercise sessions, it's possible to adapt future rehabilitation session according to the patient's current conditions. In the second part of the job is described the design of a Non-Linear Adaptive Controller (based on the arm's characteristic) to help the patient during the rehabilitation exercises. A local optimal control approach is used for the off-line design of several gains of a Proportional-Derivative (PD) controller, using the previous estimates of the impedance to personalize the therapy. The gains change during the repetitive exercise, according to the patient's ability to follow a moving target along predetermined trajectory. In this way it's possible to emulate the help of the physiotherapist, teaching the patient the correct execution of the exercise only if necessary. The idea of this algorithm is to make the code as simple as possible to be used in cheap rehabilitation systems. Some experiments have been carried out with healthy subjects, to demonstrate the effective functioning of identification and control strategies. As a further development of this thesis, new experimental tests should be performed, in order to prove the effectiveness of the motor recovery in actual patients.

Chapter 1

Introduction

1.1 Medical Background

The ability to move the body independently or to reach the normal everyday goals of life is an essential prerequisite for a good and healthy life. For this reason in the latest years, the detection of body posture and activity received a significant interest in the field of the physical rehabilitation aimed at providing advanced medical therapies to patients who have some motor function disabilities related to the Upper Motor Neuron (UMN) and Lower Motor Neuron (LMN) syndromes [77] and caused by stroke, joint replacements/reconstructions, amputation, or Parkinson's diseases ([88], [67]). There is an implicit assumption that a causal relationship exists between spasticity (present in the previous pathologies) and activity limitations, partecipation restrictions, including independence [16], because it's usually associated with a lesion (or lesions) involving both the "pyramidal" and "parapyramidal" systems (the cortico-reticular pathways that connect the primary motor cortex (MI) and all other cortex area with the motor neurons mediating voluntary movements, and the reticulospinal and vestibulospinal cord) [20], [44]. Nevertheless, progresses in medicine have made treatments of such pathologies possible, reducing the severity of their effects and increasing the survival rate. In fact it has been demonstrated that the treatment of spasticity is a central part to the clinical management of patients with injuries to the UMN pathway. For this reason it's important to remember that, one fundamental function of MI is to control voluntary movements. Recent evidence suggests that this role emerges from distributed networks rather than discrete representations and that in adult mammals these networks are capable of modification. Neuronal recordings and activation patterns revealed with neuroimaging methods have shown considerable plasticity of MI representa-

tions and cell properties following pathological or traumatic changes and in relation to everyday experience, including motor-skill learning and cognitive motor actions. The intrinsic horizontal neuronal connections in MI are a strong candidate substrate for map reorganization: They interconnect large regions of MI, they show activity-dependent plasticity, and they modify in association with skill learning. These findings suggest that MI cortex is not simply a static motor control structure. It also contains a dynamic substrate that participates in motor learning and possibly in cognitive events as well [71]. This is the basis on which every kind of rehabilitation is based, from that with physiotherapist to the most modern robotic rehabilitation. Now, a focus to the main pathology will be presented to understand better the need to develop new solutions for ever-increasing demand of rehabilitation assistance.

1.1.1 Strokes

The current World Health Organization definition of stroke (introduced in 1970 and still used) is *" rapidly developing clinical signs of focal (or global) disturbance of cerebral function, lasting more than 24 hours or leading to death, with no apparent cause other than that of vascular origin "* [56]. Stroke is one of the most common diseases in the developed world and its incidence continues to rise [4]. Every year in the US and Europe there are between 200 and 300 new cases per 100,000, in which 30% of them survive with serious disabilities and limitations on daily activities, mainly due to a deterioration in motor control and the loss of dexterity in the use of limbs [76], [79]. Specifically, as reported on the site of the Italian Ministry of Health in [6], in Italy stroke is the third cause of death after ischemic heart disease and neoplasms; it causes $10 - 12\%$ of all deaths per year and represents the first cause of invalidity. Every year there are about 196,000 strokes in Italy, of which 20% are recurring. $10 - 20\%$ of people affected by stroke die within a month and another 10% within the first year of life. Only 25% of patients surviving a stroke recover completely, 75% survive with some form of disability, and half of them carry a deficit so severe that they lose self-sufficiency. Stroke is more frequent after 55 years, its prevalence doubles after every decade; 75% of stroke occurs in people over 65 years of age. The prevalence of stroke in 65-84 years of age is 6.5% (in men 7.4%, in women 5.9%) and considering the rise in the average age of the population, stroke is a growing phenomenon over the next few years. The process of forming the stroke can be explained as the cessation of blood supply due to occlusion or hypoperfusion in a cerebral vessel, death of neuronal cells in the core of the infarcted area takes place within minutes. The area around the core, called ischemic penumbra, has

cells functionally involved but still vital for the presence of collateral circles. This area may turn into infarction for secondary neuronal damage induced by the cascade of biochemical events that occur after ischemia leading to cytotoxic and excitotoxic effects. In the following section will be shown the different ways in which a stroke may occur.

1.1.1.1 Different types of stroke

Stroke is a damage caused by vascular causes. The brain receives blood from different arteries (blood vessels that carry blood and oxygen throughout the body from the heart): front of two arteries called carotid (right and left) and posteriorly from the vertebral arteries, which protrude on both sides of the neck. The brain, in order to work properly, needs more than any other organ of a continuous supply of oxygen and nourishment through the blood, the smooth functioning of the blood vessels and the normal contraction of the heart. Depending on how it is presented it can be divided mainly into two principal cases [1],[73], also shown in the Fig. 1.1:

- **Ischemic stroke**

  It represents the most frequent form of stroke (approximately 80%) and affects mainly subjects over the age of 65, more often than men and women; In ischemic forms, the part of the brain that is sprayed by the occluded vessel is no longer fed with blood and oxygen, which is essential for the survival of the brain cells, which is therefore due to cell death (necrosis) and that brain area loses its function, manifesting the symptom of stroke. In order to achieve this situation, it is necessary that the period of ischemia is prolonged and persistent, otherwise if it lasts for a short time and then there is a complete recovery of the brain functions, the one that is classified as T.I.A (Transient Ischemic Attack) or minor stroke. It is a transient ischemic attack with the duration of the event less than 24 hours (typically a few minutes). Transient cerebral ischemic episodes occur in about a third of subjects who subsequently exhibit a definitive ischemic stroke and thus represent an important factor in identifying subjects at risk of severe cerebrovascular disease. Patients with mild ischemic stroke have a long-term prognosis similar to that of patients with TIA, so many believe that there is no specific utility in treating them separately.

- **Hemorrhagic stroke**(Primary intracerebral hemorrhage)

  It accounts for $15-20\%$ of cases and affects slightly younger subjects, always with mild prevalence for men and has a high rate of acute mor-

tality;. Is a condition determined by the presence of non-traumatic intracerebral hemorrhage (often caused by hypertension). A particular case of haemorrhagic stroke is the subarachnoid hemorrhage (ESA). It is a condition in which the presence of blood in the subarachnoid space occurs and it's predominantly present in feminine subjects of about 50 years.

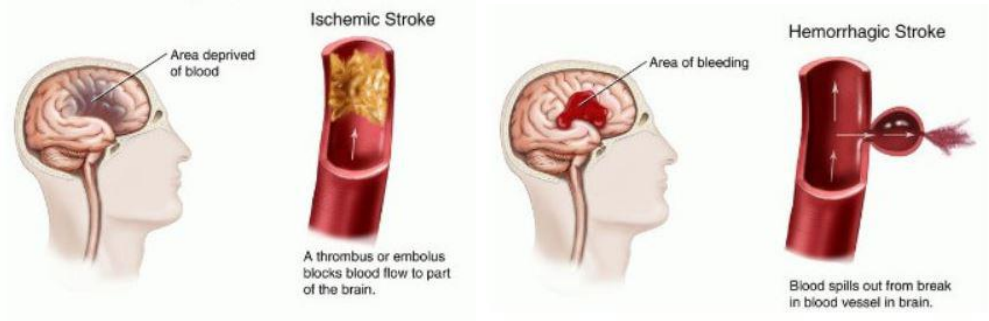

Figure 1.1: Types of stroke [2]

1.1.1.2 Risk factors and symptoms

A risk factor is something that increases your likelihood of getting a disease or condition. It is possible to have a stroke without the risk factors listed below. However, if a lot of risk factors are present in a person's life, It is more likely to have a stroke. The main types of risk factors are divided in three main branches:

1. **Medical Conditions**:

   - Hypertension: It is the leading risk factor for stroke. Blood pressure is the force of blood on walls of arteries. High blood pressure is when this pressure is higher than expected over a prolonged period of time. Normal blood pressure is in the range of 120/80 mm Hg. Hypertension is defined as blood pressure 140/90 mm Hg. If you have diabetes or chronic kidney disease, it is defined as 130/80 mm Hg. Hypertension causes turbulent blood flow that can damage blood vessels walls and overtime causes them to weaken. If you have hypertension and are not keeping your blood pressure in a specific target range, you have an increased risk of having a stroke. Hypertension has no symptoms, so it is important to have your blood pressure checked regularly.

- Cardiovascular Diseases: Cardiovascular diseases are major contributors to stroke. Many chronic conditions, such as coronary artery disease or atrial fibrillation , affect heart function, making it difficult to meet the body's demands. Long-term problems cause damage to blood vessels, increasing the risk of blockage (ischemic stroke) or bleeding (hemorrhagic stroke).
- Vascular Dementia: Vascular dementia is a type of dementia that is caused by problems with blood supply to the brain. These deficits may be caused by multiple TIAs. Both conditions are signs of increased risk of having a major stroke.
- Psychological Disorders: Having certain psychological disorders, such as depression, panic disorder, anxiety, or prolonged emotional or occupational stress are associated with an increased risk of stroke. Some disorders and treatments may lead to poor lifestyle choices, such as smoking, weight gain, or lack of physical exercise.
- Sleep Apnea: Obstructive sleep apnea (OSA) is a disorder characterized by repeated episodes of complete or partial airway obstruction during sleep. The disorder is associated with disrupted sleep patterns and decreased oxygen saturation (the amount of oxygen carried in the bloodstream). OSA has been linked to several disorders, including cardiovascular disease and early death. OSA is also an independent risk factor for hypertension, heart failure, diabetes, and heart attack.

2. **Factors That Cannot Be Changed**:

- Age: Brain function normally decreases as we age. This decrease is generally not enough to cause problems, but can increase the risk of developing cardiovascular disease, which can lead to a stroke. Some changes include stiffer blood vessels, small breaks in blood vessels, and minor cognitive and memory loss
- Sex: The risk of stroke increases as you age. Although men are more likely to have a stroke at a younger age, women overall tend to have more strokes and die from them. This may be due to risk factors that are unique to women in combination with standard ones.

- Genetics and Ethnicity: Having family members that have had a stroke or history of cardiovascular disease increases your risk as well. You are also at a higher risk if you have certain genetic abnormalities. For example, your blood may have a tendency to clot, which can increase the risk of narrowed or blocked arteries. About the ethnicity, African Americans have a higher incidence of hypertension than Caucasians and, therefore, a higher risk of having a stroke. Stroke risk is also higher among American Indians and Native Alaskans.

3. **Factors That Can Be Modified or Changed**:

- Smoking: it is a major contributing factor to stroke. Smoking can irritates and narrows blood vessels which can narrow blood vessel and decrease blood flow, contributes to the build up of arterial plaque and raises heart rate and blood pressure which can place extra pressure on weakened blood vessel walls. As a result, cigarette smokers are 2-4 times as likely as nonsmokers to have a stroke than nonsmokers. Nonsmokers who are exposed to smoking are at risk as well.
- Dietary Choices: A diet that is high in trans fat, saturated fat, and low in fruits, vegetables, whole grains, and fiber increases your risk of having a stroke. Poor diet contributes to to high cholesterol , obesity , and glucose intolerance disorders such as metabolic syndrome and diabetes , which are all independent risk factors for stroke.
- Physical Inactivity: Physical inactivity doubles your risk for a heart attack or stroke. Regular moderate to intense exercise improves heart function and promotes healthy arteries. It also helps reduce the chance of other stroke risk factors such as hypertension, high cholesterol, and diabetes.
- Excess Alcohol Intake: Drinking too much alcohol can increase blood pressure, blood triglycerides that contribute to plaque build up, and increase the risk of abnormal heart rhythms (arrhythmia). Drinking too much alcohol can increase blood pressure and lead to other cardiovascular problems.

- Drug Use: Illicit drug use, especially cocaine, can cause blood vessel damage, which can lead to blood clots and arterial spasms. Strokes are more likely in people with vascular damage.

With control and treatment of the risk factors it's possible to reduce the increasing number of strokes in the world [45]. For subjects who are at risk, it's good to know the main symptoms of stroke, in order to intervene in time. For this purpose, it better to remember the acronym F.A.S.T [62], that means:

F ace drooping: If you notice a droop or uneven smile on a person's face, this is a warning sign.

A rm weakness: Arm numbness or weakness can be a warning sign. Asking the person to raise their arms It's a warning sign if the arm drops down or isn't steady.

S peech difficulty: Slurred speech can indicate that the person is having a stroke.

T est

This is a stroke identification instrument to recognize the possible start of a stroke. Other important signs are:

- Loss of strength on one side of the body: hemiplegia or emiparesi;
- Dizziness, loss of balance;
- Sudden trouble seeing in one or both eyes;
- Tingling and loss of sensitivity on one side of the body (paresthesia) and diminished response to stimulation (emiypoesthesia);
- Sudden severe headache with no known cause.

Accurate identification of stroke by pre-hospital personnel could expedite triage of patients to acute stroke units and facilitate delivery of acute stroke therapies either in hospital or in the community. in fact, acting fast if someone is experiencing stroke symptoms it' possible to reduce the effects of this pathology and to obtain the best result with the future rehabilitation, if necessary.

1.1.1.3 Neuromuscular rehabilitation after stoke

Rehabilitation is the process by which the person affected by stroke is helped, after the post-acute phase, to achieve, recover or maintain the highest level of autonomy allowed by the disease [7]. It allow the achievement of the best quality of life possible for surviving patients, paying particular attention to the psychosocial issues that this pathology entails. Already in the period of acuity, it is necessary to pursue rehabilitation-related goals, namely prevention of disability (early mobilization and rehabilitation), integrated with the diagnostic program and emergency treatment. The stage of acuity also includes the period of clinical stabilization, during which the patient can not be required to perform special care. The post-acute phase (also referred to as the "Rehabilitation" or "Recovery phase") begins when the person is no longer in immediate danger of life, does not risk further deterioration and starts to stabilize his general conditions. It is at the this stage that a progressive improvement of the person's functions and abilities can take place, which takes the name of recovery [33]. Generally, the post-acute phase begins one to two weeks after the stroke, and ends when the person has reached the maximum possible improvement based on brain damage and his general physical condition. Some studies have revealed that the brain reorganizes after stroke in relation to recovery of motor function [59],[64]. The result of these studies suggests that training after a lesion may revive neural plasticity and functional recovery of the limb. Rehabilitation therapy, in fact, avoids further loss of hand representation in the intact bark and induces expansion of the hand territory into the adjacent cortex, in conjunction with the recovery of skill movements. Although in recent years several scientists had seen the possibility of a cortical reorganization after a lesion, the scientific world has definitively accepted this thesis only after the publication of Liepert, Taub et al. [51] confirming not only the fact that the human brain is physiologically sensitive to experience, but above all that this plasticity is maintained in cases of injury. This is the first demonstration in the human being of a long-term alteration in brain function associated with rehabilitation-induced improvement after neurological damage. About the intensity of the rehabilitation, more and longer training sessions have positive recovery effects in the post-acute phase and also in chronic phase. So, it is clear that training intensity is crucial to promote cortical reorganization after stroke, and so to obtain better rehabilitation progresses [86],[50]. Current stroke rehabilitation guidelines (described in [61],[35]) are generally centred around physiotherapy and occupational therapy regimens and are often focused on decreasing disability from stroke-induced impairment, to encourage patient independence as much as possible. For this purpose, in traditional physical rehabilitation, the

physiatry, physiotherapist and neuro-orthopedic work together, using motor re-education and specific exercises to avoid worsening spasticity. There are two main types of individual exercises [9]:

- **Physical therapy**: For most stroke patients, physical therapy (PT) is the cornerstone of the rehabilitation process. A physical therapist uses training, exercises, and physical manipulation of the stroke patient's body with the intent of restoring movement, balance, and coordination. The aim of PT is to have the stroke patient relearn simple motor activities such as walking, sitting, standing, lying down, and the process of switching from one type of movement to another.
- **Occupational therapy**: Another type of therapy involving relearning daily activities is occupational therapy (OT). OT also involves exercise and training to help the stroke patient relearn everyday activities such as eating, drinking, dressing, bathing, cooking, reading and writing, and toileting. The goal of OT is to help the patient become independent or semi-independent.

These therapies are based on rehabilitation, neuroscience and motor learning theories but, also, on the past experiences of the rehabilitation's team. In particular, after the acute phase, physiotherapists continuously tailor the exercises according to patient's impairments, challenging them to improve their skills. Patients performances and progresses are subjectively evaluated by therapist's perceptions. In this way it's possible to get customized assistance to get the best possible recovery result. On the other hand, for society, it costs a lot of time to devote a physiotherapist to a single person and it becomes impossible if one looks at the ever-increasing trend of stroke evolution in the world. Therefore, a new rehabilitation strategy is underway in recent years to cut costs and improve the results of rehabilitation therapies. It is robot-assisted rehabilitation.

1.2 Robotic Rehabilitation

The field of automated or robot-assisted motor rehabilitation has emerged since the 1990s and is rapidly developing. Traditional physical therapies can improve post-stroke functional recovery but are expensive, require a lot of workforce and need to be durable [52]. Accordingly, intelligent machines may offer a solution to increase the intensity of therapy. In fact, the rehabilitation robotics in recent years has become essential in the field of neuroradiation because the amount of recovery is directly proportional to the number of repetitions of the exercises carried out. Advanced robotics are able to provide continuous therapy at a lower cost compared to the rehabilitation activity performed by physiotherapists, giving patients more chance of recovery. Furthermore, for physicians and therapists, a rehabilitation system based on haptic interfaces[1] is highly desirable. Ideally, a sophisticated man-machine interaction should try to simulate the experienced hand of the therapist guiding the paretic limbs in a gentle manner, avoiding abrupt perturbations and providing as little assistance as necessary. So, one physiotherapist can follow several patients at the same time, reducing the cost of rehabilitation. Furthermore, it is an efficient measurement system that allow, using the several typologies of sensors (e.g. position sensors, force/torque sensors and electromyography (EMG) sensors), to evaluate the patient conditions in order to improve the rehabilitation tasks. Finally, taking advantage of recent improvements in robotics and information technology, traditional rehabilitation practice can be enriched providing advanced and more technological tools. The latter can better enhance and quantify rehabilitation and, concurrently, productivity and, in turn, optimize the quality of care.

1.2.1 State of the art of robots for rehabilitation

Below, it will shown some of the most famous examples of robots and existing rehabilitation control systems, giving you a brief description of the state of the art.

[1] A haptic interface is a computer-controlled mechanism designed to detect motion of a human operator without impeding that motion, and to feed back forces from a teleoperated robot or virtual environment [28]

1.2.1.1 Upper limb rehabilitation

Our motor system enables the selective movement of the shoulder, elbow, wrist and finger joints in multiple ways, either isolated or within movement chains. No machine can compete with this incredible movement variety at present, and any additional degree of freedom (DoF) of any applied robot arm causes exponential costs. A restriction of movements to be practised was thus inevitable, nevertheless aiming at a generalized motor recovery of the whole upper limb. Below is a brief description of some famous rehabilitation robots.

MIT-Manus

The first clinically tested robot was a planar robot for the rehabilitation of the upper limb in the 1997, called MIT-Manus [48]. It consists of a 2 degree of freedom (DOF) robot manipulator with a SCARA configuration, characterized by low inertia and friction, with which it's possible to assists shoulder and elbow movements by applying different force to the arm, acting on the robot's end-effector, to which the patient is connected via a manipulator. In rehabilitation therapies, the patient is assisted in movements on the horizontal plan in order to reach, with the sick arm, the visual targets that a graphic interface indicates on the monitor, as shown in Fig. 1.2.

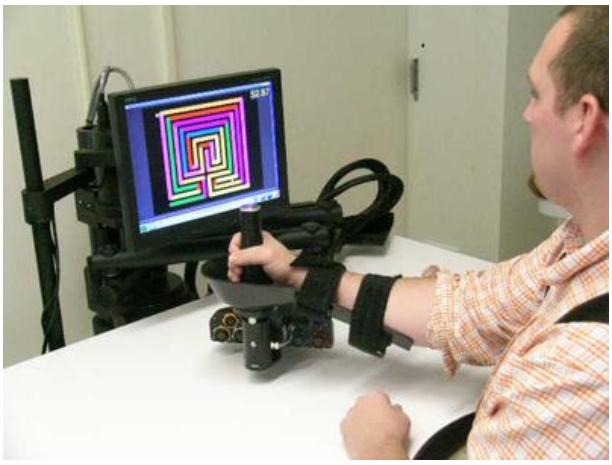

Figure 1.2: MIT-Manus [10]

For the first evaluation of the MIT-Manus, several controlled randomized trials were conducted on a total of 96 acute hemiparetic subjects for an average of 2/3 weeks after their first single stroke [11],[82],[81]. In the experimental activity, these patients performed an hour per day for 5 days a week, with a minimum of 1500 repetitions of goal-directed movements over the whole treatment period. Another consideration to do is that the MIT-Manus is modular, in fact it's possible to add other three DOF using a robot for the manipulation and rehabilitation of the wrist [49]. In this way, the MIT-Manus can become a robot that manages three-dimensional movements, in addition to planar ones in the horizontal axis. Finally, it's necessary to discuss briefly about the control law implemented in this robot. it has to interact with the patient, so it needs to transmit forces and control the movements of the patient safely, avoiding to damage more the injured limb. This specific result was obtained using impedance controls that modulate the way the robot reacts to mechanical perturbations. These controls are designed to simulate the manual manual made by the experienced therapist, transmitting light and delicate corrections of the movements.

MIME

The Mirror Image Movement Enabler (MIME) is a therapy system for the upper limb rehabilitation (focuses on shoulder and elbow function) [55], designed by Burgar and his collaborators at Stanford University [19]. This device consists of two arm supports, modified to limit movement to the horizontal plane only, and a 6 (DOF) manipulator (Staubli PUMA-560) that transmits forces and pairs to the patient's arm in a three-dimensional space by the robot's end-effector (Fig. 1.3). Currently MIME operates in unimanual and bimanual modes. For unimanual opertions the control can operates in three different ways:

1. **Passive control**: The subject is relaxed and the robot moves the limb to a target with predetermined trajectory.
2. **Active-assisted**: The patient voluntarily triggers the movement towards a target working with the robot, which partially assists the movement.
3. **Active-bound**: The robot provides a viscous resistance in the desired movement direction.

Figure 1.3: MIME [10]

About the bimanual mode there are two different control law:

1. **Master/Slave control**: The robot assistance of the affected limb is obtained by the healthy arm of the patient if possible, mirroring the movements and allowing the subject to perform coordinated movements, bi-manuals and at a speed determined by the patient himself.
2. **Different bimanual control**: The two limbs are stressed differently using one of the techniques previously described for the unimanual modes.

NeReBot

NeReBot is a cable robot (Fig. 1.4) for the rehabilitation of the upper limbs developed by a team of Padua University [29],[70]. Three nylon cables convert the rotary motion of three motors into c.c. in a spatial trajectory for the patient's limb. Real-time software manages phases of acquisition of points and cyclic repetition of spatial trajectories obtained by interpolation of acquired points. So, the firs step is the manual movement of the patient's arm, acquiring motion data. Once a certain position has been reached, the therapist starts the automatic movement, reproducing the real one in a comfortable way for the patient. The first clinical trial of 30 patients demonstrated the efficacy of the robot in the post-stroke rehabilitation treatment of sub-acute patients [58].

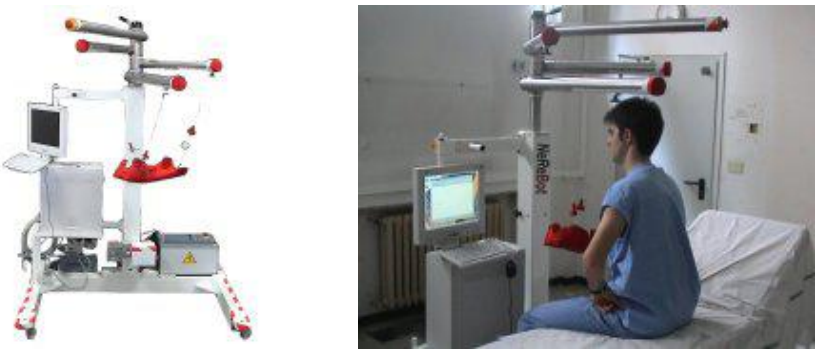

Figure 1.4: NeReBot [8]

ARM-Guide

Less sophisticated device are the Assisted Rehabilitation and Measurement (ARM) Guide [38] shown in Fig. 1.5. The robot consists of a manipulator, powered by a single motor, that follows a linear constraints. The manipulator can be oriented with different pitch and yaw angles to allow to reach all working areas. It is used for the evaluation and treatment of hemiparetic patients:

1. **Diagnostic tool**: With the ARM-Guide it's possible to evaluate several key motor impairments, including abnormal tone, incoordination and weakness (for more details, see[69].
2. **Therapeutic tool**: Using the same stategies described before for the unimanual configuration of the MIME, the ARM-Guide applies support or obstruction forces to the patient in order to perform linear movements within the work space [46].

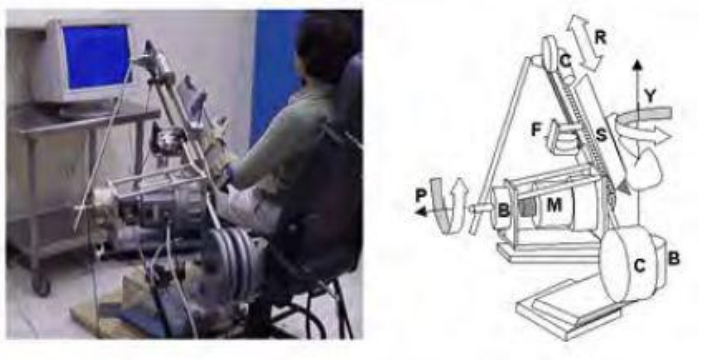

Figure 1.5: ARM-Guide [69]

1.2.1.2 Lower limb rehabilitation

Three months after the incident one third of the surviving patients has not yet regained independent walking ability, and those ambulatory walk in a typical asymmetric manner, as they avoid to load the paretic limb. At the same time their walking velocity and endurance are markedly reduced. Stairs, sudden obstacles,uneven terrain or other perturbations further challenge the patients' gait ability outside the clinic. The rehabilitation process toward regaining a meaningful mobility can be divided into three phases [72]:

1. The bedridden patient has to be mobilized into the wheelchair to avoid more problems related to the inactivation of the muscles.

2. Restoration of gait, using rehabilitation robot to improve the effects of the exercise. In fact, they relieve the physiotherapists from hard manual labour and enable an increase in training intensity for the patients. In this phase, the patient regains the ability to walk, even without support.

3. Improvement of gait in order to meet the requirements of daily mobility.

To achieve these results, robots allow more effective training sessions. For example, still in [72], 1000 steps within a typical training session of 15–20 min are possible, whereas during manually assisted training only approx. 100 steps/session were performed. A second major effect is the relief of the physiotherapists, who can now concentrate on training supervision. The ideas behind the realization of this type of devices are mainly two: machines that applies the principle of *movable footplates* and the *exoskeleton type machines*.

Movable footplates machines

- **GT I Gait Trainer**
  Hesse and co-workers [36] presented the electromechanical gait trainer, GT I, aimed at relief of the strenuous effort of therapists during locomotor therapy on the treadmill when setting the paretic limbs. Each of the patients feet is positioned on a separate footplate whose movements are controlled by a planetary gear system, simulating foot motion during stance and swing. Cadence and stride length can be set individually.

Figure 1.6: GT I Gait Trainer [5]

- **HapticWalker**
  The device is a robotic walking simulator for gait rehabilitation based on the principle of programmable foot plates; i.e., it continues the successfully applied approach of movable foot plates and allows patient-physiotherapist interaction during training [37]. The HapticWalker accomplishes the paradigm for optimal training, because it is the first gait rehabilitation device which is not restricted to training of walking on even ground. In contrast to all treadmill bound machines, it enables the patient to train arbitrary gait trajectories and daily life walking situations.

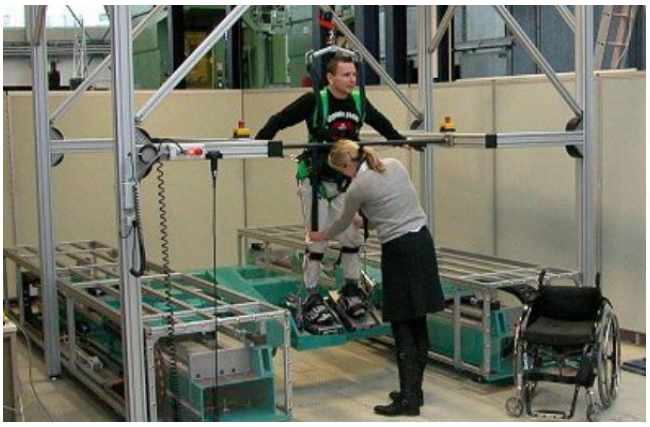

Figure 1.7: HapticWalker [72]

Exoskeleton type machines

- **LOKOMAT**
  The Lokomat (Hocoma AG) consists of a robotic gait orthosis and an advanced body weight support system, combined with a treadmill [25]. Many algorithms based on position, impedance or adaptive controllers, have been implemented in order to obtain the desired movement for rehabilitation. To achieve the pre-fixed goals it uses computer controlled motors (drives) which are integrated in the gait orthosis at each hip and knee joint (Fig. 1.8). It has been extensively used in many clinical researches, in fact it is the most clinically evaluated system and one of the firsts of its type [83],[42],[84].

Figure 1.8: LOKOMAT [3]

- **AAFO**
  The AAFO is largely composed of a polypropylene AFO [32] with a hinged ankle joint, the sensor unit, the controller and the series elastic actuator. The sensor unit detects the gait phase during walking and the controller controls dorsiflexion/plantarflexion based on the output signals from the sensors. The series elastic actuator provides the movement of an ankle joint based on signals from the controller [40]. It is shown in Fig. 1.9:

Figure 1.9: AAFO [40]

1.3 Project

In recent years, due to an increase in the number of patients affected by various diseases such as stroke, neurological lesions and musculoskeletal disorders, many projects and research studies have begun the development of specific robotic systems, focusing on particular robotics rehabilitation in order to reduce the total cost of traditional rehabilitation. This has also become necessary due to an increase in the elderly population (particularly susceptible to previous pathologies), which is expected to increase further in the coming years, as reported by the World Health Organization (WHO) [66] and shown in Fig. 1.10.

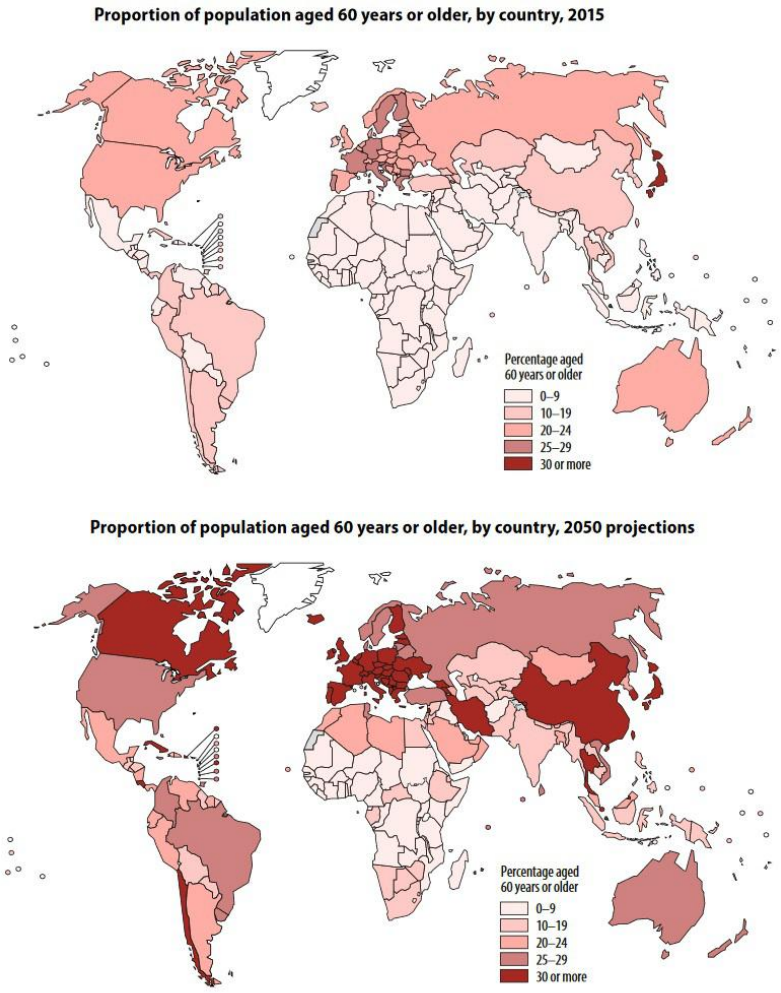

Figure 1.10: Increasing of elderly people in the world [66]

This situation and the improvement in medical treatments of previous pathologies (particularly stroke, as described above) have led to a reduction in the mortality rate, increasing the demand for rehabilitation therapies to return to a life of full autonomy [65].

1.3.1 Purpose of the project

One of the biggest challenges of recent years is the low-cost development of robots and rehabilitation techniques for rehabilitation. In this regard, more and more projects start with the aim of lowering the development costs of these machines, in order to make robotized rehabilitation more accessible at the patient's home. At the same time, they must ensure satisfactory results that simulate the behavior of the physiotherapist during a rehabilitation exercise, possibly giving a quantifiable idea of the results obtained by the patient. Starting from a pre-existing project sponsored by the Ministry of Health, whose Padua University is a partner, an alternative way of reducing the computational cost of planar rehabilitation robots algorithm, developed by Davide Pilastro in the PhD thesis [68], has been considered in this Master thesis. In this regard, starting from the widely used industrial model identification techniques that use only position encoders (usually present in every equipment to be controlled) and low-cost accelerometers (i.e. MEMS), we tried to model and parametrize the impedance of the end point of the human arm, then quantify it by experimental data. This allows to include the parameters related to the physical condition of the patient directly into the control system, by customizing the rehabilitation process according to the initial needs and improvements achieved during the therapy. As regards the development of the control algorithm, it is based on the idea of optimizing different controllers at specific points of the task required by the physiotherapist, taking into account about the different parameters of the patient's arm, depending on the arm configuration during the execution of the exercise and the required level of assistance. All this is done off-line using simple optimal control techniques. In addition, the main purpose is to create a system that implements an adaptive help control that emulates the physiotherapist's help when needed, using only standard position sensors. To this end, a control mechanism has been implemented that can adapt the on-line help force depending on the patient's degree of compromise. In conclusion, using this method, it is possible to obtain a control system that can assist the patient during repetitive exercises, taking into account the physical condition of the subject and the ability to follow the predetermined trajectories.

1.3.2 Structure of the Thesis

The explanation of the project is subdivided into three chapters, excluding the present chapter (Chapter 1). Chapter 2 presents modelization, parametrization and identification of the system used, taking into account the human arm pattern reported at the end-effector of this one. This model also includes the non-linearity of the mechanical and electrical system, purging the arm estimate not only from the mechanical model of the motor, but also from overlapping noise / errors. This will then show the approach used (includes a non-linear identification procedure and a sensor fusion algorithm) and the relative results obtained experimentally to verify the validity of this method. Chapter 3, however, presents the adaptive control system designed to emulate the help of the physiotherapist during rehabilitation exercises. Experiments are shown to evaluate the functioning of the adaptation system implemented. Unfortunately, there have been no specific clinical trials with patients with pathological illnesses for lack of time, so this will be one of the future work. In the end, in Chapter 4, some conclusions about the work done are reported.

Chapter 2

Impedance of the Human Arm End-Point

2.1 Identification of Human Arm Impedance

As describe in Chapter 1, Purpose of the project, the main point of this thesis is the development of an adaptive controller that take into account about the patient conditions to customize the rehabilitation session to improve the benefits of the exercises. But the investigation of human motor control is not simple and have led to a wide variety of viewpoints concerning the strategy of the central nervous system (CNS) in controlling limb movements. Several researchers, for example [31] and [39], have proposed the control of mechanical impedance as an important means of human motor control. For this kind of control it's necessary to simplify the complex joint-based model of the human arm presented in [39] as a Cartesian impedance model, propagating the internal model of the arm out to the human arm end-point in the horizontal plane [26]. So, stiffness, damping, and mass become three basic components of mechanical impedance of the human arm end-point, relating force to position, velocity, and acceleration, respectively. To use this modeling to take account of human-machine interaction in rehabilitation systems, an estimate of the impedance of the end-point of the human arm it's necessary. For this purpose, different parametric [1] and non-parametric [2] approach are used in literature. The main difference presented in this Chapter is the improvement of the estimation using a parametric approach considering the non-linear Coulomb friction of the motor and based on the combination of the RLS estimator and a state observer (aaKF).

[1] i.e Recursive Least Square estimator (RLS)

[2] i.e Empirical transfer function estimate (ETFE) method [53])

2.1.1 System Modeling

First of all it is necessary to decide an appropriate representation of the considered system. So, modeling the human arm as a mass-damper-spring system concentrated at the end point of the arm (model present in literacture, as [80] and [13]) it is possible to add the human arm model to the model of the motor in a simple way (Fig. 2.1, the meaning of all parameters are in Tab. 2.1). The closed-loop position control of the system is used to fix the working-point position using a band limited random white noise as the input. In this way the system is properly excited and in the same time are avoiding too big unknown movements.

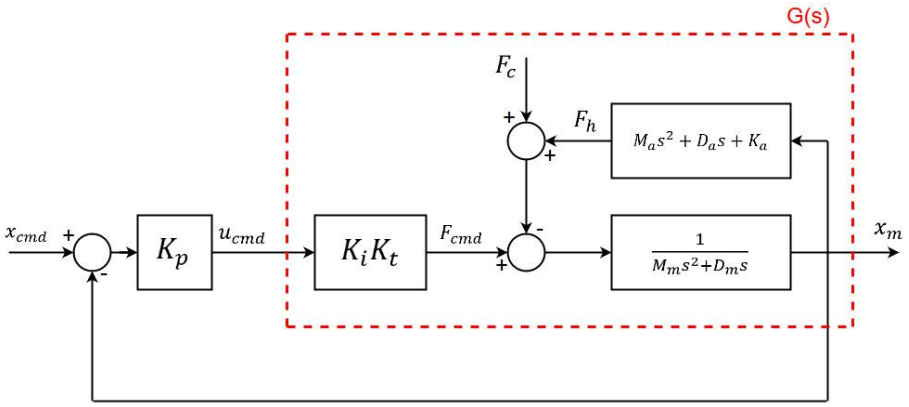

Figure 2.1: Block Diagram of that include Motor and Arm model

From Fig. 2.1 it's possible to obtain the transfer function between voltage and position:

$$G(s) = \frac{X_m(s)}{U_{cmd}(s)} = \frac{\frac{K_t K_i}{M_m s^2 + D_m s}}{1 + \frac{M_a s^2 + D_a s + K_a}{M_m s^2 + D_m s}} = \frac{K_t K_i}{M s^2 + D s + K_a} \tag{2.1}$$

With:

$$M = M_m + M_a \ , \qquad D = D_m + D_a$$

Eq. 2.1 represents the continuous model of the system, with a physical meaning. For a correct implementation in a digital environment it's necessary to discretize the previous system using the Zero-Order Holder (ZOH) method. The relationship between Dicrete and Continuous parameters, using ZOH is shown in Appendix A. In this way, the problem changes from the estimation of the arm parameters to estimation of the discrete parameters of the following system:

x_{cmd}	Command position (White noise) $[m]$
u_{cmd}	Command Voltage $[V]$
K_t	Thrust Constant $[\frac{N}{A}]$
K_i	Trans-conductance $[\frac{A}{V}]$
K_p	Position Gain $[\frac{V}{m}]$
F_c	Coulomb Friction $[N]$
F_h	Reaction Force of the Human Arm $[N]$
M_m	Motor Mass $[kg]$
D_m	Motor Damping factor $[\frac{Ns}{m}]$
M_a	Human Arm Mass $[kg]$
D_m	Human Arm Damp. fact. $[\frac{Ns}{m}]$
D_m	Human Arm Stiffness $[\frac{N}{m}]$
x_m	Real position of the motor with Arm $[m]$

Table 2.1: Meaning of the Fig. 2.1 parameters

$$G_d(z) = \frac{X_m(z)}{U_{cmd}(z)} = \frac{z^{-1}b_1 + z^{-2}b_0}{1 + z^{-1}a_1 + z^{-2}a_0} \tag{2.2}$$

In eq. 2.2 the Discrete Transfer Function between "digital voltage" and "digital output position" is presented. But in this way it is not possible to take into account about the non-linearity of the motor, like Coulomb Friction, because Gd is a linear dynamic model. To solve that problem, a modification in the input signal definition is necessary, i.e.:

$$\begin{aligned} u_{cmd}(k) &= u_{ref}(k) - \frac{F_c}{K_i K_t} = \dots \\ \dots &= u_{ref}(k) - \frac{f_c sign(\dot{x}_m(k))}{K_i K_t} = u_{ref}(k) - u_c(k) \end{aligned} \tag{2.3}$$

In Fig. 2.2 it is possible to see the Block Diagram of the Discrete System defined in this way. Furthermore, in the same figure it is possible to see the

model that generates the data under noisy condition (like encoder quantization or other unknown noise).

To take into account about this problem, the representation with Discrete Transfer Function (with abuse of notation) is obtain using an ARMAX [60] model:

$$\begin{aligned} x_{enc}(k) &= \frac{B(z)}{A(z)}u_{cmd}(k) + \frac{C(z)}{A(z)}e(k) = ... \\ ... &= \frac{z^{-1}b_1 + z^{-2}b_0}{1 + z^{-1}a_1 + z^{-2}a_0}u_{cmd}(k) + \frac{1 + z^{-1}c_1 + z^{-2}c_0}{1 + z^{-1}a_1 + z^{-2}a_0}e(k) \end{aligned} \tag{2.4}$$

The regression form of the previous system is obtained by combining eq. 2.3 and the Discrete Time representation of eq. 2.4, obtaining:

$$\begin{aligned} x_{enc}(k) &= v_{state}^T(k)C_d(k) + e(k) = ... \\ ... &= \begin{bmatrix} -x_{enc}(k-1) \\ -x_{enc}(k-2) \\ u_{ref}(k-1) \\ u_{ref}(k-2) \\ e(k-1) \\ e(k-2) \\ -sign(\dot{x}_m(k-1)) \\ -sign(\dot{x}_m(k-2)) \end{bmatrix}^T \begin{bmatrix} a_1(k) \\ a_0(k) \\ b_1(k) \\ b_0(k) \\ c_1(k) \\ c_0(k) \\ \frac{f_c b_1}{K_i K_t}(k) \\ \frac{f_c b_0}{K_i K_t}(k) \end{bmatrix} + e(k) \end{aligned} \tag{2.5}$$

Where the estimation of e(k) is:

$$\widehat{e}(k|k-1) = x_{enc}(k) - v_{state}^T(k)\widehat{C}_d(k-1) \tag{2.6}$$

And the estimation of the Coulomb friction becomes:

$$\widehat{f_c} = \widehat{f_{c_1}} = \frac{\widehat{f_c b_1}}{K_i K_t}\frac{K_i K_t}{\widehat{b_1}} = \widehat{f_{c_2}} = \frac{\widehat{f_c b_0}}{K_i K_t}\frac{K_i K_t}{\widehat{b_0}} \;\mapsto\; \widehat{f_c} = \frac{\widehat{f_{c_1}} + \widehat{f_{c_2}}}{2} \tag{2.7}$$

The Regression form allows to describe the system as a sum of two terms. The first describe the system behavior and the second is a white noise[3] $e(k)$ that is independent of $v_{state}(k)$, in fact it is possible to see that in eq. 2.6 $e(k)$ is obtained from the new data $x_{enc}(k)$,), removing the behavior of the previous states $(k-1,\ k-2,\ etc...)$.

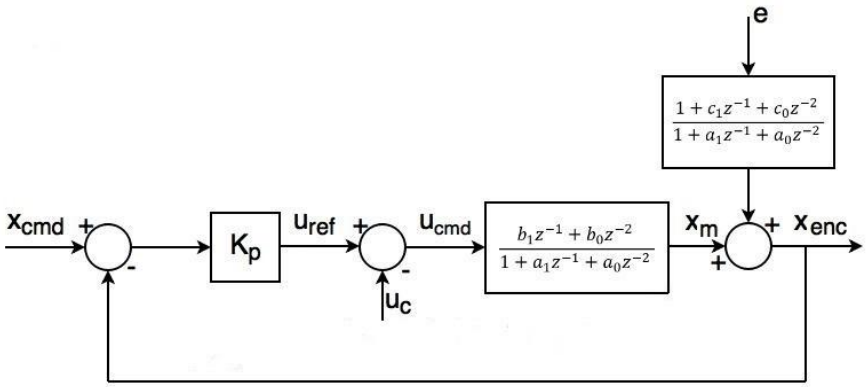

Figure 2.2: Block Diagram of Discrete System

To obtain the estimation of the real parameters of the arm using the estimation of the discrete system, see appendix A.

2.1.2 Recursive Least Square estimator (RLS)

In least square estimation, unknown parameters of a linear model are chosen in such a way that the sum of the squares of the difference between the actually observed and the computed values is a minimum [14]. The result of this method can be viewed as a filter that averages the data to give optimal estimates. Averaging is a good strategy if parameters of the model are constant in nature. However, many times the parameters that it's necessary to estimate are time-varying. So, for a better estimation, another similar approach is used to keep track of the variations. In fact, Human-Arm- parameters are not constant and the RLS estimator with forgetting factor is used. To use this approach, an assumption is needed, that is, the parameters of the model

[3]Sequence of independent, identically distributed (i.i.d.) random variables with zero mean.

must be considered slowly varying in the time if the patient doesn't move his limb, as it's possible to see in [63].

2.1.2.1 Theory

The RLS estimator with forgetting factor is useful if the parameters vary continuously but slowly. That is the concept of forgetting in which older data is gradually discarded in favor of more recent information. In the least square method, forgetting can be viewed as giving less weight to older data and more weight to recent data. The 'loss-function' is then defined as follows:

$$J(C_d, k) = \frac{1}{2} \sum_{i=1}^{k} \beta_{ff}^{k-i} [x_{enc}(k) - v_{state}^T(k) \widehat{C}_d(k)]^2 \tag{2.8}$$

Where $v_{state}^T(k)\widehat{C}_d(k-1)$ is the estimate of the system output in the sample k using the previous values.

$0 < \beta_{ff} \leq 1$ is called forgetting factor and it is useful for:

- Tracking time varying parameters
- Recovering a correct estimate by starting from an imprecise initial estimate (i.e. discarding the effect of the initial conditions)

The forgetting factor can be determined as follows:

$$\beta_{ff} = e^{-\frac{T_s}{T_f}} \tag{2.9}$$

Where T_s is the sampling time and T_f is the time constant of the exponential forgetting (i.e. the time after which old data is weighted less than 37% with respect to new data). Using the model described in eq. 2.5 it is possible to provide a "correct" estimate $\widehat{C}_d$ of the "true" value of C_d thanks to the use of the RLS estimator with data generated under "noisy" conditions. "Correct" estimate, as describe in [27] and in [24] means that the estimation of C_d is:

- Unbiased, i.e $E[\widehat{C}_d] = C_d$ [4]
- Consistent, i.e $[\widehat{C}_d] \mapsto C_d$ as $k \to \infty$[5]

[4] $E(\bullet)$ denotes the expectation operator.

[5] The limit has to be considered in some statistical sense. Mean square convergence is a possibility, which implies to analyze the behavior of the estimation variance as the number of observation grows.

2.1.2.2 Implementation

Solving 2.8 for the minimizing parameters and considering the recursive form that update the estimates on-line, the implementation is given by:

$$\widehat{C}_d(k) = \widehat{C}_d(k-1) + K(k)\epsilon(k) \tag{2.10}$$

Where $\widehat{C}_d(k-1)$ represent the old values of plant parameters, which is updated through an appropriate innovation weighing. $\epsilon(k)$ is the innovation and it is defined as:

$$\widehat{\epsilon}(k|k-1) = x_{enc}(k) - v_{state}^T(k)\widehat{C}_d(k-1) \tag{2.11}$$

It takes into account the error between the output value at time k, $y(k)$, and the estimated output using the old values of the estimated parameters and regression variable $v_{state}(k)$. If $\epsilon(k) = 0$, the estimated parameters correctly describe the system in case of constant values. To implement RLS estimator, the gain $K(k)$ that minimizes the estimation error is derived as follows:

$$\begin{aligned} K(k) &= P(k)v_{state}(k) = ... \\ ... &= P(k-1)v_{state}(k)[\beta_{ff} + v_{state}^T(k)P(k-1)v_{state}(k)]^{-1} \end{aligned} \tag{2.12}$$

With the covariance matrix:

$$P(k) = \frac{1}{\beta_{ff}}[I - K(k-1)v_{state}^T(k)]P(k-1) \tag{2.13}$$

That represents the confidence with which it is possible to estimate the parameters of the system. It is very important to evaluate the contribution of the new output value into parameters estimates. In fact the main difference with the classic least square method is how the covariance matrix $P(k)$ is updated. In the classic RLS the covariance vanishes to zero with time, losing its capability to keep track of changes in the parameter. In equation 2.14 however, the covariance matrix is divided by $\beta_{ff} < 1$ at each update. This slows down fading out of the covariance matrix.

The exponential convergence of the above scheme is shown in some textbooks and research papers (see e.g. the proof provided in [43] or [17]) for the case of unknown but constant parameters. In general, exponential convergence in the constant case implies a certain degree of tracking capability in the time varying case [21]. However rigorous mathematical analysis of tracking capabilities of an estimator when the parameters are time-varying

is rare in the literature and many properties are demonstrated through simulation results. Campi [21] provides rigorous mathematical arguments that if the covariance matrix of the estimator is kept bounded the tracking error will remain bounded. Ljung and Gunnarsson present a survey of algorithms for tracking time-varying systems in [54]. For the conversion to physical parameters see eq. A.7 and A.8 in Appendix A

2.2 State Estimator

In real systems there are several types of disturbances that impede a correct estimation of the real state of the system. Different solution have been implemented to solve this problem. To improve the estimation of the systems parameters, a method to reduce the effect of the output position noise and to estimate the velocity in the best way, a State Estimator will be used [15].

2.2.1 Theory

In almost all processes it is practically impossible to access to all the real state variables. Therefore, it is necessary to make use of an appropriate estimators that are able to reconstruct the state in acceptably accurate manner, relying solely on the input and the output (or only the outputs) of the observation process, in order, for example, to use this estimate as a feedback from the state (as shown in Fig. 2.3).

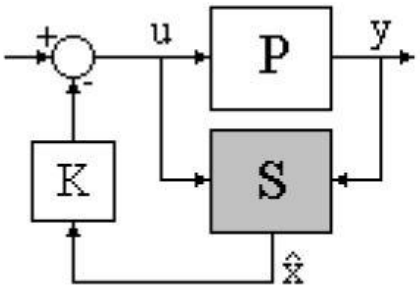

Figure 2.3: Scheme with a feedback from estimated state

So, being the real system suffering from noise (unaccessible input), it is necessary to include in the mathematical model of the estimator a term that weighs the difference between the real and estimated output. There are many different type of estimator, but the main ones are the asymptotic estimator.

- **PREDICTOR FORM**

  The model of this estimator is the following:

$$\widehat{x}(k+1) = F\widehat{x}(k) + Gu(k) + L[y(k) - H\widehat{x}(k)] \tag{2.14}$$

  Where $H\widehat{x}(k)$ represents the actual output $y(k)$ estimation and $y(k) - H\widehat{x}(k)$ represents the innovation error.

  If the model of the system is:

$$\begin{cases} x(k+1) = Fx(k) + Gu(k) \\ y(k) = Hx(k) \end{cases} \tag{2.15}$$

  It is simple to derive the behavior of the estimation error, that is:

$$e(k+1) = \widehat{x}(k+1) - x(k+1) = [F - LH]e(k) \tag{2.16}$$

  In eq. 2.16 it is shown that, if it is possible to design L so that all the eigenvalues (λ) of $[F - LH]$ are stable ($|\lambda| < 1$), the estimator that is obtained is asymptotic ($\lim_{k\mapsto\infty} e(k) \mapsto 0$).

  Furthermore, in this case, the calculations of the estimator necessarily require a time less than the sampling period T_s. This means that the predicted state $\widehat{x}(k+1)$ will be available before the instant $(k+1)T_s$ and it will be retained by a Zero-Holder in order to synchronize the feedback signal with the sampling instants (Fig. 2.4).

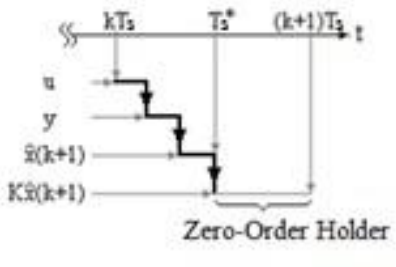

Figure 2.4: Steps of asymptotic estimator in predictor form

- **CORRECTOR FORM**

  The basic principle is similar to that of the previous estimator, but in this case the estimation is done in several steps:

  1. $\widehat{x}(k+1|k) = F\widehat{x}(k|k) + Gu(k)$
  2. $\widehat{y}(k+1|k) = H\widehat{x}(k+1|k)$
  3. $\widehat{x}(k+1|k+1) = \widehat{x}(k+1|k) + L[y(k+1) - \widehat{y}(k+1|k)]$

  In this way, the estimation error is governed by $[F - LHF]$ instead of $[F - LH]$. The advantage is that there is a static connection between state and output, so the estimate is better but there is time-shift and it may cause an alteration in the discretization of the system if the state is used like a feedback. In order to obtain L, Discrete Kalman Filter will be presented in the next section.

2.2.2 Discrete Time Kalman Filter

Consider the following discrete system:

$$\begin{cases} \bar{x}(k+1) = F\bar{x}(k) + Gu(k) + \bar{\eta}_d(k) \\ y_q(k) = H\bar{x}(k) + w(k) \end{cases} \tag{2.17}$$

This system is used very often in the configuration where $\bar{x}$ is a vector that represent the state of the system (for example position x, velocity $\dot{x}$ etc...), while y_q represents the measured position x_{enc}. This system represents the actual case in which, in addition to the required inputs, are present unknown inputs (noises) and hardly measurable. The two noises $w(k)$ and $\bar{\eta}_d(k)$, considered Gaussian White Noises with zero mean, are respectively measurement noise and process noise.

1. **Measurement noise**

   It is mainly due to the quantization noise present in an encoder (Fig. 2.5):

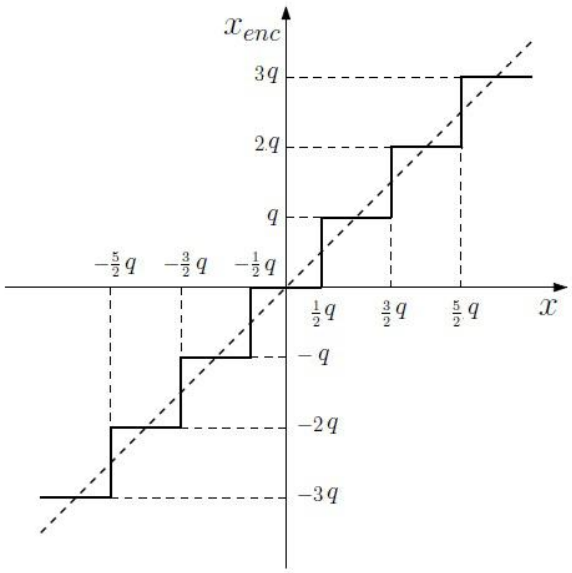

Figure 2.5: Encoder quantization

For each measurement, it belongs to the range $[-\frac{q}{2}, \frac{q}{2}]$ because it can be modeled as a uniform distribution with density shown in Fig. 2.6:

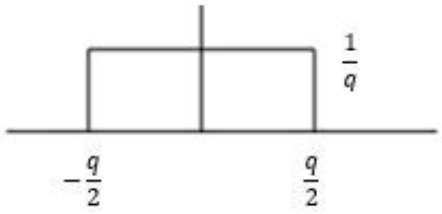

Figure 2.6: Model noise of the quantizer

This is an equivalent stochastic model of the quantizer and the variance of this type of noise (considering a lot of measurements and using the central limit theorem to consider this noise as a normal distribution [18]) is $R = \frac{q^2}{12}$, where q is the quantization step (resolution) of the encoder. If other kind of sensor are used, a specific experiment to evaluate the variance of the noise is needed.

2. **Process noise**

   It is impossible to perfectly know the real model of a system. So, the process noise is used to represent the imperfect knowledge of the real system. This translates, for a motor, to take into account the unknown effects of:

   - Non-linear friction
   - Non-linearity at input (there is a DAC)
   - Variation of motor parameters $J_m, B_m, K_t K_i$
   - Electrical noise

   In this case an analytical approach is really difficult, therefore, to determine the variance Q_d of this error it is necessary to go to attempts with experimental tuning procedure of Kalman Filter's parameters.

Kalman filter uses these values of the variances of noise as a lower limit of the state error variance estimation in order to obtain the best possible estimation of the state of the model, avoiding the stop of the update of some state parameters. The implementation of the Kalman Filter algorithm is divided in two steps: Prediction Step and Corrector Step. In the Prediction Step the algorithm use the state space model of the system (ignoring the noises because unpredictable), described in the eq. 2.17 to update the current estimation with the data from the previous time step. In this way there are some errors due to the difference between real and mathematical system. To solve this problem the Corrector Step provides a method to correct the estimation, taking into account about the innovation error between the actual output value of the system and the previous prediction. A weight L is used to know how much and when the innovation error modify the estimation, taking into account about the variance of the estimation error $P(k) = Var\{x(k) - \widehat{x(k)}\}$. To model L, the Kalman Filter algorithm use an optimal technique that minimize the expected value of the square error between the real (unknown) and estimate states of the system. Using a generic representation of a discrete system (eq. 2.17), the code used to implement the Kalman Filter algorithm is [47]:

Prediction Step

$$\begin{aligned} \widehat{\widehat{x}}(k|k-1) &= F\widehat{\widehat{x}}(k-1|k-1) + Gu(k-1) \\ P(k|k-1) &= FP(k-1|k-1)F^T + Q_d \end{aligned} \tag{2.18}$$

Corrector Step

$$\begin{aligned} L(k) &= P(k|k-1)H^T[HP(k|k-1)H^T + R_d]^{-1} \\ \widehat{\widehat{x}}(k|k) &= \widehat{\widehat{x}}(k|k-1) + L(k)[y_q(k) - H\widehat{\widehat{x}}(k|k-1)] \\ P(k|k) &= [I - L(k)H]P(k|k-1) \end{aligned} \tag{2.19}$$

With $P(0) = P_0 = I\delta$ (where δ is a constant value) symmetric and positive semidefinite matrix and $\widehat{x}(0) = 0$ if some informations about the state of the system are not available.

2.2.3 Accelerometer Aided Kalman Filter (aaKF) estimator

Normally, Kalman Filter algorithm uses the output of the encoder and a mathematical-mechanical model of the system, that uses the voltage (or force) like an input, to describe the behavior of the state. In this case the problem is that Kalman Filter provides an optimal estimation for a single system. The aaKF is an implementation of a sensor fusion algorithm that provides to solve some problems of a classic algorithm:

- Measurements are provided, respectively, by position sensor, such as linear encoder, and accelerometers placed in the motion part of the motor where will be attached the arm
- They are fused by the aaKF in order to obtain better system position, velocity and acceleration estimations in terms of reduced residual noise.
- The robustness of the estimate is enhanced by making use of a kinematic model in the aaKF. With this choice, no mechanical parameters of the system are necessary in the aaKF implementation, thus ensuring an accurate estimate even in case of large variations of such parameters (like the parameters of different arms)
- The aaKF estimator is also insensitive to the input disturbance and friction forces acting on the plant (Process noise).

The filter model has been developed considering kinematic relation between acceleration and position of rigid single-DOF motor-load system [41] and the added noise in the motor position and load acceleration measurements [12]. For the encoder noise see the description of Measurement noise.

If the acceleration sensor is not able to provide an accurate acceleration measurements (for example when the measurements are provided by low cost MEMS sensors), a model of the error of the accelerometer is required. The common problems of this type of sensors are the bias, drifts and noise, caused by variations of temperature and other stochastic factors. To take into account about these problems, an augmented model for acceleration measurement has been considered:

$$\ddot{x}_{acc} = \ddot{x}_{acc} + b + w_{acc} \tag{2.20}$$

Where:

- $\ddot{x}_{acc}$ is the acceleration measured with the sensor
- $\ddot{x}_m$ is the real acceleration of the motor. It is obtained from the jerk $\dddot{x}_m = \frac{\mathrm{d}\ddot{x}_m}{\mathrm{d}t} = \eta_a$ like a random walk (η_a) is a white random process), avoiding to use the mathematical-mechanical model of the motor/arm
- b is the bias that affect the measurements. It is modeled as a random walk because the real variations of the bias are unknown (η_b is a white random process);
- w_{acc} is an additional Gaussian with zero-mean noise that corrupt the measurements.

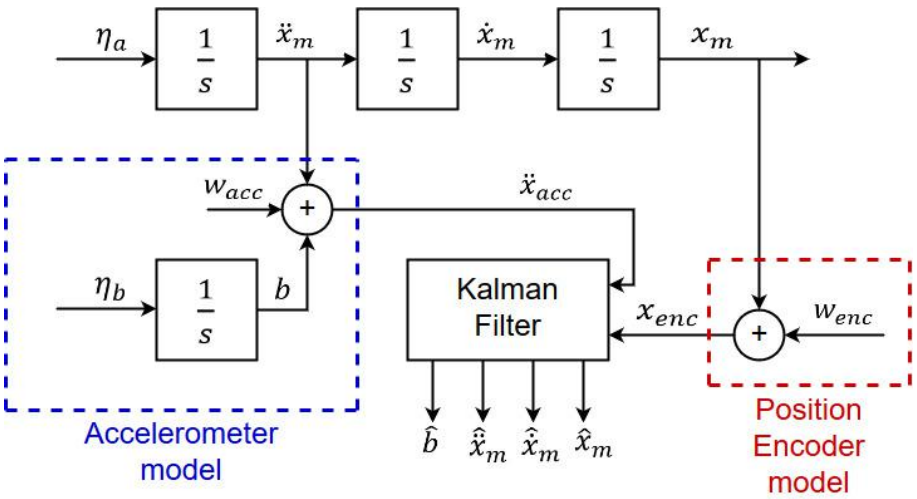

Figure 2.7: Block Diagram of Kinematic Model used for Kalman Filter

Taking into account about the model shown in Fig. 2.7, it is possible to describe the system with the Space State approach in the Continuous Time:

$$\begin{cases} \dot{\bar{x}}(t) = \begin{bmatrix} \dot{x}_m \\ \ddot{x}_m \\ \dddot{x}_m \\ \dot{b} \end{bmatrix} = \begin{bmatrix} 0 & 1 & 0 & 0 \\ 0 & 0 & 1 & 0 \\ 0 & 0 & 0 & 0 \\ 0 & 0 & 0 & 0 \end{bmatrix} \begin{bmatrix} x_m \\ \dot{x}_m \\ \ddot{x}_m \\ b \end{bmatrix} + \begin{bmatrix} 0 \\ 0 \\ 0 \\ 0 \end{bmatrix} 0 + \begin{bmatrix} 0 & 0 \\ 0 & 0 \\ 1 & 0 \\ 0 & 1 \end{bmatrix} \begin{bmatrix} \eta_a \\ \eta_b \end{bmatrix} = \ldots \\ \ldots = Ax(t) + Bu(t) + B_\eta \bar{\eta}(t) \\ \bar{y}(t) = \begin{bmatrix} 1 & 0 & 0 & 0 \\ 0 & 0 & 1 & 1 \end{bmatrix} \begin{bmatrix} x_m \\ \dot{x}_m \\ \ddot{x}_m \\ b \end{bmatrix} + \begin{bmatrix} w_{enc} \\ w_{acc} \end{bmatrix} = C\bar{x}(t) + \bar{w}(t) \end{cases} \tag{2.21}$$

An important condition for the convergence of the estimate is that the (A,C) pair must be observable. So, the following relationship is the Observability matrix [74]:

$$O = \begin{bmatrix} C \\ CA \\ CA^2 \\ CA^3 \end{bmatrix} = \begin{bmatrix} 1 & 0 & 0 & 0 \\ 0 & 0 & 1 & 1 \\ 0 & 1 & 0 & 0 \\ 0 & 0 & 0 & 0 \\ 0 & 0 & 1 & 0 \\ 0 & 0 & 0 & 0 \\ 0 & 0 & 0 & 0 \\ 0 & 0 & 0 & 0 \end{bmatrix} \tag{2.22}$$

In this case the rank of the Observability matrix is full and the system is fully observable.

In the implementation of aaKF, process noises $\bar{\eta}(t) = [\eta_a \quad \eta_b]^T$ and measurements noises $\bar{w}(t) = [w_{enc} \quad w_{acc}]^T$ are considered uncorrelated white Gaussian random noises, with zero-mean and variances $\eta_a \mapsto \sigma_a^2$, $\eta_b \mapsto \sigma_b^2$, $w_{enc} \mapsto \sigma_{enc}^2$, $w_{acc} \mapsto \sigma_{acc}^2$.

In this way, the corresponding process noise covariance matrix is:

$$Q = E[(B_\eta \bar{\eta}(t))(B_\eta \bar{\eta}(t))^T] = \begin{bmatrix} 0 & 0 & 0 & 0 \\ 0 & 0 & 0 & 0 \\ 0 & 0 & \sigma_a^2 & 0 \\ 0 & 0 & 0 & \sigma_b^2 \end{bmatrix} \tag{2.23}$$

And measurement noise covariance matrix is:

$$R = E[\bar{w}(t)\bar{w}^T(t)] = \begin{bmatrix} \sigma_{enc}^2 & 0 \\ 0 & \sigma_{acc}^2 \end{bmatrix} \tag{2.24}$$

To use eq. 2.18 and 2.19 as an implementation of aaKF, it is necessary to discretize the model in eq. 2.21 and it is necessary to know the variance of the noises. As regards the measurement noises, they can be divided as:

- Noise of the accelerometers
- Noise of the encoder, related with the quantization error

For the first noise, an experiment is required to see the output of the accelerometer without movement of the system. In this way it is possible to calculate the variance of the accelerometer's noise. About the quantization error, it's described previously in Measurement noise. The result is $R_d = R$. In aaKF, the process noises are related to the velocity of change of motor acceleration and bias signals, so the correct values of the variances are set following the physical meaning. In fact σ_b^2 is set very small compared to σ_a^2 because the bias is like a constant disturbance. For σ_a^2 it's necessary an experimental tuning of the aaKF, that will be presented later, in the subsection Tuning of Accelerometer Aided Kalman Filter. Q_d is the discrete version of Q and it's possible to obtain this one thinking the noises as two "unaccessible" inputs in the State Space Model of the system (eq. 2.21). So, the result is:

$$E[\bar{\eta}_d(k)\bar{\eta}_d^T(k)] = Q_d = \int_0^{T_s} e^{A\sigma} Q (e^{A\sigma})^T \, d\sigma \tag{2.25}$$

This quantity describes the noise variance watching how state values disperse in a sampling time Ts, after an excitement due to the unaccessible inputs.

To solve this equation it is necessary to approximate $e^{A\sigma}$ with the Taylor expansion:

$$e^{A\sigma} = I + A\sigma + \frac{A^2\sigma^2}{2} + ... + \frac{A^n\sigma^n}{n!}; \quad with\ n \mapsto \infty \tag{2.26}$$

For the experiment it is possible to approximates $e^{A\sigma}$ with a second order system $e^{A\sigma} = I + A\sigma + \frac{A^2\sigma^2}{2}$. So, now, it is possible to define explicitly:

$$Q_d = \begin{bmatrix} \frac{\sigma_a^2 T_s^5}{20} & \frac{\sigma_a^2 T_s^4}{8} & \frac{\sigma_a^2 T_s^3}{6} & 0 \\ \frac{\sigma_a^2 T_s^4}{8} & \frac{\sigma_a^2 T_s^3}{3} & \frac{\sigma_a^2 T_s^2}{2} & 0 \\ \frac{\sigma_a^2 T_s^3}{6} & \frac{\sigma_a^2 T_s^2}{2} & \sigma_a^2 T_s & 0 \\ 0 & 0 & 0 & \sigma_b^2 T_s \end{bmatrix} \tag{2.27}$$

Referred to the system describe in eq. 2.17, the method to obtain the other matrices necessary to complete the implementation of the aaKF is the ZOH method, with: $F = e^{AT_s}$; $G = \int_0^{T_s} e^{A\sigma} B\, d\sigma$; $H = C$

2.2.4 Reset of the State Estimation

The model described in eq. 2.17 and used for aaKF is only an approximation of the real system and some unknown behaviour are not considering, so it may produce inconsistent estimation of the state compared with the actual measurements. To take into account about this problem, a reset of the state estimation is required ([87] and [68]) . Using the model of the quantization error of the encoder in a specific sample k, it is possible to define a range where it is sure to find the real actual position of the motor, i.e:

$$x_{enc}(k) - \frac{q}{2} \leq x_m(k) \leq x_{enc}(k) + \frac{q}{2} \tag{2.28}$$

In the same way, using the discrete derivative of the real actual position $x_m(k)$ it is possible to obtain the estimation of the real actual velocity $\widehat{\dot{x}}_m(k) = \frac{x_m(k) - x_m(k-1)}{T_s}$, where Ts is the sampling time. Combine this one with eq. 2.28, an equation to take into account about the range where it is possible to find the real velocity, is obtained:

$$\frac{x_{enc}(k) - x_{enc}(k-1)}{T_s} - \frac{q}{T_s} \leq \widehat{\dot{x}}_m(k) \leq \frac{x_{enc}(k) - x_{enc}(k-1)}{T_s} + \frac{q}{T_s} \tag{2.29}$$

Using eq. 2.28 and 2.29 it is simple to define the boundaries of the estimation, to be sure that aaKF code is able to provide consistent estimation

(between prediction and correction step in eq. 2.18 and 2.19) with the real position and velocity.

2.3 Experimental Set-up

The experimental setup used for the experiments explained in this thesis is divided in five parts (Fig. 2.8):

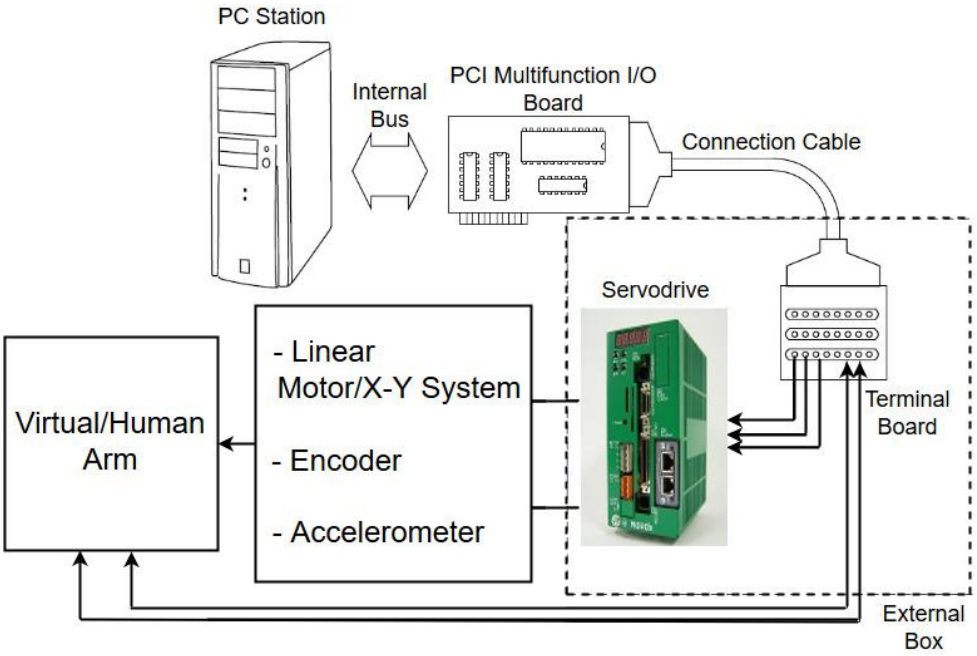

Figure 2.8: Experimental Setup

Now it will be briefly presented each of the various components of the setup:

⇒ **PC Station** is used as a HMI (Human-Machine Interface) to allow the tracking and the controlling of the motor and controller's parameters. It is possible with RTAI Application Interface, a modification of the source code of the Linux kernel used to simulate a Real-Time system direct using C-code [57]; it allows rapid prototyping or hardware-in-the-loop simulation of the control system and signal processing algorithms.

⇒ **PCI Multifunction I/O Board** is the interface between the servo-drive and the PC station. It allows to manage digital and analog I/O with an ADC/DAC. The principal parameters are:

Interface	Parameters	Description
PCI - D/A	Type	PCI-3340
	Resolution	16 bit
	Output	±5 [V] or ±10 [V]
	Channels	8
	Conversion time	5 [μs]
PCI - A/D	Type	PCI-3178
	Resolution	16 bit
	Output	±5 [V] or ±10 [V]
	Channels	4
	Conversion time	20 [μs]
Counter Boards	Type	PCI-6201 (Linear Motors)
		PCI-6205C (X-Y System)
	Resolution	16 bit
	Input	5 [V]
	Channels	4 (Linear Motors)
		8 (X-Y System)
	Max input freq.	1 [MHz] (Linear Motors)
		2 [MHz] (X-Y System)

⇒ **External Box** includes a terminal board, used to connect the external encoder and the servo drive to the PCI. The main parameters are:

Interface	Parameters	Description
Servo-Driver	Type	SVFM1 DSP-model
	Trasconductance K_i	0.2 [$\frac{A}{V}$]
	Voltage (Vmax/rms)	±5 [V] or ±10 [V]
	Voltage	V_{max} = 84 [V]
		V_{rms} = 59.4 [V]
	Current	A_{max} = 2.75 [A]
		A_{rms} = 2.0 [A]

The current loop reference must be limited to ±2 [A] to avoid exceeding the maximum current so, the maximum voltage became 10 [V] using K_i value.

⇒ **Linear Motor/X-Y System + Encoder + Accelerometer** is the "chain" used to control the Virtual Arm/Human Arm. Following, the parameters of Linear motor, X-Y System, Encoder and Accelerometer:

Interface	Parameters	Description
X-Y system Two equal Linear Motors	Type	S160Q
	Thrust constant	$K_t = 33\ [\frac{N}{A}]$
	Mover weight (without sliders)	$M_m = 0.3$ [kg]
	Windings Resistance	R = 43 [ω]
	Max voltage	240 [V]
	Continuous Current (rms)	0.62 [A]
	Acceleration Current (rms)	2.5 [A]
Encoder	Type	RGH24Y30A30A
	Resolution	0.1 [μm]
Accelerometer	Type	ARJ-200A
	Capacity	200 [$\frac{m}{s^2}$]
	Frequency range	0 - 500 [Hz]

⇒ **Virtual Arm/Human Arm** are the loads applied to the two different systems. The Virtual Arm is another linear motor (Fig. 2.9, Motor 2) with the same nominal specifications as before.

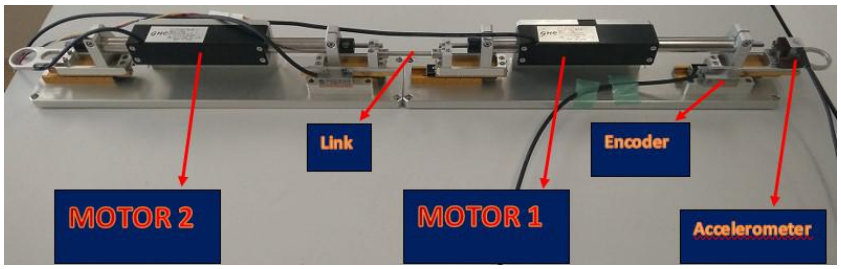

Figure 2.9: Linear Motor + Virtual Arm connected with a link

About the Human Arm, an experimental test is necessary to obtain the parameters using the configuration shown in Fig. 2.10

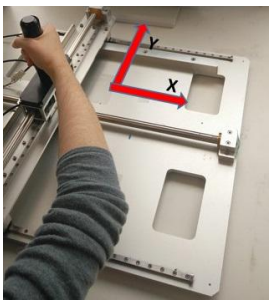

Figure 2.10: X-Y System with Human Arm

2.4 Experimental Testing

The principal purpose of this section is to describe the sequence of experiments to test the effectiveness and practical implementation of the estimator previously discussed. It is divided into the following steps: Experiment description

2.4.1 Experiment description

2.4.1.1 Preliminary Tests

Preliminar test is conducted to find the nominal value of the Mass, Damping factor and coulomb friction of the linear motors.

- MASS For the Mass the strategy is very simple and it consists in evaluating the necessary force to counteract the weight force of the motor. So, the motors are positioned in vertical position to let the movable part free to move under its own weight force. The values of two mass are obtained using the relation between force, mass and acceleration:

$$F = ma = M_m g = M_m 9.81 \tag{2.30}$$

So, if the value of the mass is correct, the force F used to counteract the weight force allow to have no movement in vertical position.

- DAMPING FACTOR (D_m) and COULOMB FRICTION (F_c) In this case, the principal relation used for the experiment is the following [22]

$$F_{tot} = F_{fric} + M_m \ddot{x}_m \tag{2.31}$$

Where:

$$F_{fric} = F_0 + F_c + F_v = F_0 + f_c sign(\dot{x}_m) + D_m \dot{x}_m \tag{2.32}$$

With:

$F_{fric} \mapsto$ Part of the input force of the motor used to compensate the friction

$F_0 \mapsto$ Static Friction: friction that tends to prevent stationary surface from being set in motion

$F_c \mapsto$ Coulomb friction: model that shows the direction and magnitude of the friction force between two bodies with dry surfaces in contact

$F_v \mapsto$ Viscous Friction: model that shows the friction force of a body that moves immersed in a fluid (air, water or other)

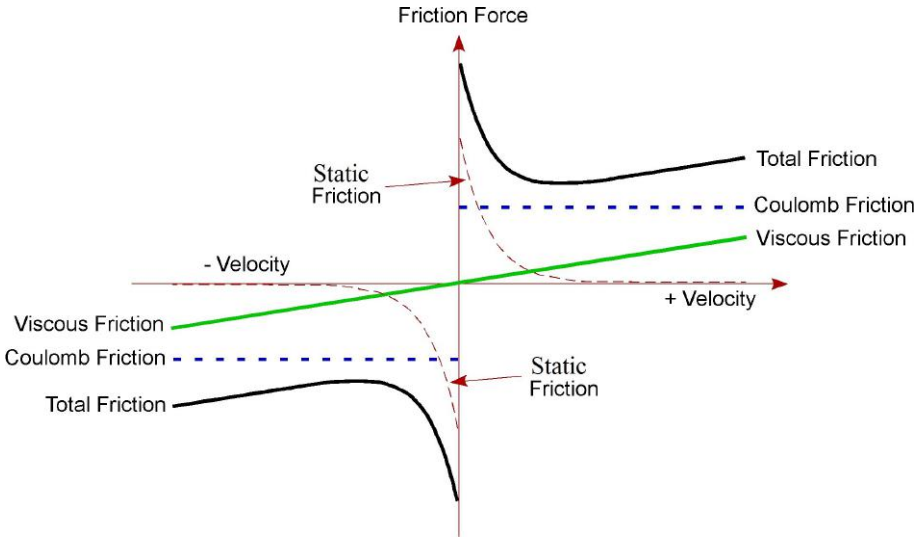

Figure 2.11: Friction model

To conduct the experiments, a digital PI controller is used to set the desired velocity ($\dot{x}_m$) to follow, that in this case is a trapezoidal velocity. With this choice it is possible to avoid to use a part of acceleration force ($M_m\ddot{x}_m$) in the part where the velocity is constant. So, the total force used by the motor is only to compensate the friction. In this way it is possible to obtain, with different velocity, an estimation of the model shown in Fig. 2.11. F_0 is ignored in the estimation because it is not used in the RLS model and it represent only the friction in a static condition. So, the model used for the estimation is only:

$$F_{fric} = f_c sign(\dot{x}_m) + D_m\dot{x}_m \tag{2.33}$$

Using the Least Square method (LS method), the estimation of the coefficient f_c of the coulomb friction and the Damping factor D_m is performed by minimizing the sum of square error between real and estimated values of the force (eq 2.33), using real input ($F_{tot} = F_{fric}$) and "real" output (estimation of the velocity using a filtered derivative) with different constant velocity.

2.4.1.2 Tuning of Accelerometer Aided Kalman Filter

As describe in the section Accelerometer Aided Kalman Filter (aaKF) estimator, an experimental tuning of aaKF is necessary to obtain the best possible result. The experimental tuning consists, firstly, in the description of the variance of the noise of the accelerometer via a further preliminary test. This test consists to take the acceleration measurements for some seconds without some input. In this way it is possible to see that the correct model to describe the noise of the accelerometers is a Gaussian white noise with zero mean (after removing the average) and σ^2_{acc} as the variance. Then, the BartLett's test is used to obtain the correct values of the variance of the process noises ([75]). It consists to compare the real value and the predicted value. If the residuals (innovation) are a white noise process (flat spectrum), it's impossible to predict better the real state because all residuals are uncorrelated and totally random, so the aaKF is an optimal state observer. it is actually better to evaluate the integral innovation being subject to less variation and more easily comparable with the ideal behavior wanted, that is a constant and growing straight line.

2.4.1.3 Estimation of a Linear Motor's parameters

This test is necessary to prove the abilities of the algorithm to estimate correctly the nominal parameters of a Linear Motor to subtract later to obtain the Human Arm parameters from the total system. The experiment is divided in two parts. The first one uses only the RLS estimator with the encoder's values and its filtered derivative to obtain the position and velocity, Fig. 2.12, where $M = M_m$, $D = D_m$ and $K = 0$).

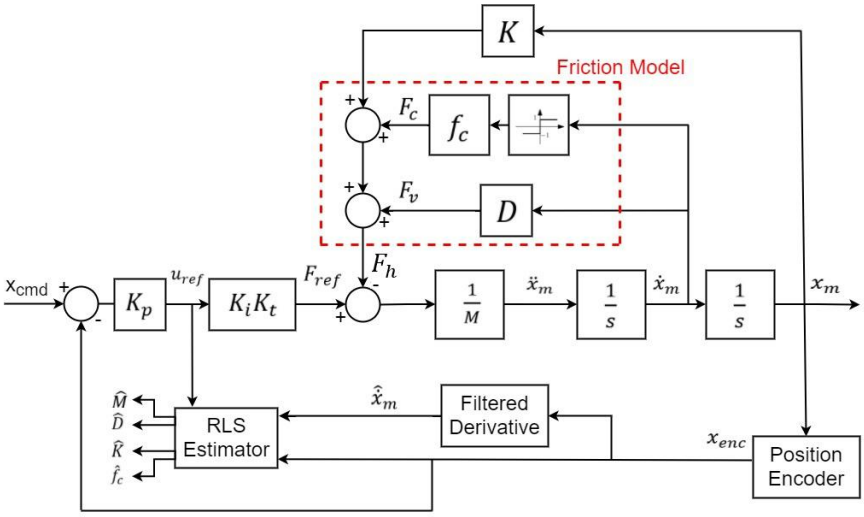

Figure 2.12: Block Diagram used for the estimation (Only Encoder)

In the second part, the aaKF observer and RLS estimator are used together to estimate M_m, D_m (Fig. 2.12).

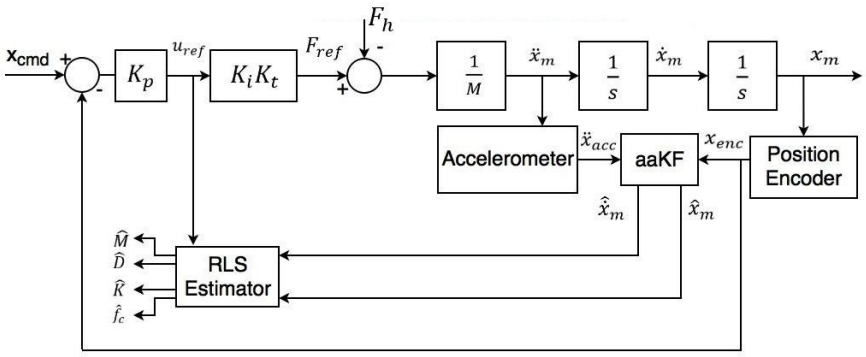

Figure 2.13: Block Diagram used for the estimation (Encoder and Accelerometer)

For both cases, a comparison with the previous nominal values, estimated in Preliminary Tests, is made.

2.4.1.4 Estimation of a Virtual Arm's Impedance

In this test, using the motor 2 (Fig. 2.9) as a Virtual Arm connected with motor 1 by a rigid link, it is possible to demonstrate that using only an encoder and an accelerometer in motor 1 is possible to evaluate the real mechanical values of the Virtual Arm. The block diagram used for the estimation is the same as before (Fig. 2.13, where $M = M_m + M_a$, $D = D_m + D_a$ and $K = K_a$). Motor 2 is used as an arm with Mass, Damping factor and Stiffness. To obtain this result, it's used a zero position control. In Fig. 2.14 it is possible to see the block diagram used for this purpose.

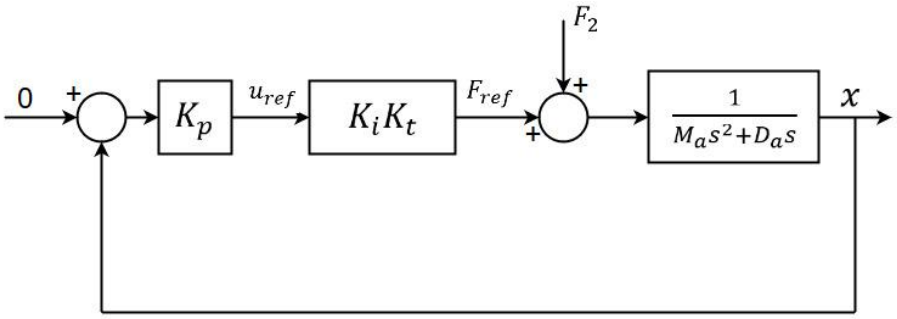

Figure 2.14: Block Diagram to control the Virtual Arm

From Fig. 2.14 it is possible to obtain the Transfer Function between F_2 and x:

$$G_h(s) = \frac{X(s)}{F_2(s)} = \frac{\frac{1}{M_as^2+D_as}}{1+\frac{K_pK_iK_t}{M_as^2+D_as}} = \frac{1}{M_as^2+D_as+K_pK_iK_t} = \frac{1}{M_as^2+D_as+K_a} \tag{2.34}$$

Motor 2 (Virtual Arm) is attached with motor 1, so F_2 represent the part of the force F_{ref} (Fig. 2.13) that is used to move Motor 2. For the same reason, x is the position of both motor. So, it is possible to write, taking into account about eq. 2.34, the following relationship:

$$F_2 = (M_as^2 + D_as + K_a)x \tag{2.35}$$

That is the same relationship used to describe the effect of the arm in Fig. 2.1. So, changing the value of K_p it is possible to obtain different nominal stiffness for the Virtual Arm.

2.4.1.5 Estimation of "mechanical" parameters of the Human Arm

For this test, the considerations are the same as before, but the configuration of the system is changed (X-Y System with Human Arm, Fig. 2.10). To get an idea about the variation of the Human Arm parameters in different conditions, a series of experiments is performed in different position. The choice of the positions where to estimate (point 1,2,3,4 shown in Fig. B.1) is related to the design of the controller.

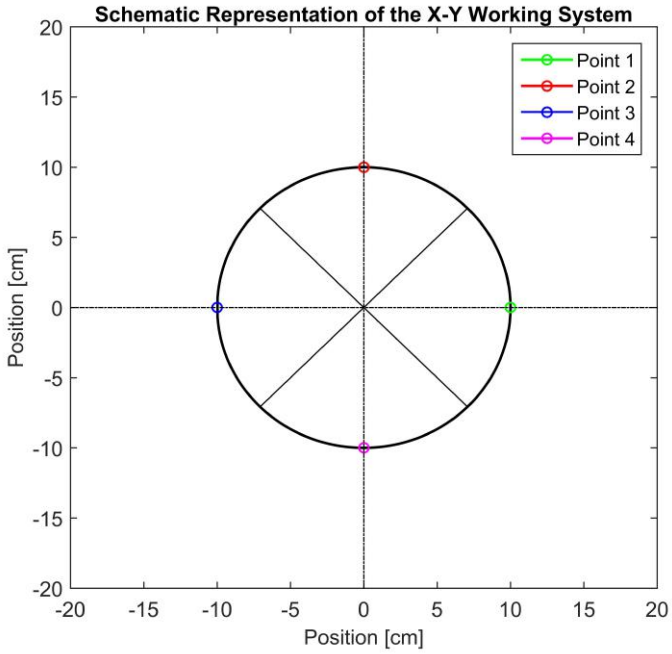

Figure 2.15: Working System, X-Y plane

The block diagram used to estimate human arm's parameters for each position and for each axis is the same as before (Fig. 2.13, where $M = M_m + M_a$, $D = D_m + D_a$ and $K = K_a$).

2.4.2 Result

The results of the experiments about the estimation's part of the project, with their comments, will be now presented, according to the previous scheme presented in section Experiment description.

2.4.2.1 Preliminary Tests

- MASS As describe before, the first step is to find the nominal values of the linear motors mass. Different values of the mass are used in eq. 2.30 to find the correct range of the real mass. The results are reported in Tab. 2.2:

	Motor 1	Motor 1
Mass [kg]	0.610 ± 0.030	0.605 ± 0.020

Table 2.2: Range of the nominal mass of two linear motors

- DAMPING FACTOR (D_m) and COULOMB FRICTION (F_c) A series of six different trapezoidal velocity are used to find the friction behavior. For each velocity, it has been considered three positive movements and three negative movements (Fig. 2.16) to allow to evaluate the average of this three situations and in the same time the variance. In Tab. 2.3 it is possible to see the averages values of the positive and negative velocity used for the experiments and the relative real values of the forces for motor 1.

Motor 1:

Prove	Force $[N]$	Velocity $[\frac{m}{s}]$	Force $[N]$	Velocity $[\frac{m}{s}]$
1	0.3118	0.0998	-0.3122	-0.1002
2	0.2583	0.0797	-0.2621	-0.0798
3	0.1604	0.0499	-0.1574	-0.0499
4	0.1392	0.0400	-0.1268	-0.0400
5	0.0771	0.0200	-0.0857	-0.0200
6	0.0570	0.0160	-0.0529	-0.0160

Table 2.3: Positive and negative velocity and force for motor 1

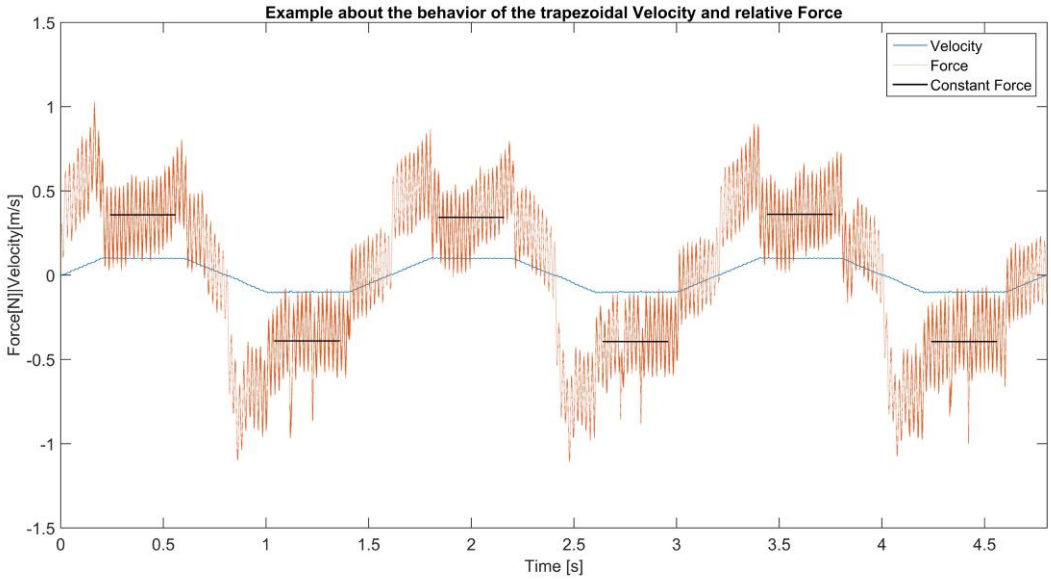

Figure 2.16: Behavior of real trapezoidal velocity and respective real Force to move the system.

In table (Tab. 2.4) the values of the positive and negative estimated friction parameters are shown.

	$f_c[N]$	$D_m[\frac{m}{s}]$
Positive Values	0.0137 ± 0.0017	3.0176 ± 0.3329
Negative Values	0.0116 ± 0.0032	3.0314 ± 0.7354
Average Values	0.0127 ± 0.0032	3.0245 ± 0.7354

Table 2.4: Estimated values of the Coulomb (f_c) and Viscous (D_m) friction parameters of the motor 1

In the same way for Virtual Arm (motor 2), the values are reported in Tab. 2.5 and Tab. 2.6.

Motor 2:

Prove	Force $[N]$	Velocity $[\frac{m}{s}]$	Force $[N]$	Velocity $[\frac{m}{s}]$
1	0.3382	0.0998	-0.3459	-0.1000
2	0.2871	0.0799	-0.2901	-0.0799
3	0.1833	0.0501	-0.1883	-0.0498
4	0.1187	0.0400	-0.1378	-0.0401
5	0.0745	0.0199	-0.0762	-0.0199
6	0.0720	0.0161	-0.0583	-0.0160

Table 2.5: Positive and negative velocity and force for motor 2

	$f_c[N]$	$D_m[\frac{Ns}{m}]$
Positive Values	0.0079 ± 0.0012	3.3559 ± 0.7718
Negative Values	0.0060 ± 0.0015	3.4692 ± 0.3113
Average Values	0.0070 ± 0.0015	3.4125 ± 0.7718

Table 2.6: Estimated values of the Coulomb (f_c) and Viscous (D_m) friction parameters of the motor 2

Fig. 2.17 shows the behavior of the friction of the motor 1, estimated using the real relation between constant velocity and force:

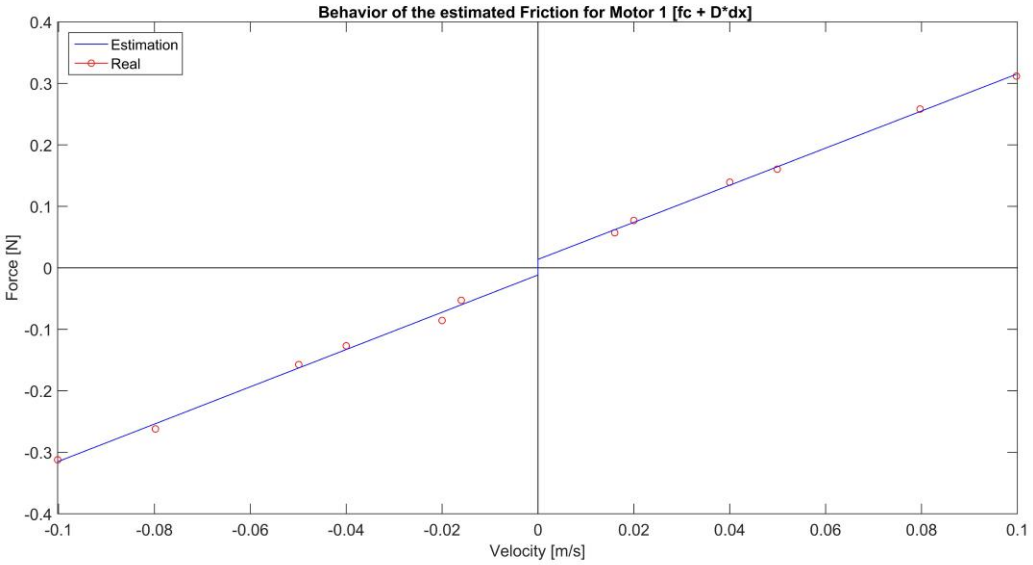

Figure 2.17: Behavior of the estimated friction for motor 1

The same is shown for motor 2 in Fig. 2.18:

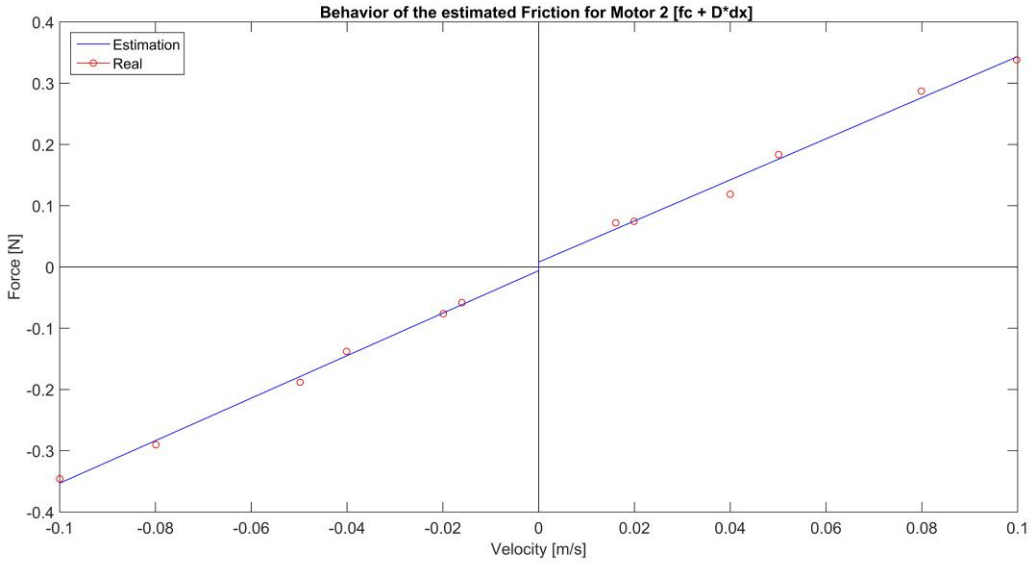

Figure 2.18: Behavior of the estimated friction for motor 2

2.4.2.2 Tuning of Accelerometer Aided Kalman Filter

To use correctly the Bartlett's test to tune the aaKF it's necessary to evaluate the variance of the accelerometer. As describe in the previous section Experiment description - Tuning of Accelerometer Aided Kalman Filter, an experiment with zero input is provided and the results are shown in Fig. 2.19. With this experiment it's possible to demonstrate that the distribution of the acceleration noise (after removing the bias value) is a Gaussian distribution with zero mean.

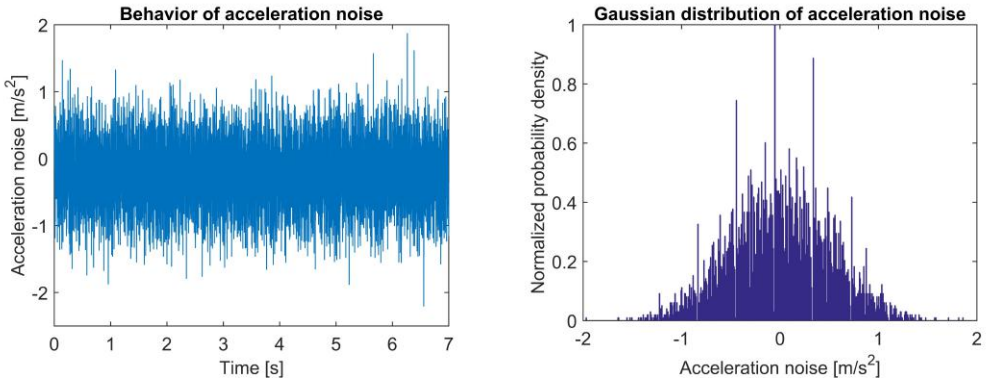

Figure 2.19: Behavior of acceleration noise and its Gaussian distribution

So, it's possible to represent the acceleration noise (after removing the bias value) as a white Gaussian noise with zero mean and sample variance:

$$\widehat{\sigma}^2_{acc} = \frac{\sum_{i=0}^{N}(\ddot{x}_i - \ddot{x}_{av})^2}{N-1} \tag{2.36}$$

Where $\ddot{x}_i$ is the sample of the instant i of the acceleration, $\ddot{x}_{av}$ is the mean value and N is the total number of samples.

The next step is the tuning of aaKF using the Bartlett's test. For motor 1, three different test are performed to see the variations in the time with the same tuning. These tests are shown in Fig. 2.20. Then, to prove that aaKF is usable with the same tuning for different configurations of the system (robustness of aaKF), the same prove it's performed with motor 1 attached to motor 2 (in configuration of Virtual Arm with different Stiffness K_a). The results of these proves are shown in Fig. 2.21

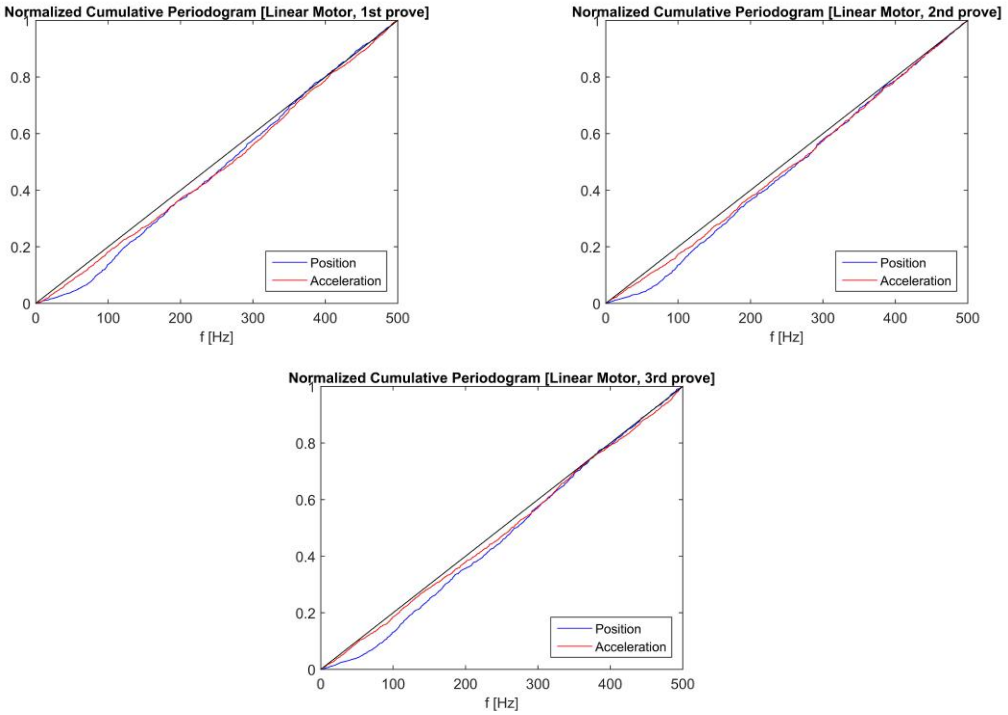

Figure 2.20: Bartlett's tests for motor 1

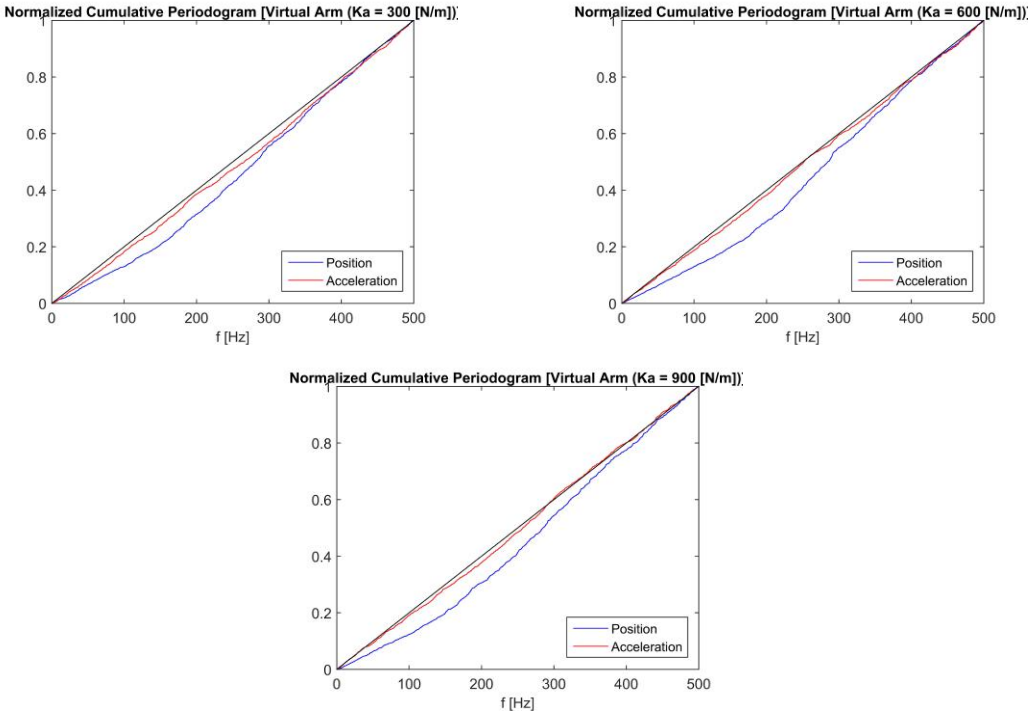

Figure 2.21: Bartlett's tests for motor 1 and Virtual Arm togheter

2.4.2.3 Estimation of a Linear Motor's parameters

In Fig. 2.22 it is possible to see the estimation of the mechanical parameters of the motor 1. As in the case of Bartlett's test, three different experiments are performed to evaluate the variation of the estimation in different time for a system with "constant" nominal values. It is possible to see that using aaKF to estimate the real position and real velocity, no particular benefits are achieved. For the value of the stiffness it is not perfectly zero because of the input disturbances (however reduced using ARMAX model in the RLS estimator), but the estimation of all other principal parameters is correct. In Tab. 2.7, the values of the estimation are reported as an average value and relative standard deviation with 95% of the probability (from time 30 [s]).

Motor (without aaKF)

Prove	$M_m[kg]$	$D_m[\frac{Ns}{m}]$	$K_m[\frac{N}{m}]$	$f_c[N]$
1	0.6099 ± 0.0030	2.8974 ± 0.0662	-0.0101 ± 0.0007	0.0130 ± 0.0011
2	0.6213 ± 0.0045	3.1111 ± 0.1355	-0.0121 ± 0.0016	0.0136 ± 0.0009
3	0.6122 ± 0.0042	3.0862 ± 0.1214	-0.0121 ± 0.0013	0.0131 ± 0.0009

Motor (with aaKF)

Prove	$M_m[kg]$	$D_m[\frac{Ns}{m}]$	$K_m[\frac{N}{m}]$	$f_c[N]$
1	0.6089 ± 0.0029	2.8813 ± 0.0695	-0.0100 ± 0.0007	0.0131 ± 0.0011
2	0.6200 ± 0.0042	3.1076 ± 0.1188	-0.0121 ± 0.0014	0.0136 ± 0.0008
3	0.6115 ± 0.0043	3.0809 ± 0.1196	-0.0121 ± 0.0013	0.0131 ± 0.0009

Table 2.7: Estimation of the motor 1 parameters

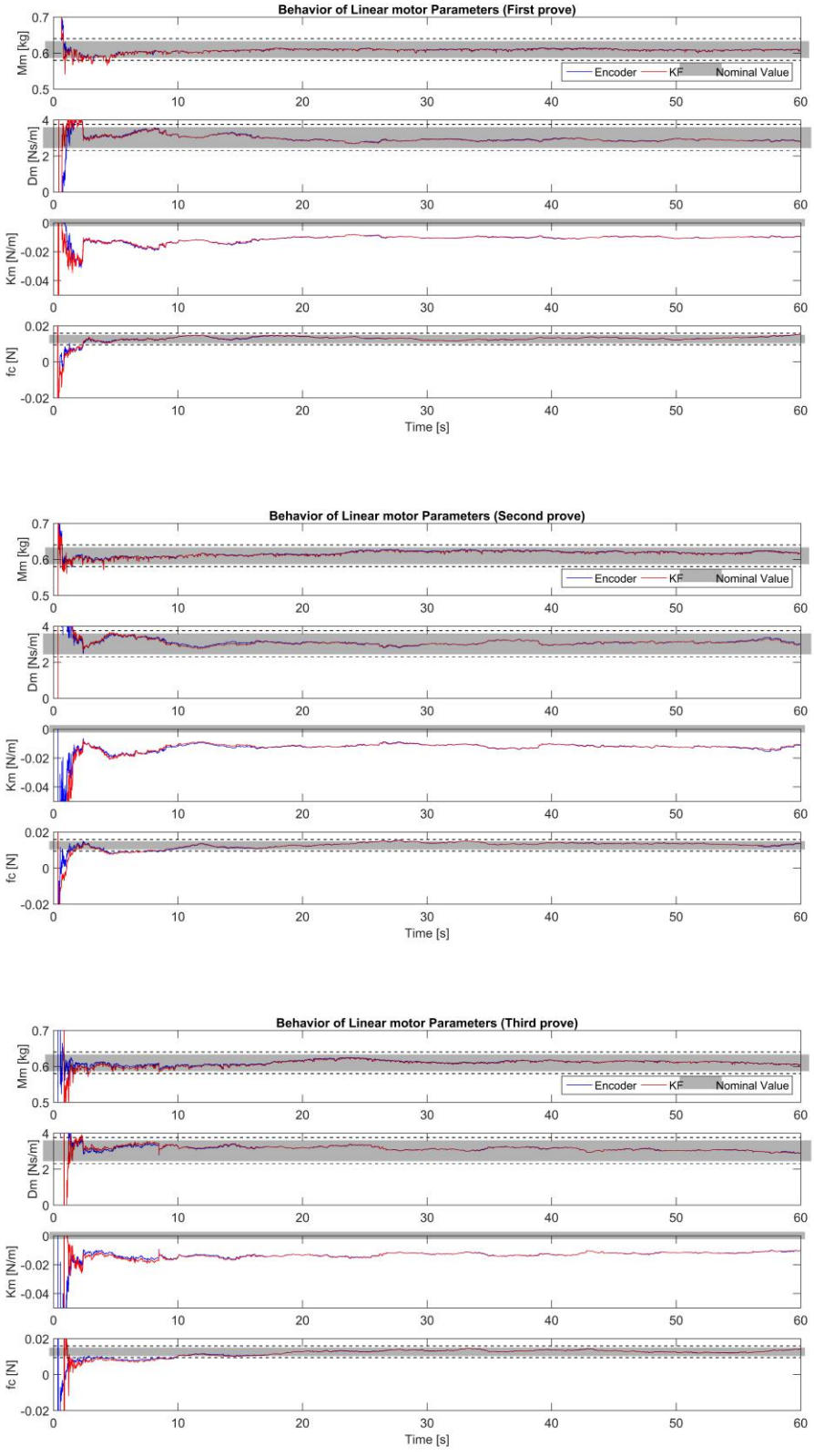

Figure 2.22: Estimation of the linear motor 1 parameters

2.4.2.4 Estimation of a Virtual Arm's Impedance

Using the same method as before, it is possible to estimate the mechanical parameters of the sum of motor 1 and 2 and subtracting the average values of the three proves estimated before it is possible to obtain the estimation of the parameters of the Virtual Arm. Three proves are performed with three different values of the stiffness, using three tipical values of the arms stiffness (reported in [13]). So, in Fig. 2.23 it is possible to see the behavior of the estimated parameters. In this case, the estimation using aaKF is better than using only RLS estimator. It is because the noise that affect the output is reduced. In the same way as before, in Tab. 2.8, the values of the Virtual Arm parameters are reported:

Virtual Arm (without aaKF)

$K_a[\frac{N}{m}]$	$M_a[kg]$	$D_a[\frac{Ns}{m}]$	$K_a[\frac{N}{m}]$	$f_c[N]$
300	0.5821 ± 0.0117	3.0628 ± 1.0873	280.8472 ± 24.2212	0.0069 ± 0.0022
600	0.5842 ± 0.0087	3.2243 ± 0.8106	580.3065 ± 28.7515	0.0070 ± 0.0021
900	0.5653 ± 0.00125	3.5093 ± 0.8985	859.2655 ± 29.1999	0.0070 ± 0.0018

Virtual Arm (with aaKF)

$K_a[\frac{N}{m}]$	$M_a[kg]$	$D_a[\frac{Ns}{m}]$	$K_a[\frac{N}{m}]$	$f_c[N]$
300	0.6033 ± 0.0086	3.6758 ± 0.2614	297.8203 ± 7.6927	0.0058 ± 0.0005
600	0.6097 ± 0.0045	3.3997 ± 0.4595	596.4068 ± 13.1209	0.0064 ± 0.0007
900	0.6075 ± 0.0071	3.5074 ± 0.5396	883.9797 ± 18.2726	0.0076 ± 0.0011

Table 2.8: Estimation of the Virtual Arm parameters

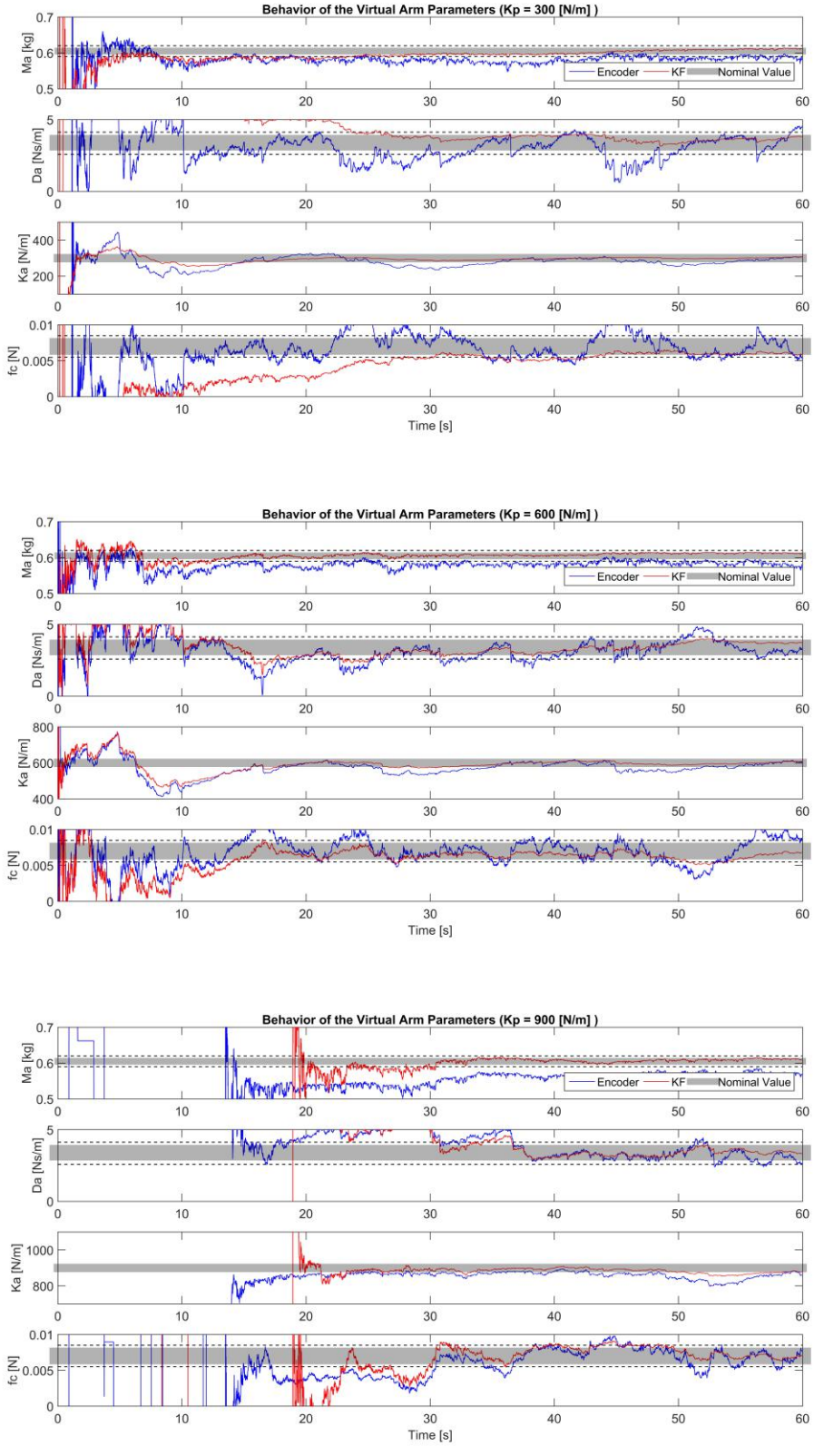

Figure 2.23: Estimation of the Virtual Arm parameters

2.4.2.5 Estimation of "mechanical" parameters of the Human Arm

This is the final step about the estimation problem. So, firstly, The estimation of the X-Y system parameters is necessary in both direction (Fig. 2.24, Tab. 2.9).

Motor

Axis	$M_m[kg]$	D_m
X	4.1408 ± 0.072	12.7184 ± 0.3777
Y	0.9548 ± 0.0023	6.2157 ± 0.1918

Table 2.9: Estimation of the parameters of the X-Y system's motors

Human Arm (X-Axis)

Point	$M_a[kg]$	$D_a[\frac{Ns}{m}]$	$K_a[\frac{N}{m}]$	$f_c[N]$
1	0.7740 ± 0.0473	21.0660 ± 1.7040	171.1142 ± 13.4549	5.7806 ± 0.2586
2	0.4236 ± 0.0342	22.3898 ± 1.8630	159.9294 ± 23.2716	5.1323 ± 0.2011
3	0.7114 ± 0.0375	31.5313 ± 4.1188	246.4368 ± 13.9612	6.0177 ± 0.2503
4	0.5460 ± 0.0331	24.7030 ± 1.7247	224.6979 ± 30.1885	6.6220 ± 0.1832

Human Arm (Y-Axis)

Point	$M_a[kg]$	$D_a[\frac{Ns}{m}]$	$K_a[\frac{N}{m}]$	$f_c[N]$
1	0.5634 ± 0.0270	44.7817 ± 9.9531	546.9010 ± 98.4803	1.7792 ± 0.1021
2	0.8420 ± 0.0429	65.8075 ± 4.0016	454.7515 ± 42.3808	1.9790 ± 0.1027
3	0.7202 ± 0.0363	52.2867 ± 5.0709	397.1847 ± 37.9193	1.9658 ± 0.0950
4	0.8002 ± 0.0397	51.9557 ± 4.3640	555.4930 ± 28.9554	2.0490 ± 0.0836

Table 2.10: Estimation of the Human Arm parameters

Then, the results of the estimation of the arm parameters in X and Y axis and for each considered point (1,2,3,4 Fig. B.1) are shown in Fig. 2.25 and reported in Tab. 2.10. This experiment is performed with an healthy subject. The results are that, in different position of the End- Point of the Human Arm and in the time, it's possible to see a variation of the condition of the Human Arm. In the same position, the variations are slow and contained within a range .

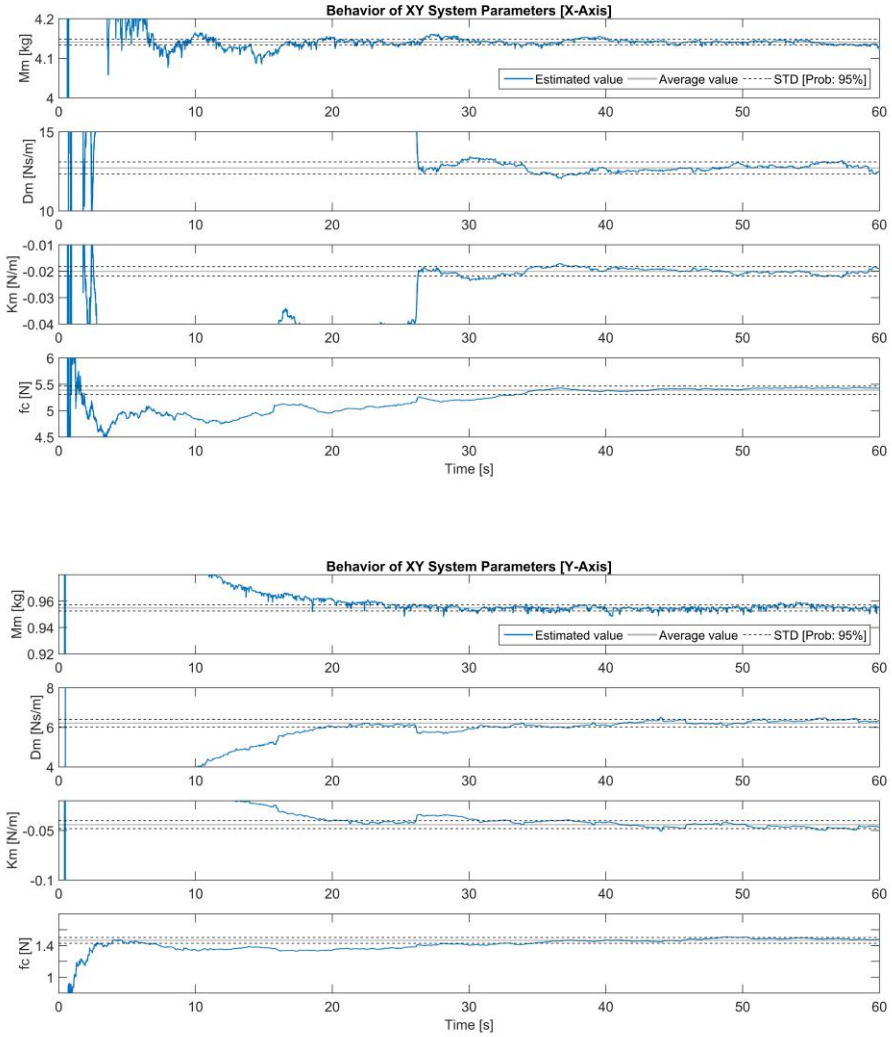

Figure 2.24: Estimation of the X-Y System parameters

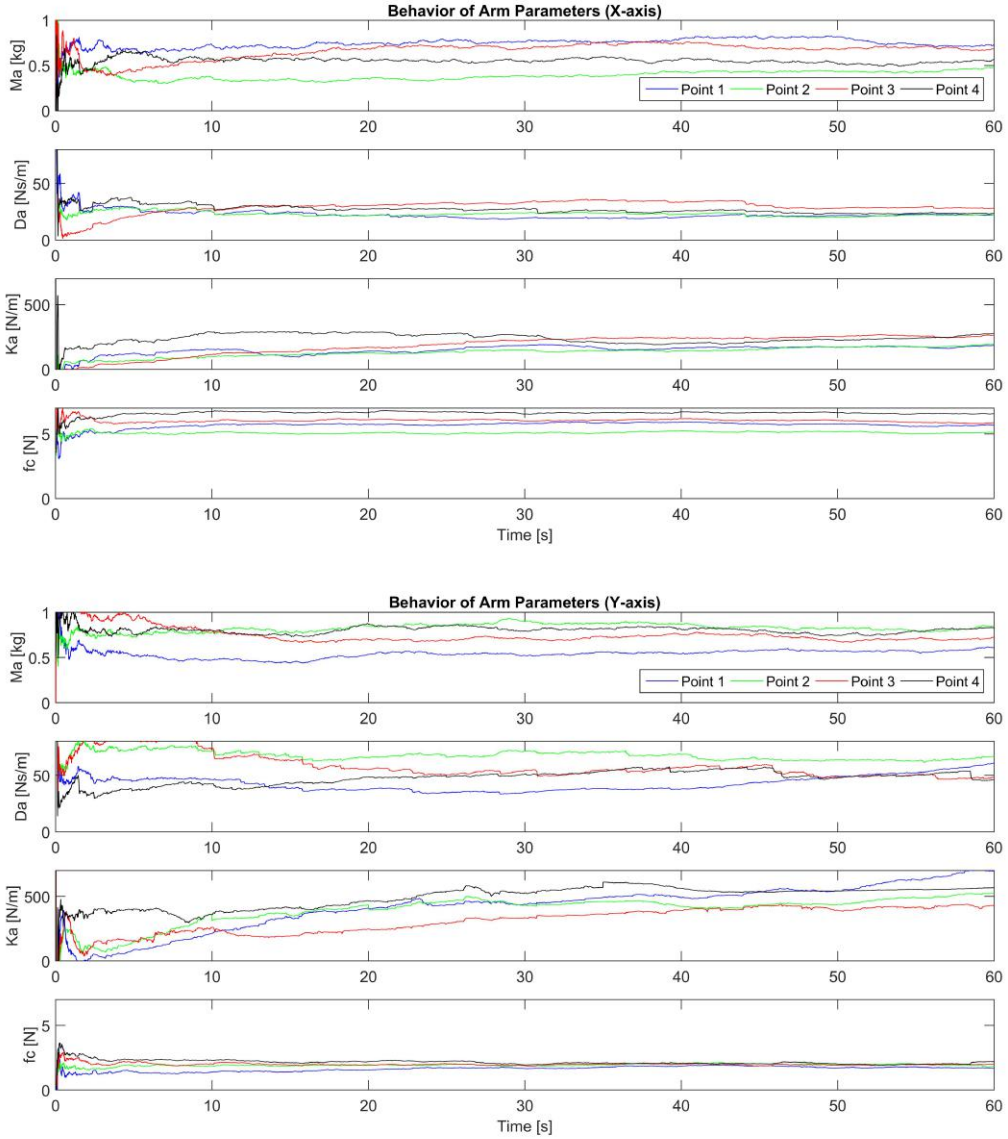

Figure 2.25: Estimation of the Human Arm parameters

As a conclusion of this chapter, a series of estimates of another healthy subject are performed to show the variable behavior of the estimation between different subject and to design the controller. The results are reported in Appendix B.

Chapter 3

Adaptive Controller

3.1 Control System Design

When a person becomes unable to interact physically with the environment, and thus able to achieve their personal goals, due to injury or illness, it's necessary to use the technology-based solutions to improve the re-learning of the basic repetitive movements. In fact, the advanced robotics is able to provide a continuous therapy at a lower cost compared to the activity carried out by physiotherapists rehabilitation, giving patients greater chance of recovery [30]. Furthermore, for doctors and therapists, a system based on haptic interfaces is highly desired, since it is an efficient system for measuring the patient condition and it can provide an intense exercise rehabilitation by providing the objective information about the progress of the patient. Another good quality of the robotic rehabilitation is that it's possible to use for a lot time the robot. In this way, in fact, the abilities of the patient can improve because the human neuromuscular system has an intrinsic dependence on the brain plasticity. For the patient, furthermore, a visual feedback from the virtual reality can improve the quality of the motion recovery. That said, one of the most important focus of the rehabilitation robots is the control law that is designed to achieve different pre-fixed goals. In this thesis, the main purpose is the emulation of the physiotherapist's help during a rehabilitation session. This one, in fact, adapts the reaction force based on the patient and his ability to properly perform the proposed exercise. So, if the patient has some problem, the physiotherapist help the patient to teach him the correct exercise. Then the patient has to try to perform the exercise with a less help to promote his partecipation and to stimulate better his plasticity. This condition need an implementation of an adaptive control type that fits its parameters according to the patient arm conditions and to the mistake

that the patient does during a repetitive exercise. In this chapter, a possible approach is proposed to achieve the previous described goals, considering a low computational cost compare to the most functional but complex work described in [68]. A simple representation of the "chain" described above is shown in Fig. 3.1

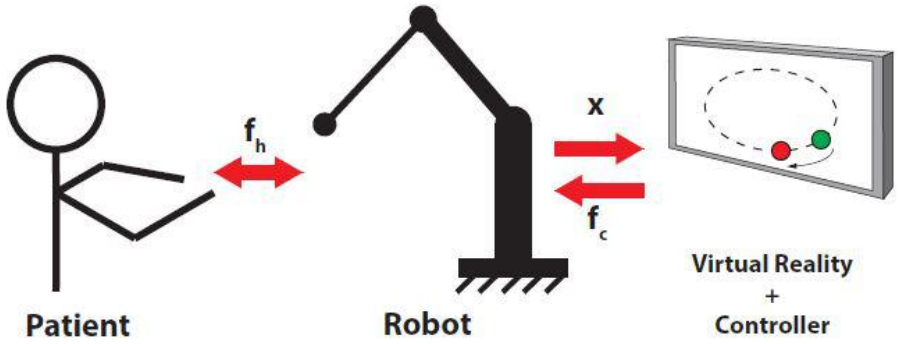

Figure 3.1: Schematic representation of a typical stand-alone robotic rehabilitation system and related therapy [68]

3.1.1 Rehabilitation Task and Control Strategy

Considering the X-Y System (shown in Fig. 2.10), a specific task is developed as an example, but the following rehabilitation controller can be used with different exercise decided in collaboration with the physiotherapist. A schematic representation of the working system with the exercise chosen to demonstrate the validity of the controller are shown in Fig. 3.2. During the exercise session, the patient (represented as Real Pos in the previous figure) has to follow the command position (Cmd Pos) around the circle in the virtual environment (created with the OPEN GL libraries). It's divided in four sectors (A,B,C,D sectors) and for each one an estimation of the arm and motor parameters in the middle point is required (1,2,3,4 point). So, using the previous estimates, it's possible to include the conditions of the patient in the design of a custom PD controller that allow to help the patient to follow correctly the specific position and velocity.

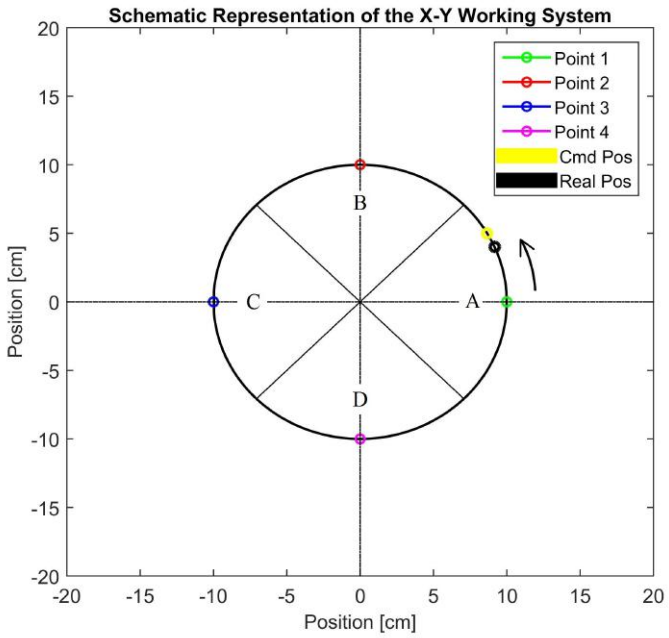

Figure 3.2: Schematic representation of the exercise in the X-Y working system

To achieve this goal and the adaptation of the assistance during the exercise, an appropriate Optimization of the controller is developed for each point and for each axis. The steps of the control strategy are shown below:

1. In the first revolution, the patient is helped to follow the command position. So, at first, the controller teaches the patient the exercise to do.

2. During the revolution, the controller evaluates, for each sector, the patient's ability to perform the exercise properly.

3. The controller adjust the gains for the next revolution. So, if the patient is able to follow correctly the reference, the help for the next revolution will be not high, allowing a high and active participation by the patient. In the other way, the controller try to re-learn the exercise, based on the error of the previous revolution.

4. This control strategy is repeated for several revolution, decided with the physiotherapist.

3.1.2 Local Optimal Design

The first step to develop the controller is the inclusion of the characteristics of the patient's arm. So, using the end-point impedance model (System Modeling) estimated with the combination of RLS and aaKF estimators, and the Optimal Control theory, it's simple to achieve this result. Following the previous control strategy to optimize the controller, the optimal control approach is developed in function of the position and velocity error (respectively, e_p and e_v) between real and command behavior and in the same time in function of the command force (F_{cmd}) used to help the patient during the exercise. So, the cost function to minimize and used for the optimization is the following:

$$\begin{aligned} J &= \sum_{k=0}^{\infty} \left\{ \begin{bmatrix} e_p(k) \\ e_v(k) \end{bmatrix}^T Q_{opt} \begin{bmatrix} e_p(k) \\ e_v(k) \end{bmatrix} + F_{cmd}^2(k) R_{opt} \right\} = \ ... \\ ... &= \sum_{k=0}^{\infty} \left\{ \begin{bmatrix} e_p(k) \\ e_v(k) \end{bmatrix}^T \begin{bmatrix} Q_{pos} & 0 \\ 0 & Q_{vel} \end{bmatrix} \begin{bmatrix} e_p(k) \\ e_v(k) \end{bmatrix} + F_{cmd}^2(k) R_{opt} \right\} \end{aligned} \tag{3.1}$$

Q_{opt} is a cost matrix 2_x2 that weight the position and velocity errors and R_{opt} is a parameter that weight the command force. So, if the costs of the errors are high compered with the cost of the input force, the optimization keep high the position and velocity gains of the control law to reduce as much as possible (in relation with the costs) the values of the errors, allowing a good tracking of the trajectory of the exercise and in the same time teaching that to the patient. In the opposite way, if the cost of the command force is the most high, the controller keep low the gains to reduce the assistance force, promoting active patient involvement. To include the human arm parameters (the estimate are shown in Appendix B) and in the same time also the motor parameters in the optimization, it's necessary to define the Algebraic Riccati Equation (ARE)

$$M_\infty = Q_{opt} + F^T M_\infty F - F^T M_\infty G[R_{opt} + G^T M_\infty G]^{-1} G^T M_\infty F \tag{3.2}$$

Where Q_{opt} and R_{opt} are defined before, while F and G represents the discrete matrix of the state space model of the motor/arm system (shown in Appendix A, section A.1 Discretization[1]).

[1]Remembering that $F_{cmd} = K_t K_i u_{cmd}$. F and G matrices are the same as the system

So, deciding a cost value of R_{opt}, keeping constant $Q_{pos} \neq 0$[2] and $Q_{vel} \neq 0$[3] and minimizing the eq. 3.1 following the method described in [34] it's possible to obtain a stable PD controller:

$$\begin{aligned} F_{cmd}(k) = [R + G^T M_\infty G]^{-1} G^T M_\infty F x(k) = [K_p \quad K_v] \begin{bmatrix} e_p(k) \\ e_v(k) \end{bmatrix} = \ ... \\ ... \ = K_{opt} \begin{bmatrix} e_p(k) \\ e_v(k) \end{bmatrix} \end{aligned} \tag{3.3}$$

The presented approach is used for both axis and for each point 1,2,3,4 represented in Fig. 3.2 separately and off-line. About this, to connect on-line the different controller's gain values between adjacent sections during the same revolution, it's possible to use a strategy that weight the two values of the position/velocity gains, depending on the angle in which the arm is located, as the following (for example for the movement from A to B):

$$\begin{bmatrix} K_{p_{1\mapsto 2}} \\ K_{v_{1\mapsto 2}} \end{bmatrix} = \begin{bmatrix} K_{p_1} \\ K_{v_1} \end{bmatrix} (1-p) + \begin{bmatrix} K_{p_2} \\ K_{v_2} \end{bmatrix} p \tag{3.4}$$

Where K_{p_1}, K_{p_2} and K_{v_1}, K_{v_1} are respectively the position and the velocity gains of the point 1 and 2. $K_{p_{1\mapsto 2}}$ and $K_{v_{1\mapsto 2}}$ are the position and velocity gains implemented directly in the controller described in eq. 3.3. "p" is a parameter that represent in percentage how much space (in term of real angle) has traveled the arm from the point 1 (sector A) to point 2 (sector B). In this way is avoided the discontinuity of the behavior of the gain from the first sector to the next.

considered in the appendix A.1 Discretization because, changing the state reference, it's possible to arrive to the same system with position and velocity error as states of the system)

[2]The value of Q_{pos} is choise $10^6[\frac{1}{m^2}]$ to weight in the same way force and position errors with different sizes of unit of measure.

[3]Q_{pos} is around the 99% of the total value of Q_{opt} because, for this implementation, the position value is the most important target.

Following, a part of the C code that describe the implementation of the solution just discussed (where "*theta_max*" represent the maximum angle between two point, that in this case is 90 degree):

```
if (theta_real>=0.0 && theta_real<theta_max)
{
        Kp_x = Kp_x_1*(1.0-theta_real/theta_max)+Kp_x_2*(theta_real/theta_max);
        Kp_y = Kp_y_1*(1.0-theta_real/theta_max)+Kp_y_2*(theta_real/theta_max);
        Kv_x = Kv_x_1*(1.0-theta_real/theta_max)+Kv_x_2*(theta_real/theta_max);
        Kv_y = Kv_y_1*(1.0-theta_real/theta_max)+Kv_y_2*(theta_real/theta_max);
}

else if(theta_real>=theta_max && theta_real<2.0*theta_max)
{
        Kp_x = Kp_x_2*(1.0-(theta_real-theta_max)/theta_max)+Kp_x_3*((theta_real-theta_max)/theta_max);
        Kp_y = Kp_y_2*(1.0-(theta_real-theta_max)/theta_max)+Kp_y_3*((theta_real-theta_max)/theta_max);
        Kv_x = Kv_x_2*(1.0-(theta_real-theta_max)/theta_max)+Kv_x_3*((theta_real-theta_max)/theta_max);
        Kv_y = Kv_y_2*(1.0-(theta_real-theta_max)/theta_max)+Kv_y_3*((theta_real-theta_max)/theta_max);
}

else if(theta_real>=2.0*theta_max && theta_real<3.0*theta_max)
{
        Kp_x = Kp_x_3*(1.0-(theta_real-2.0*theta_max)/theta_max)+Kp_x_4*((theta_real-2.0*theta_max)/theta_max);
        Kp_y = Kp_y_3*(1.0-(theta_real-2.0*theta_max)/theta_max)+Kp_y_4*((theta_real-2.0*theta_max)/theta_max);
        Kv_x = Kv_x_3*(1.0-(theta_real-2.0*theta_max)/theta_max)+Kv_x_4*((theta_real-2.0*theta_max)/theta_max);
        Kv_y = Kv_y_3*(1.0-(theta_real-2.0*theta_max)/theta_max)+Kv_y_4*((theta_real-2.0*theta_max)/theta_max);
}

else if(theta_real>=3.0*theta_max && theta_real<=4.0*theta_max)
{
        Kp_x = Kp_x_D*(1.0-(theta_real-3.0*theta_max)/theta_max)+Kp_x_A*((theta_real-3.0*theta_max)/theta_max);
        Kp_y = Kp_y_D*(1.0-(theta_real-3.0*theta_max)/theta_max)+Kp_y_A*((theta_real-3.0*theta_max)/theta_max);
        Kv_x = Kv_x_D*(1.0-(theta_real-3.0*theta_max)/theta_max)+Kv_x_A*((theta_real-3.0*theta_max)/theta_max);
        Kv_y = Kv_y_D*(1.0-(theta_real-3.0*theta_max)/theta_max)+Kv_y_A*((theta_real-3.0*theta_max)/theta_max);
}
```

Figure 3.3: C-code about the weighing of the controller gains

In the same figure it's possible to see that the variation of the controller, during the transition between two points, depends on the actual real position of the hand (referring to the angle of the circumference and represent as "*theta_real*" describe in the sub-section Waiting system in Fig. 3.7), and not from the one commanded. So, if the patient fails to move his arm, there will be no sudden changes in term of gains.

3.1.3 Variable weight cost for the input Force (F_{cmd})

The principal point of this sub-section is to define R_{opt} to allow to take into account on-line about the variation of the abilities of the patient to perform correctly the exercise. As describe before, R_{opt} represent the cost about the use of the control energy that in this case it is the force used to help the patient to do the rehabilitation exercise (F_{cmd}).

Using only the classic Optimal Control approach describe in the previous sub-section Local Optimal Design it's not possible to fully replicate on-line the physiotherapist's intervention during the exercise:

- **PROBLEM**: The control law is always the same for each revolution and it's possible to choose only if the reaction force to help the patient is:
  - Strong (R_{opt} "low" $\mapsto$ K_{opt} "high"): The patient is helped a lot in exercising because the controller tries to keep the position and velocity errors very small, so he will never be moved to participate actively.
  - Weak (R_{opt} "low" $\mapsto$ K_{opt} "high"): The controller, is this case, not help a lot the patient, so he is always invited to participate actively in the exercise, even in the case of a lot of difficulties. This situation is not very good because morally, the patient may be affected by the fact that he is never able to finish the exercise and in the same time the plasticity of the brain is not trained.
  - Not weak and not strong (R_{opt} "middle" value $\mapsto$ K_{opt} "middle" value): The system tries to mediate between a small error and a non-excessive reaction force. This is not a bad situation, but the patient never provided complete help to learn the exercise well in the event of difficulty and at the same time, he is never left "free" to perform the exercise to actively participate in the rehabilitation session.
- **PROPOSED SOLUTION**: To avoid the previous situation and to promote the participation of the patient, using the force to help only if necessary and with the correct intensity, a simple strategy is implemented (another kind of Assist-as-Needed Controller is shown in [85] and [68]).

The proposed approach can be divided into two parts:

- Off-line part: The idea is to set a constant value of Q_{opt} and pre-calculate off-line different values of Optimal Control Gains for each point 1,2,3,4 of the exercise and for both axis, depending of the variation of R_{opt} (that is different for each sector A,B,C,D and for both axis). Then, a law that connect the variations of the gains with the variation of the input cost R_{opt} is developed using the previous Optimal gains.
- On-line part: Finally, an on-line strategy to update the values of R_{opt} is necessary to evaluate, during the revolution M (actual revolution), the gains of the controller that will be used in the M+1 revolution (next revolution).

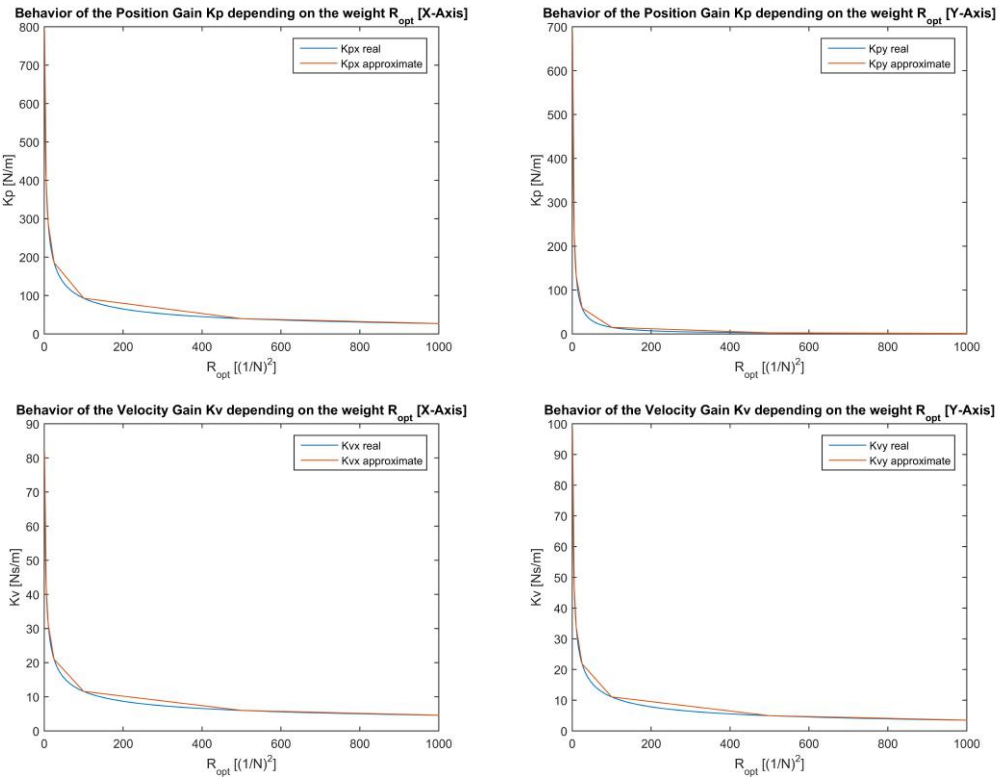

Figure 3.4: Comparison between real and approximate behavior of K_{p_1} and K_{v_1} in function of R_{opt} (Point 1, both axis)

About the off-line part of the design of the adaptive control law, a series of optimal control design have been carried out for each point (1,2,3,4 in Fig. 3.2) and for each axis, varying the value of R_{opt} from 1 to 1000 $[\frac{1}{N^2}]$ (with step of 1 $[\frac{1}{N^2}]$). In this way it's possible to describe off-line the behavior of K_{opt} in function of R_{opt}, shown, as an example for the point 1, in Fig. 3.4. In the same figure are shown the approximation of the law to limit the computational cost to reproduce correctly the same relationship for the on-line application. So, a series of straight line are implemented to connect 7 different values of the gains using the simple relation of a straight through two point. Therefore, depending on the range in which the R_{opt} values falls, the correct linear relationship will be chosen on-line. An example of the implementation of this solution in sector A for the point 1 and for X-axis is shown in Fig. 3.5 (For all other sector and for Y-axis the implementation is the same):

```
if (R_opt_x_A >= 1.0 && R_opt_x_A<=5.0)
{
        Kp_x_1 = (R_opt_x_A-1.0)/(5.0-1.0)*(Kp_x_1_R5 - Kp_x_1_R1)+Kp_x_1_R1;
        Kv_x_1 = (R_opt_x_A-1.0)/(5.0-1.0)*(Kv_x_1_R5 - Kv_x_1_R1)+Kv_x_1_R1;
}
else if (R_opt_x_A > 5.0 && R_opt_x_A<=1.0)
{
        Kp_x_1 = (R_opt_x_A-5.0)/(10.0-5.0)*(Kp_x_1_R10 - Kp_x_1_R5)+Kp_x_1_R5;
        Kv_x_1 = (R_opt_x_A-5.0)/(10.0-5.0)*(Kv_x_1_R10 - Kv_x_1_R5)+Kv_x_1_R5;
}
else if (R_opt_x_A > 10.0 && R_opt_x_A<=25.0)
{
        Kp_x_1 = (R_opt_x_A-10.0)/(25.0-10.0)*(Kp_x_1_R25 - Kp_x_1_R10)+Kp_x_1_R10;
        Kv_x_1 = (R_opt_x_A-10.0)/(25.0-10.0)*(Kv_x_1_R25 - Kv_x_1_R10)+Kv_x_1_R10;
}
else if (R_opt_x_A > 25.0 && R_opt_x_A<=100.0)
{
        Kp_x_1 = (R_opt_x_A-25.0)/(100.0-25.0)*(Kp_x_1_R100 - Kp_x_1_R25)+Kp_x_1_R25;
        Kv_x_1 = (R_opt_x_A-25.0)/(100.0-25.0)*(Kv_x_1_R100 - Kv_x_1_R25)+Kv_x_1_R25;
}
else if (R_opt_x_A > 100.0 && R_opt_x_A<=500.0)
{
        Kp_x_1 = (R_opt_x_A-100.0)/(500.0-100.0)*(Kp_x_1_R500 - Kp_x_1_R100)+Kp_x_1_R100;
        Kv_x_1 = (R_opt_x_A-100.0)/(500.0-100.0)*(Kv_x_1_R500 - Kv_x_1_R100)+Kv_x_1_R100;
}
else if (R_opt_x_A > 500.0 && R_opt_x_A<=1000.0)
{
        Kp_x_1 = (R_opt_x_A-500.0)/(1000.0-500.0)*(Kp_x_1_R1000 - Kp_x_1_R500)+Kp_x_1_R500;
        Kv_x_1 = (R_opt_x_A-500.0)/(1000.0-500.0)*(Kv_x_1_R1000 - Kv_x_1_R500)+Kv_x_1_R500;
}
```

Figure 3.5: C-code about the behavior of the gains in relation to the R_opt in the point 1, sector A, X-axis

All pre-calculated gains (Position Gains $[\frac{N}{m}]$ and Velocity Gains $[\frac{Ns}{m}]$) used to develop the controller's law are shown in Tab. 3.1 for both axis.

Point	$K_{p_{x_{R1}}}$	$K_{p_{x_{R5}}}$	$K_{p_{x_{R10}}}$	$K_{p_{x_{R25}}}$	$K_{p_{x_{R100}}}$	$K_{p_{x_{R500}}}$	$K_{p_{x_{R1000}}}$
1	787.7902	397.2571	288.3015	185.7766	92.9947	39.9039	27.1804
2	785.6777	395.6752	286.8034	184.3411	91.6218	38.6279	25.9712
3	786.9422	393.8043	284.4925	181.7795	89.0130	36.2283	23.7478
4	787.1622	395.3552	286.2245	183.6059	90.8269	37.8755	25.2646

Point	$K_{v_{x_{R1}}}$	$K_{v_{x_{R5}}}$	$K_{v_{x_{R10}}}$	$K_{v_{x_{R25}}}$	$K_{v_{x_{R100}}}$	$K_{v_{x_{R500}}}$	$K_{v_{x_{R1000}}}$
1	81.3090	42.2169	31.2933	20.99878	11.5812	6.0231	4.6055
2	81.2393	42.1962	31.2779	20.9730	11.5586	5.9821	4.5541
3	81.6969	42.3290	31.3587	21.0135	11.5578	5.9311	4.4792
4	81.4977	42.4203	31.3235	20.9980	11.5656	5.9702	4.5333

Point	$K_{p_{y_{R1}}}$	$K_{p_{y_{R5}}}$	$K_{p_{y_{R10}}}$	$K_{p_{y_{R25}}}$	$K_{p_{y_{R100}}}$	$K_{p_{y_{R500}}}$	$K_{p_{y_{R1000}}}$
1	684.9462	230.3403	132.4906	58.9382	15.0526	2.5687	1.0898
2	758.9197	281.5911	171.5351	82.5351	23.3698	4.5824	2.1728
3	775.3160	298.5336	185.8500	92.3205	27.2652	5.5303	2.6654
4	766.9077	292.5020	180.9285	88.9779	25.9000	5.1816	2.4787

Point	$K_{v_{y_{R1}}}$	$K_{v_{y_{R5}}}$	$K_{v_{y_{R10}}}$	$K_{v_{y_{R25}}}$	$K_{v_{y_{R100}}}$	$K_{v_{y_{R500}}}$	$K_{v_{y_{R1000}}}$
1	98.0700	46.9666	33.8870	21.8287	11.0640	4.9676	3.5108
2	98.7983	47.7983	34.7346	22.5999	11.5781	5.2232	3.6946
3	97.5739	47.4080	34.5295	22.5531	11.6182	5.2574	3.7207
4	97.3545	47.2541	34.3835	22.4205	11.5234	5.2079	3.6847

Table 3.1: Position and Velocity pre-calculated gains

This kind of implementation is developed considering the actual R_{opt} in the revolution M to evaluate the future values of the gains in the revolution M+1. With this in mind, all R_{opt} have to change on-line to adapt the values of the gains in relation to the abilities of the patient to follow the target. The idea to update the values of R_{opt} is the evaluation of the average of the position square error of the patient in the sector in which the arm is present. In this way the update law depends only on the magnitude of the error (the error can be present in both directions, positive and negative), giving more weight to the average for bigger errors due to the quadratic form of the error. So, taking as an example the evaluation of the error in sector A related to the Fig. 3.2, the on-line law becomes:

$$R_{opt_{x_A}} = par_1 + \frac{par_2}{\frac{\sum_{i=0}^{N-1} e^2_{p_{x_A}}(i)}{N}} = par_1 + \frac{par_2}{e_{A_{index}}} \tag{3.5}$$

Where par_1 and par_2 are two parameters used to design the behavior of the weight in the desired way solving a simple equation system shown below:

$$\begin{cases} 1 = par_1 + \frac{par_2}{max(e_{A_{index}})} \\ 1000 = par_1 + \frac{par_2}{min(e_{A_{index}})} \end{cases} \tag{3.6}$$

1 and 1000 are, respectively, the minimum and the maximum values of R_{opt}. These two values are the limit values of the R_{opt}'s range. $max(e_{A_{index}}$ and $min(e_{A_{index}}$ are respectively the decided maximum and minimum values of the average square error desired. They are chosen by the physical considerations made by the physiotherapist in relation of the approximation of a constant minimum and maximum desired error during the exercise. So, changing that values, it's possible to weigh more or less the mistake made by the patient, affecting the intensity of help on the next revolution.

3.1.4 Waiting system

In order to obtain a safe and correct behavior for the patient, another constrain is applied to the controller. In fact, if the patient has some problem to follow the command target (for example, for a sudden stiffening of the arm that prevents movement in one of the two directions), the error between command position and real position could become to high and the reaction of the controller could be dangerous for the patient. Anyway, if K_{opt} is high, the controller help the patient to follow the target, so this constrain is useful only in the situation where K_{opt} in the visited area is not high and the patient has to follow the target "alone". In fact, in this situation, a too high discrepancy between the command and real position angle may arise because the reaction force initially is not very high (K_{opt} is not high) and changing the normal gain values update (Fig. 3.3), creating discontinuities and sharp movement in wrong directions. This situation is shown in Fig. 3.6.

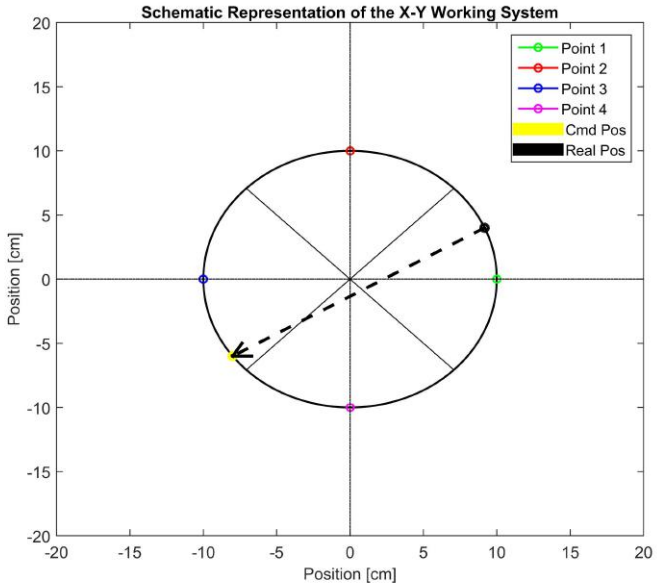

Figure 3.6: Wrong direction of the movement caused by the controller

The implementation of the constrain is not just thought to avoid movement outside of the area around the circle caused by controller. In fact, setting that, if the error between θ_{cmd} and θ_{real} is more big than a pre-fixed value, θ_{cmd} doesn't change its value until this error will be reduced (Fig. 3.7). So, it is also used to increase the patient's self-confidence, that will see the target position to reach move depending on their abilities.

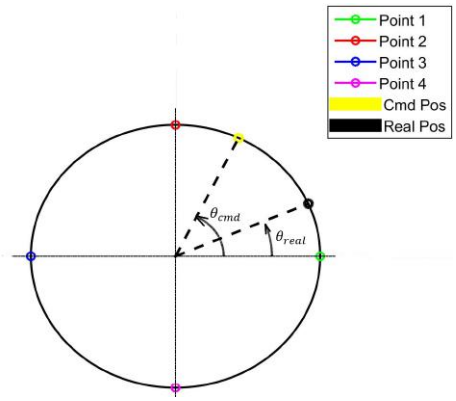

Figure 3.7: θ_{real} and θ_{cmd}

Finally, it's better to specify that the values of θ_{real} and θ_{cmd} are calculated from the position of the two linear motor using X and Y coordinates in the following way:

$$\begin{aligned} \theta_{cmd} &= atan2(\frac{y_{cmd}}{x_{cmd}})\frac{180}{\pi} \\ \theta_{real} &= atan2(\frac{y_{real}}{x_{real}})\frac{180}{\pi} \end{aligned} \tag{3.7}$$

Defined in the range $[-180°, 180°]$ and with the conditions:

if $\theta_{cmd} < 0$
  $\theta_{cmd} = 360° + \theta_{cmd}$
end

if $\theta_{real} < 0$
  $\theta_{real} = 360° + \theta_{real}$
end

3.2 Experimental Set-up

To test the validity of the controller, the X-Y system set-up described in the section Experimental Set-up of Chapter 2 is used in the way shown in Fig. 3.8:

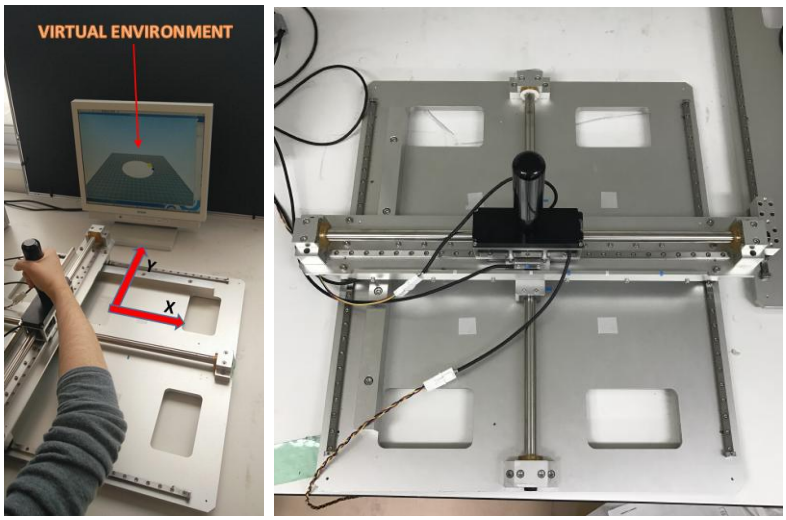

Figure 3.8: X-Y System with/without Human Arm

3.3 Experimental Testing

The implementation of the control law, based on the scheme in Fig. 3.9, is used in the X-Y system shown in Fig. 3.8 to test the validity of the emulation of the physiotherapist's help during the exercise and the waiting system implemented.

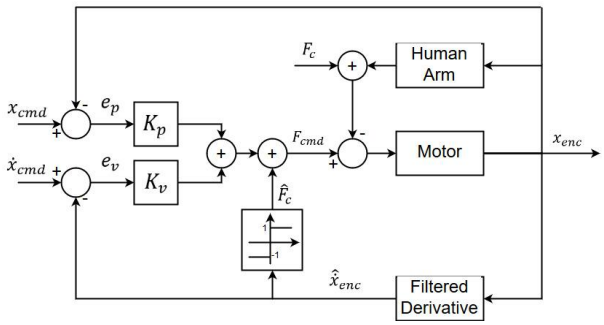

Figure 3.9: Scheme used to control the system during the rehabilitation task

In order to reduce the effect of the non-linear Coulomb friction during the exercise (not considered in the previous design of the controller) a compensation is performed using the previous estimated parameters f_c and the estimation of the velocity [4].

3.3.1 Experiment description

3.3.1.1 Test to validate the replication of the physioterapist intervention

This experiment is performed to prove that the controller law works in the correct way. So, for this purpose, the healthy subject under the test (his impedance parameters are listed in the Appendix B) tried to follow the command target with his own arm. In Fig. 3.10 it is possible to see the real behavior of the arm during five revolutions of the circle starting from point 1 and proceeding in counterclockwise direction.

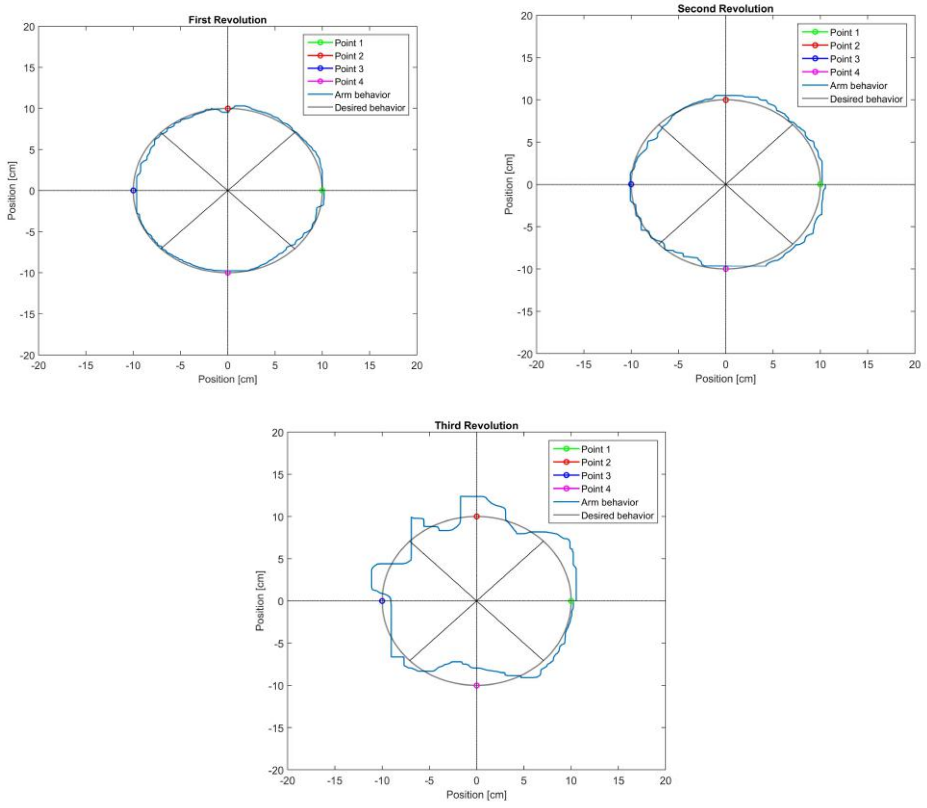

[4]Here shown only with a filtered derivative for lack of two accelerometers with which to implement for both axis an aaKF estimator to improve the effectiveness

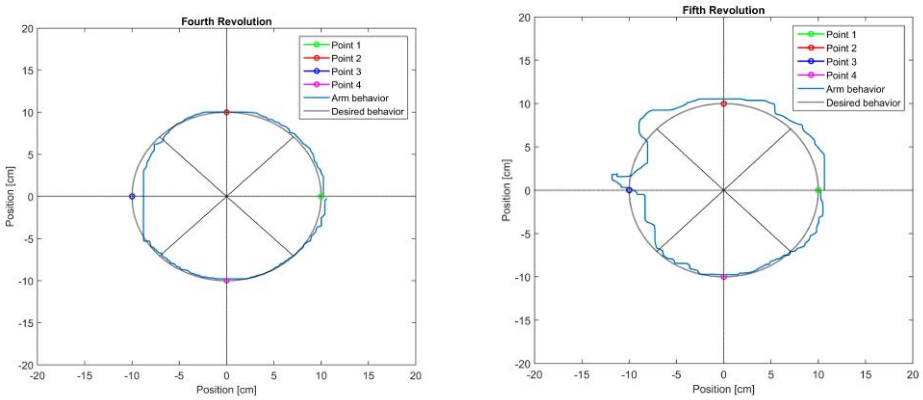

Figure 3.10: Revolutions during the exercise

3.3.1.2 Test to validate the waiting system

In a second time, the subject under the test tried to simulate the situation in which the patient has a big problem to follow the target with "minimal" assistance, blocking the movement of the arm, until reaching the limit constrain about the difference between θ_{cmd} and θ_{real}, selected for this test as 30°.

3.3.2 Result

3.3.2.1 Test to validate the replication of the physioterapist intervention

In Fig. 3.11 a representation of the square error committed by the subject and the relative behavior of the position gain (the most important) is shown (for both axis). It is possible to see that, during the revolution with a low gain, it is possible to commit some error because the patient has to try to follow the target alone. But, if the error is high, the gains increases for the following revolution, teaching the patient the right path to follow.

3.3.2.2 Test to validate the waiting system

The final test shows, in Fig. 3.12 the correct operation of the waiting system. In fact, when the subject blocked the arm, θ_{cmd} continues for another 30°, then the system block the target, waiting the movement of the patient.

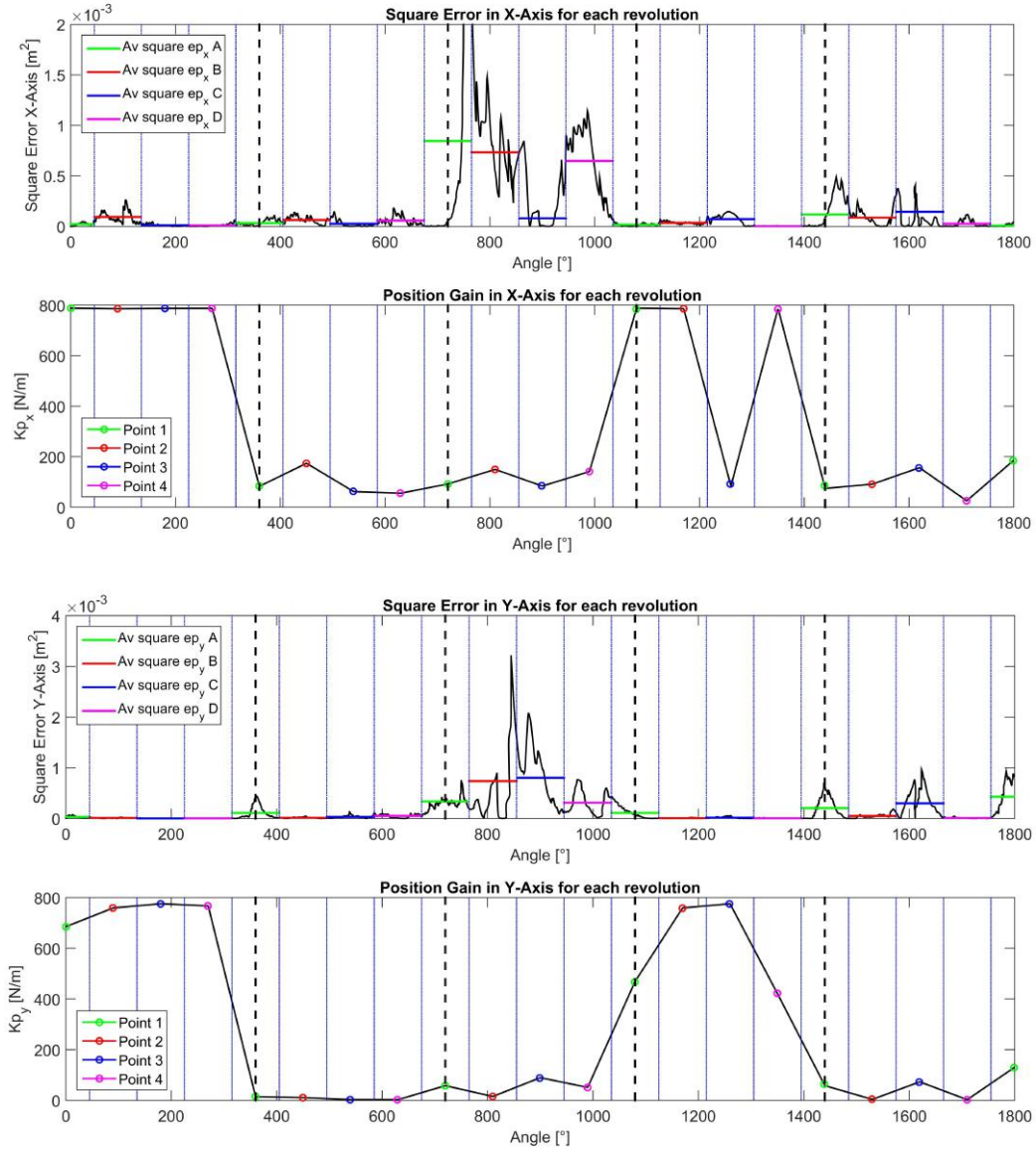

Figure 3.11: Behaviors of the square error and position gain for both axis

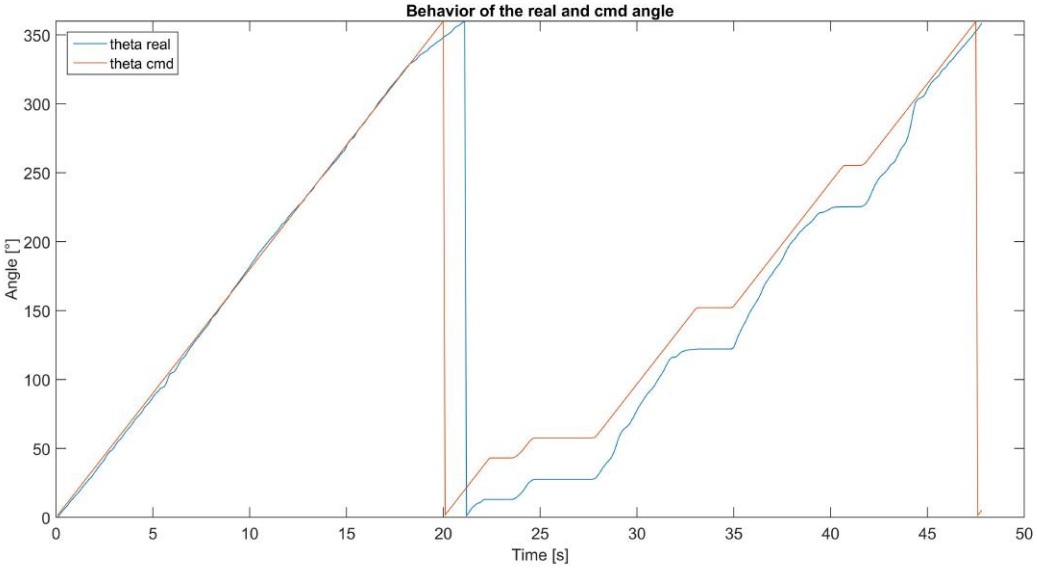

Figure 3.12: Stop of the θ_{cmd} to wait the patient

The last thing to clarify is that, after a training session is over, it's possible to re-evaluate the condition of the patient, by adjusting the controller depending on the improvements achieved.

Chapter 4

Conclusions

After commenting the experiment results, the main final considerations are now reported. Firstly, the estimation of the human arm parameters allows to know better the real condition of the patient. For example, the estimation of the stiffness of the arm is a parameter that could be used to understand if there have been improvements with the rehabilitation training, leaving any medical consideration to the subjectivity of the doctor or physiotherapist. To obtain a good result of the estimates, an appropriate system model is necessary to describe it in the best way. It's possible to model the arm as a Mass-Damper-Stiffness system (many examples of this kind of model for the arm exist in literature , for example [78]). But the real system with the motor is affected by unknown noises and non-linearity, so a state space approach, using the RLS estimator with an ARMAX model, allows to obtain a proper estimation of the total system. Then, subtracting the mechanical values of the motor it is possible to obtain an accurate estimation of the arm parameters. In this thesis, it has also been demonstrated that, using a state observer, it is possible to achieve a better result. In fact, using aaKF it's possible to remove the quantization noise of the encoder, obtaining a better estimation of the velocity (used to take into account about the non-linear Coulomb friction in the system). The implementation of the aaKF, in addition, allows to solve the problem about the variation of the human arm parameters for different patients. So, it is not necessary to tune the aaKF for each patient. Finally, using the average values of the arm's estimation, it has been shown an implementation of a control law that allows to design an appropriate controller that is different for each person. This control law changes during the exercise, allowing to follow the condition and the capabilities of the patient, improving the reaction force to help the patient to follow the command target if the error committed is high, and in the opposite way, relaxing the reaction force if the patient is able to follow the target. In this

way the patient is more motivated to continue the exercise and the brain plasticity is exiting to remember better the correct movement. More experiment are necessary in the future to understand better the benefits of this approach, especially with affected arms. Furthermore, the development of a more accurate arm's model is necessary to consider other effects, for example the combined response of the x and y directions during the movements.

Appendix A

Zero-Order Holder discretization of the system

The Zero-Order Holder discretization method is a technique used to go from continuous time to discrete time. There are many reasons why it's important to discretize a continuous-time system. First of all, a lot of system now are controlled by digital controller, so it's better to uniform the controller with the plant to control. Another reason is that a lot of identification code are more easily implementable in discrete time because the systems are described as a linear function of the previous and actual sample. So, taking into account about the holder H (that keep constant the input $u(t)$ from to different step) and about the sampling device S (that take an information from the continuous output $x(t)$ of the system in form of sample in the step k) it's simple to describe a continuous sistem as a "digital" system. Thanks the system used for taking into account about the discretization, this method is called also "Step-Invariant Trasformation" and a schematic representation is shown in Fig. A.1. For more details about the theory of this kind of discretization, see [23].

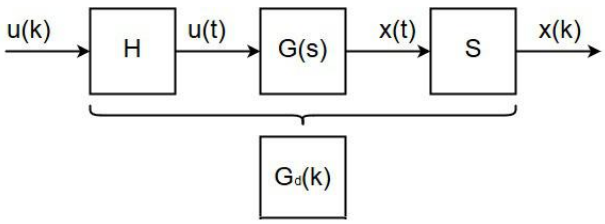

Figure A.1: Step Invariant Trasformation

A.1 Discretization

The purpose of this appendix is to show the mathematical approach to connect the continuous time (used to describe the natural system consisting of motor and arm) with the discrete time (used to describe the system in an appropriated form for the identification and for the controller). So, firstly, only the part of the figure used for the Model of the system is reported here (Fig. A.2):

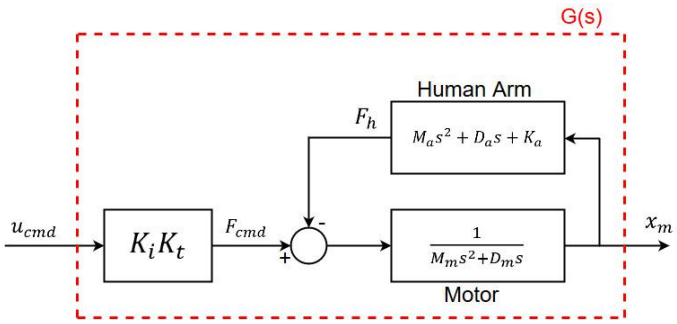

Figure A.2: Block Diagram to describe the Motor-Arm system

For the same reason, eq. 2.1 is reported only for semplicity of comprehension:

$$G(s) = \frac{X_m(s)}{U_{cmd}(s)} = \frac{\frac{K_t K_i}{M_m s^2 + D_m s}}{1 + \frac{M_a s^2 + D_a s + K_a}{M_m s^2 + D_m s}} = \frac{K_t K_i}{M s^2 + D s + K_a} \tag{A.1}$$

With: $M = M_m + M_a, D = D_m + D_a$

Using eq. A.1 in the Continuous Time Domain is possible to obtain the State Space Model representation:

$$\begin{cases} \begin{bmatrix} \dot{x}_m(t) \\ \ddot{x}_m(t) \end{bmatrix} = \begin{bmatrix} 0 & 1 \\ -\frac{K_a}{M} & -\frac{D}{M} \end{bmatrix} \begin{bmatrix} x_m(t) \\ \dot{x}_m(t) \end{bmatrix} + \begin{bmatrix} 0 \\ \frac{K_i K_t}{M} \end{bmatrix} u_{cmd}(t) = \ \ldots \\ \quad \ldots \ = \begin{bmatrix} 0 & 1 \\ \alpha & \beta \end{bmatrix} \begin{bmatrix} x_m(t) \\ \dot{x}_m(t) \end{bmatrix} + \begin{bmatrix} 0 \\ \gamma \end{bmatrix} u_{cmd}(t) = A \begin{bmatrix} x_m(t) \\ \dot{x}_m(t) \end{bmatrix} + B u_{cmd}(t) \\ y(t) = x_m(t) = [1 \ \ 0] \begin{bmatrix} x_m(t) \\ \dot{x}_m(t) \end{bmatrix} = C \begin{bmatrix} x_m(t) \\ \dot{x}_m(t) \end{bmatrix} \end{cases} \tag{A.2}$$

The next step is the discretization of the system using the Zero-Order Holder method, considering T_s as a sample time from two different samples, where the signals are keeping constant. So, the discrete version of the State Space Model describe before is the following:

$$\begin{cases} \begin{bmatrix} x_m(k+1) \\ \dot{x}_m(k+1) \end{bmatrix} = \begin{bmatrix} F_{11} & F_{12} \\ F_{21} & F_{22} \end{bmatrix} \begin{bmatrix} x_m(k) \\ \dot{x}_m(k) \end{bmatrix} + \begin{bmatrix} G_1 \\ G_2 \end{bmatrix} u_{cmd}(k) = \ ... \\ \qquad\qquad ... \ = F \begin{bmatrix} x_m(k) \\ \dot{x}_m(k) \end{bmatrix} + G u_{cmd}(k) \\ y(k) = x_m(k) = [1 \ \ 0] \begin{bmatrix} x_m(k) \\ \dot{x}_m(k) \end{bmatrix} = H \begin{bmatrix} x_m(k) \\ \dot{x}_m(k) \end{bmatrix} \end{cases} \tag{A.3}$$

Where:

$$\begin{cases} F = e^{AT_s} = I + AT_s + \dfrac{A^2T_s^2}{2} + ... + \dfrac{A^nT_s^n}{n!}, (n \mapsto \infty) \approx I + AT_s + \dfrac{A^2T_s^2}{2} + \dfrac{A^2T_s^3}{3!} = \ ... \\ ... \ = \begin{bmatrix} 1 + \alpha\frac{T_s^2}{2} + \alpha\beta\frac{T_s^3}{6} & T_s + \beta\frac{T_s^2}{2} + (\alpha+\beta^2)\frac{T_s^3}{6} \\ \alpha T_s + \alpha\beta\frac{T_s^2}{2} + \alpha(\alpha+\beta^2)\frac{T_s^3}{6} & 1 + \beta T_s + (\alpha+\beta^2)\frac{T_s^2}{2} + [\alpha\beta + \beta(\alpha+\beta^2)]\frac{T_s^3}{6} \end{bmatrix} \\ G = \int_0^{T_s} e^{A\sigma} B \, d\sigma = \begin{bmatrix} \frac{\gamma}{2}T_s^2 + \frac{\beta\gamma}{6}T_s^3 + \frac{(\alpha+\beta^2)\gamma}{24}T_s^4 \\ \gamma T_s + \frac{\beta\gamma}{2}T_s^2 + \frac{(\alpha+\beta^2)\gamma}{6}T_s^3 + \frac{\alpha\beta+\beta(\alpha+\beta^2)]\gamma}{24}T_s^4 \end{bmatrix} \\ H = C = [1 \ \ 0] \end{cases} \tag{A.4}$$

Using the Z-transform in the system A.3, the Discrete Transfer Function becomes:

$$\begin{aligned} G_d(z) = \frac{X_m(z)}{U_{cmd}(z)} = H(zI - F)^-1GU = \frac{zG_1 + (-F_{F_{22}G_1 + F_{12}G_2})}{z^2 + z(-F_{22} - F_{11}) + (F_{11}F_{22} - F_{21}F_{12})} = \ ... \\ ... \ = \frac{zb_1 + b_0}{z^2 + za_1 + a_0} = \frac{z^{-1}b_1 + z^{-2}b_0}{1 + z^{-1}a_1 + z^{-2}a_0} \end{aligned} \tag{A.5}$$

In this way, a simple discrete representation of the initial system was created.

A.2 Connection between Discrete and Continuous Systems

When the estimation of the discrete system is achieved, it's necessary to return to the initial continuous system to obtain an information about the condition of the patient. For this purpose, from A.3, eq. A.4 and A.5 it's possible to define an approximation of the coefficients a_1, a_0, b_1, b_0:

$$\begin{cases} a_1 = \alpha(-T_s^2 - \beta\frac{T_s^3}{2}) - 2 - \beta T_s - \beta^2\frac{T_s^2}{2} - \beta^3\frac{T_s^3}{6} \\ a_0 = 1 + \beta T_s + \beta^2\frac{T_s^2}{2} + \beta^2\frac{T_s^2}{2} + \beta^3\frac{T_s^3}{6} - \alpha^2\frac{T_s^4}{12} - \alpha^3\frac{T_s^6}{36} + \alpha^2\beta\frac{T_s^5}{12} - \alpha\beta^2\frac{T_s^4}{6} \\ b_1 = \frac{\gamma}{2}T_s^2 + \frac{\beta\gamma}{6}T_s^3 + \frac{(\alpha+\beta^2)\gamma}{24}T_s^4 \\ b_0 = -\{1 + \beta T_s + (\alpha+\beta^2)\frac{T_s^2}{2} + [\alpha\beta + \beta(\alpha+\beta^2)]\frac{T_s^3}{6}\}b_1 + [T_s + \beta\frac{T_s^2}{2} + \ ... \\ ... \ + (\alpha+\beta^2)\frac{T_s^3}{6}]\{\gamma T_s + \frac{\beta\gamma}{2}T_s^2 + \frac{(\alpha+\beta^2)\gamma}{6}T_s^3 + \frac{[\alpha\beta+\beta(\alpha+\beta^2)]\gamma}{24}T_s^4\} \end{cases} \tag{A.6}$$

With these equations system is possible to estimate the value of the parameters α, β, γ. Using these last parameters it's simple to derive the information of the total continuous system:

$$\begin{cases} \widehat{M} = \frac{K_i K_t}{\widehat{\gamma}} \\ \widehat{D} = -\widehat{\beta}\widehat{M} \\ \widehat{K}_a = -\widehat{\alpha}\widehat{M} \end{cases} \tag{A.7}$$

To obtain the parameters of the Arm, the final step is only to remove the values of the motor from the total values estimated:

$$\begin{cases} \widehat{M}_a = \widehat{M} - \widehat{M}_m \\ \widehat{D}_a = \widehat{D} - \widehat{D}_m \\ \widehat{K}_a = \widehat{K}_a - 0 \end{cases} \tag{A.8}$$

Appendix B

Second Subject Estimation Results

In this appendix some test are conducted to test with another subject the estimation code and in the same way to obtain the specific results of Mass, Damping factor and Stiffness to use to design the controller. The estimation are performed in four different point of the X-Y working system and in both direction, as shown in Fig. B.1 for the previous estimation and here reported to understand better the situation:

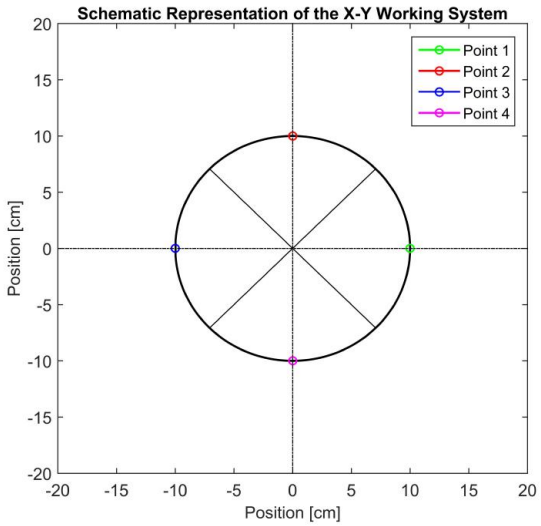

Figure B.1: Working System, X-Y plane

The circle represent only the behavior to follow by the patient during the exercise. The choice of only four point is related with the necessity to limit

the stress of the patient's arm before the exercise session. So, in Tab. B.1 the average values with the standard deviation of the Human Arm of the second subject are reported and in Fig. B.2 are shown the behavior for each estimation for each point and for each axis.

Human Arm (X-Axis)

Point	$M_a[kg]$	$D_a[\frac{Ns}{m}]$	$K_a[\frac{N}{m}]$	$f_c[N]$
1	0.4615 ± 0.0428	9.6650 ± 2.2057	93.3894 ± 15.7535	5.7186 ± 0.1698
2	0.4788 ± 0.0184	15.5574 ± 1.1058	124.8165 ± 17.1971	5.4962 ± 0.1469
3	0.3724 ± 0.0051	17.2736 ± 1.7418	177.6957 ± 6.3052	5.4710 ± 0.1573
4	0.4179 ± 0.0126	12.5843 ± 0.7528	139.9010 ± 21.1631	5.8165 ± 0.1132

Human Arm (Y-Axis)

Point	$M_a[kg]$	$D_a[\frac{Ns}{m}]$	$K_a[\frac{N}{m}]$	$f_c[N]$
1	0.4546 ± 0.0494	40.1667 ± 6.0451	554.4791 ± 45.1490	1.8232 ± 0.1034
2	0.4225 ± 0.0196	44.8716 ± 2.3351	354.6298 ± 51.3641	1.7328 ± 0.1062
3	0.5859 ± 0.0183	44.2142 ± 2.9372	375.6720 ± 25.6326	2.5645 ± 0.0634
4	0.6082 ± 0.0145	42.3212 ± 2.6487	407.8477 ± 123.4616	1.9870 ± 0.0920

Table B.1: Estimation of the Human Arm parameters of the second subject

Human Arm (X-Axis)

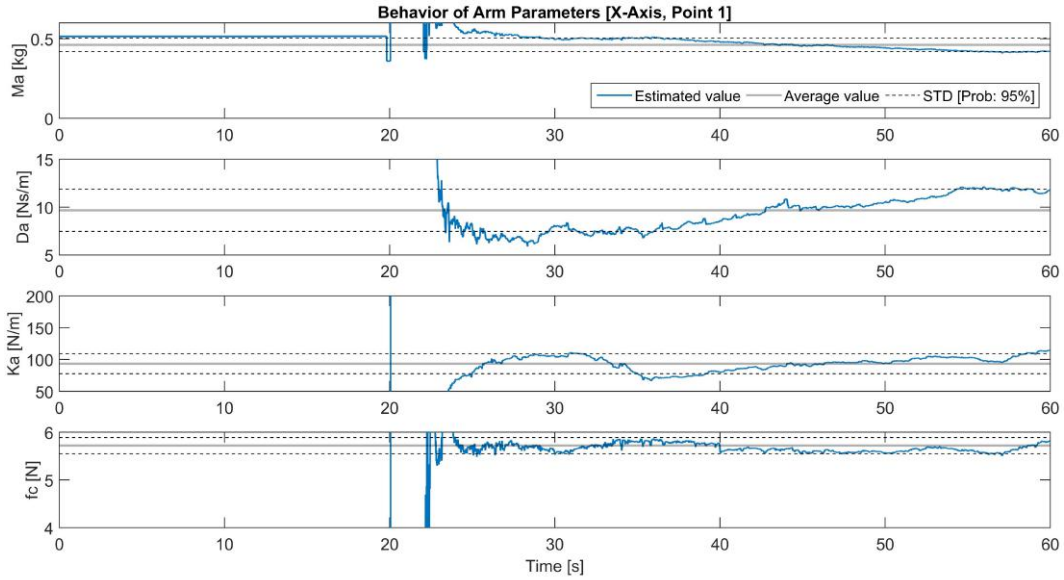

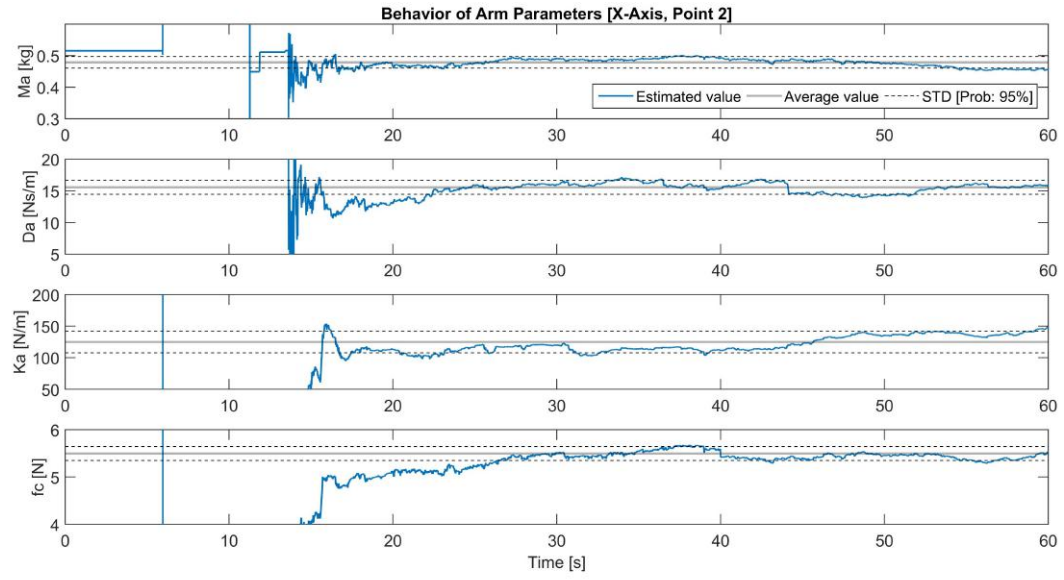

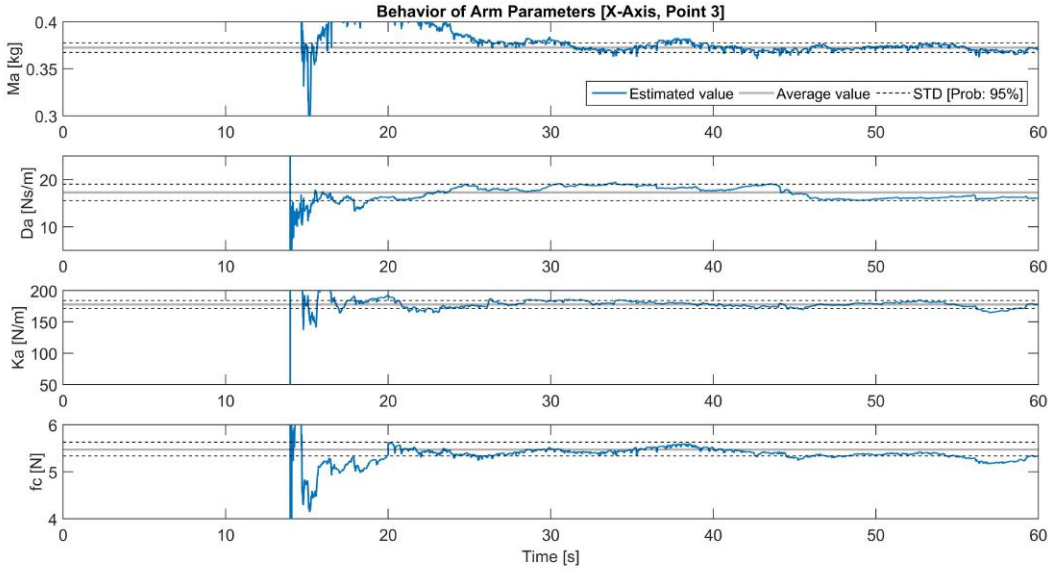
Behavior of Arm Parameters [X-Axis, Point 3]
Ma [kg]
Da [Ns/m]
Ka [N/m]
fc [N]
Estimated value
Average value
STD [Prob: 95%]
Time [s]

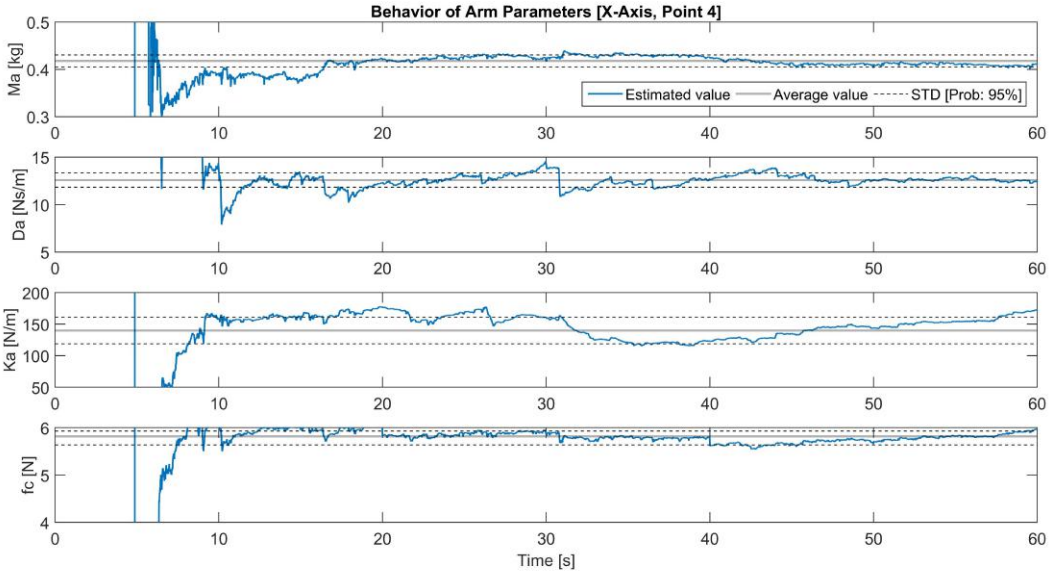
Behavior of Arm Parameters [X-Axis, Point 4]
Ma [kg]
Da [Ns/m]
Ka [N/m]
fc [N]
Estimated value
Average value
STD [Prob: 95%]
Time [s]

Human Arm (Y-Axis)

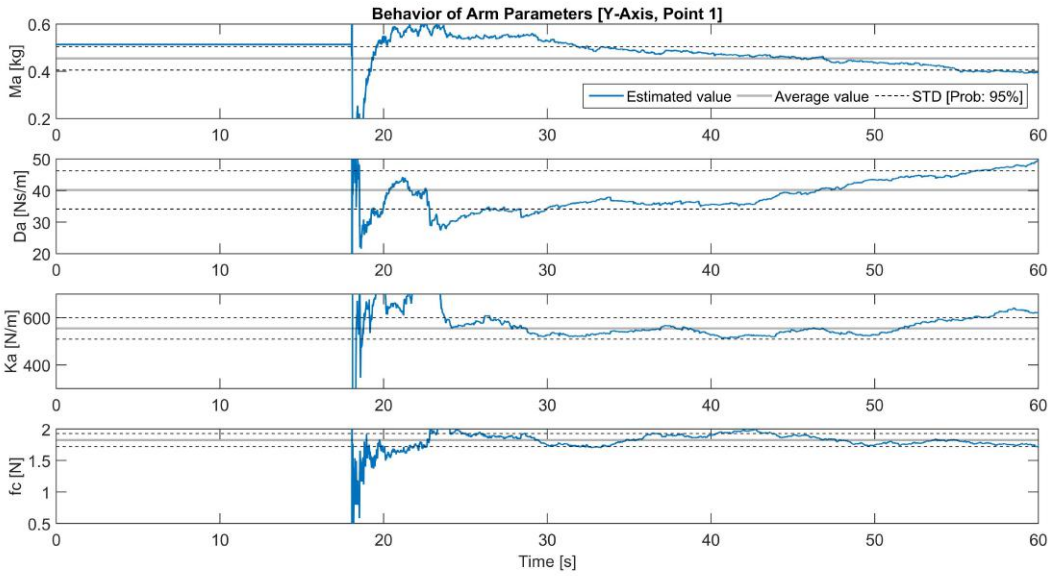

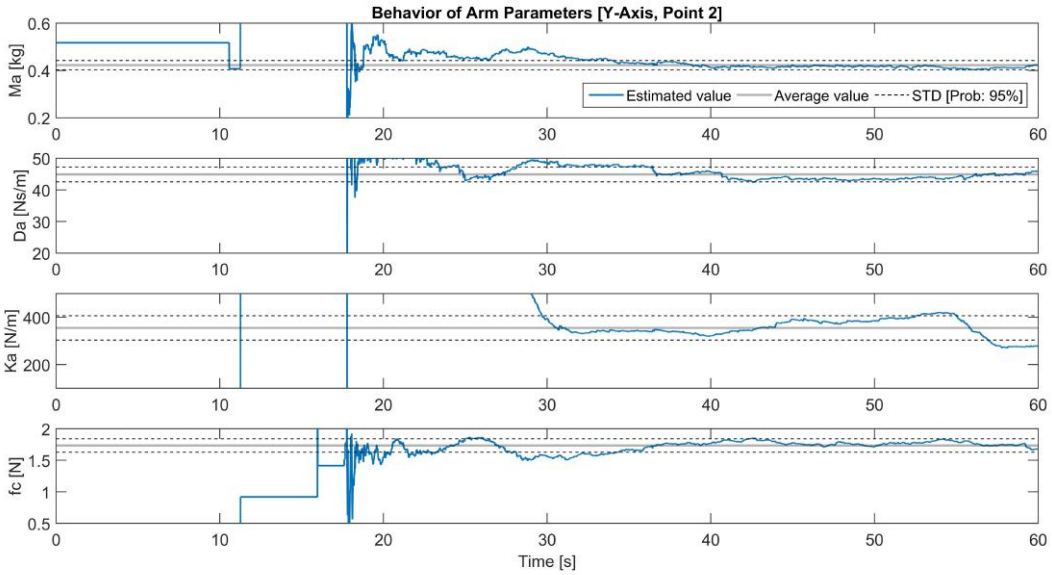

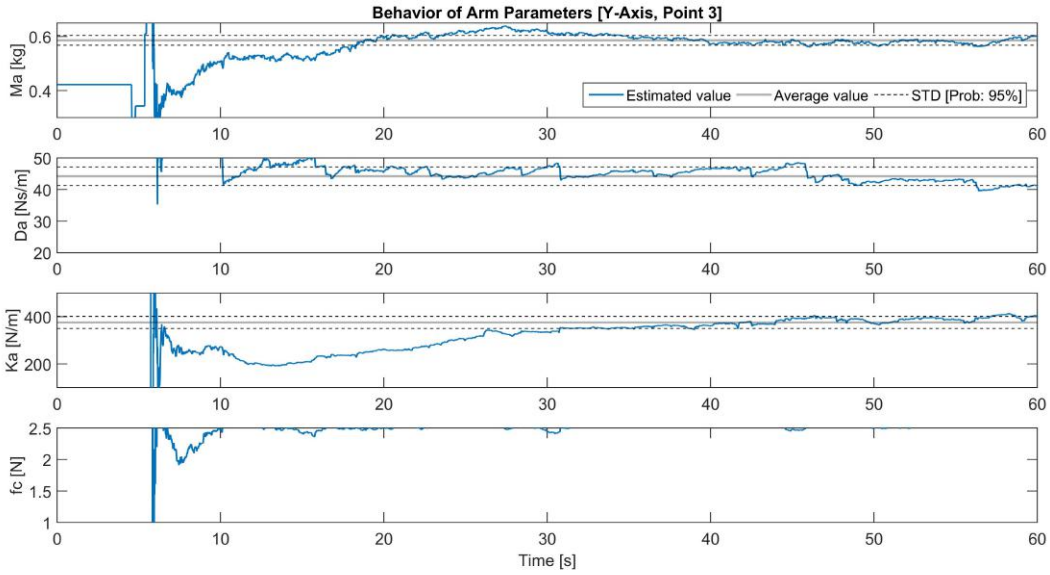

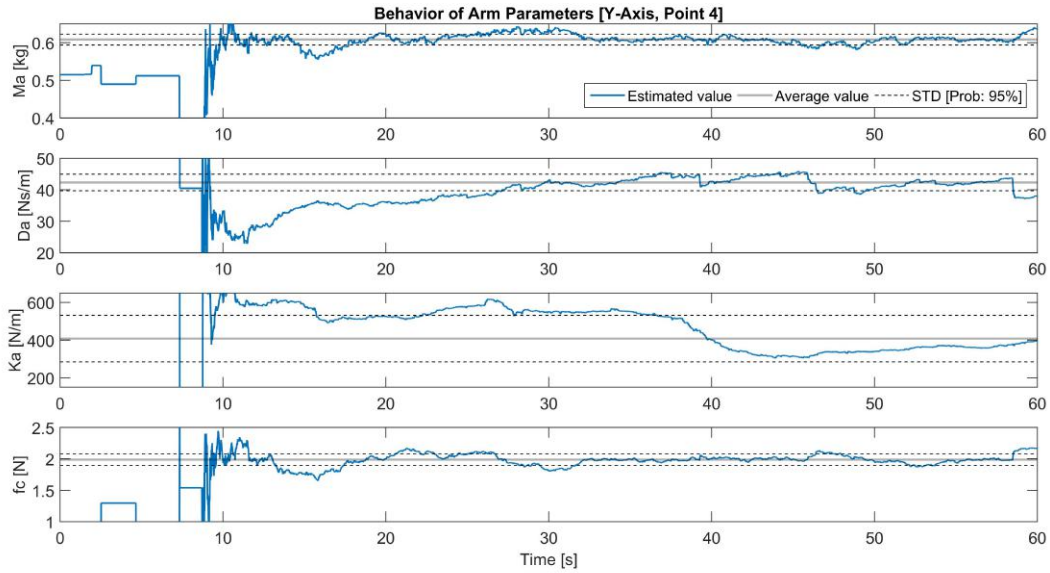

Figure B.2: Estimation of the Human Arm parameters of the second subject

Bibliography

[1] http://www.strokefoundation.com.au/.

[2] http://www.womens-health-advice.com/photos/stroke.html/.

[3] http://airindo.com/product/lokomat/.

[4] A. s. association [online]. http://www.strokeassociation.org/. Available on line.

[5] Gait retraining after neurological disorders. https://www.researchgate.net/publication/229747966_Gait_Retraining_After_Neurological_Disorders.

[6] Ictus in italia. http://http://www.salute.gov.it/portale/salute/p1_5.jsp?id=28&area=Malattie_cardiovascolari/. Available on line.

[7] Il percorso di cura della persona colpita da ictus: la fase post acuta e riabilitativa. https://www.ulss.tv.it/.

[8] Nerebot. http://www.mechatronics.it/.

[9] Rehabilitation therapy. https://www.ninds.nih.gov/Disorders/Patient-Caregiver-Education/Hope-Through-Research/Stroke-Hope-Through-Research#1105_23/.

[10] Robotic therapy helps stroke patients regain function. http://news.mit.edu/.

[11] Mindy Lipson Aisen, H Igo Krebs, Neville Hogan, Fletcher McDowell, and Bruce T Volpe. The effect of robot-assisted therapy and rehabilitative training on motor recovery following stroke. *Archives of neurology*, 54(4):443–446, 1997.

[12] Riccardo Antonello, Kazuaki Ito, and Roberto Oboe. Acceleration measurement drift rejection in motion control systems by augmented-state kinematic kalman filter. *IEEE Transactions on Industrial Electronics*, 63(3):1953–1961, 2016.

[13] Riccardo Antonello and Roberto Oboe. Force controller tuning for a master-slave system with proximity based haptic feedback. In *Industrial Electronics Society, IECON 2014-40th Annual Conference of the IEEE*, pages 2774–2779. IEEE, 2014.

[14] Karl J Åström and Second edition Wittenmark, Björn. *Adaptive control*. Addison Wesley, 1995.

[15] Karl Johan Åström and Björn Wittenmark. *Computer-Controlled Systems: Theory and Design*. Courier Corporation, 2011.

[16] Michael P Barnes. An overview of the clinical management of spasticity. *Upper motor neurone syndrome and spasticity: clinical management and neurophysiology*, pages 1–11, 2001.

[17] S Bittanti, P Bolzern, M Campi, and E Coletti. Deterministic convergence analysis of rls estimators with different forgetting factors. In *Decision and Control, 1988., Proceedings of the 27th IEEE Conference on*, pages 1530–1531. IEEE, 1988.

[18] Bruce M Brown et al. Martingale central limit theorems. *The Annals of Mathematical Statistics*, 42(1):59–66, 1971.

[19] Charles G Burgar, Peter S Lum, Peggy C Shor, and HF Machiel Van der Loos. Development of robots for rehabilitation therapy: The palo alto va/stanford experience. *Journal of rehabilitation research and development*, 37(6):663–674, 2000.

[20] David Burke. Spasticity as an adaptation to pyramidal tract injury. *Advances in neurology*, 47:401, 1988.

[21] Marco Campi. Performance of rls identification algorithms with forgetting factor: A -mixing approach. *Journal of Mathematical Systems Estimation and Control*, 7:29–54, 1997.

[22] Carlos Canudas, K Astrom, and Konrad Braun. Adaptive friction compensation in dc-motor drives. *IEEE Journal on Robotics and Automation*, 3(6):681–685, 1987.

[23] Tongwen Chen, Bruce Francis, and Tomomichi Hagiwara. Optimal sampled-data control systems. *Proceedings of the IEEE*, 86(4):741–741, 1998.

[24] Gregory C. Chow and An loh Lin. Best linear unbiased interpolation, distribution, and extrapolation of time series by related series. *The Review of Economics and Statistics*, 53(4):372–375, 1971.

[25] Iñaki Díaz, Jorge Juan Gil, and Emilio Sánchez. Lower-limb robotic rehabilitation: literature review and challenges. *Journal of Robotics*, 2011, 2011.

[26] John M Dolan, Mark B Friedman, and Mark L Nagurka. Dynamic and loaded impedance components in the maintenance of human arm posture. *IEEE Transactions on Systems, Man, and Cybernetics*, 23(3):698–709, 1993.

[27] Friedhelm Eicker et al. Asymptotic normality and consistency of the least squares estimators for families of linear regressions. *The Annals of Mathematical Statistics*, 34(2):447–456, 1963.

[28] Randy E Ellis, Ossama M Ismaeil, and Michael G Lipsett. Design and evaluation of a high-performance haptic interface. *Robotica*, 14(3):321–327, 1996.

[29] Claudio Fanin, Paolo Gallina, Aldo Rossi, Umberto Zanatta, and Stefano Masiero. Nerebot: a wire-based robot for neurorehabilitation. In *Proceedings of the 8th International Conference on Rehabilitation Robotics*, pages 23–25, 2003.

[30] Susan E Fasoli, Hermano I Krebs, Joel Stein, Walter R Frontera, and Neville Hogan. Effects of robotic therapy on motor impairment and recovery in chronic stroke. *Archives of physical medicine and rehabilitation*, 84(4):477–482, 2003.

[31] AG Feldman. Change in the length of the muscle as a consequence of a shift in equilibrium in the muscle-load system. *Biophysics*, 19:544–548, 1974.

[32] Daniel P Ferris, Keith E Gordon, Gregory S Sawicki, and Ammanath Peethambaran. An improved powered ankle–foot orthosis using proportional myoelectric control. *Gait & posture*, 23(4):425–428, 2006.

[33] Hilde M Feys, Willy J De Weerdt, Beat E Selz, Gail A Cox Steck, Ruth Spichiger, Luc E Vereeck, Koen D Putman, and Gustaaf A Van Hoydonck. Effect of a therapeutic intervention for the hemiplegic upper limb in the acute phase after stroke. *Stroke*, 29(4):785–792, 1998.

[34] Ettore Fornasini and Giovanni Marchesini. *Appunti di teoria dei sistemi*. Libreria Progetto, 1988.

[35] Neil F Gordon, Meg Gulanick, Fernando Costa, Gerald Fletcher, Barry A Franklin, Elliot J Roth, and Tim Shephard. Physical activity and exercise recommendations for stroke survivors. *Stroke*, 35(5):1230–1240, 2004.

[36] S Hesse, TH Sarkodie-Gyan, and D Uhlenbrock. Development of an advanced mechanised gait trainer, controlling movement of the centre of mass, for restoring gait in non-ambulant subjects-weiterentwicklung eines mechanisierten gangtrainers mit steuerung des massenschwerpunktes zur gangrehabilitation rollstuhlpflichtiger patienten. *Biomedizinische Technik/Biomedical Engineering*, 44(7-8):194–201, 1999.

[37] Stefan Hesse, Henning Schmidt, and Cordula Werner. Machines to support motor rehabilitation after stroke: 10 years of experience in berlin. *Journal of rehabilitation research and development*, 43(5):671, 2006.

[38] Stefan Hesse, Henning Schmidt, Cordula Werner, and Anita Bardeleben. Upper and lower extremity robotic devices for rehabilitation and for studying motor control. *Current opinion in neurology*, 16(6):705–710, 2003.

[39] Neville Hogan. Mechanical impedance control in assistive devices and manipulators. In *Proc. of the 1980 Joint Automatic Control Conference, pp. TA10-B*, 1980.

[40] Sungjae Hwang, Jungyoon Kim, Jinbock Yi, Kisik Tae, Kihong Ryu, and Youngho Kim. Development of an active ankle foot orthosis for the prevention of foot drop and toe drag. In *Biomedical and Pharmaceutical Engineering, 2006. ICBPE 2006. International Conference on*, pages 418–423. IEEE, 2006.

[41] Soo Jeon and Masayoshi Tomizuka. Benefits of acceleration measurement in velocity estimation and motion control. *Control Engineering Practice*, 15(3):325–332, 2007.

[42] Saso Jezernik, Gery Colombo, and Manfred Morari. Automatic gait-pattern adaptation algorithms for rehabilitation with a 4-dof robotic orthosis. *IEEE Transactions on Robotics and Automation*, 20(3):574–582, 2004.

[43] C Richard Johnson. *Lectures & adaptive parameter estimation*. Prentice-Hall, Inc., 1988.

[44] Garth R Johnson, MP Barnes, and GR Johnson. Measurement of spasticity. *Upper motor neurone syndrome and spasticity*, pages 79–95, 2001.

[45] Lenore N Joseph, Viken L Babikian, Nancy C Allen, and Michael R Winter. Risk factor modification in stroke prevention. *Stroke*, 30(1):16–20, 1999.

[46] Leonard E Kahn, Michele L Zygman, W Zev Rymer, and David J Reinkensmeyer. Robot-assisted reaching exercise promotes arm movement recovery in chronic hemiparetic stroke: a randomized controlled pilot study. *Journal of NeuroEngineering and Rehabilitation*, 3(1):12, 2006.

[47] Rudolph Emil Kalman et al. A new approach to linear filtering and prediction problems. *Journal of basic Engineering*, 82(1):35–45, 1960.

[48] H Igo Krebs, Neville Hogan, Mindy L Aisen, and Bruce T Volpe. Robot-aided neurorehabilitation. *IEEE transactions on rehabilitation engineering*, 6(1):75–87, 1998.

[49] Hermano Igo Krebs, Bruce T Volpe, Dustin Williams, James Celestino, Steven K Charles, Daniel Lynch, and Neville Hogan. Robot-aided neurorehabilitation: a robot for wrist rehabilitation. *IEEE Transactions on Neural Systems and Rehabilitation Engineering*, 15(3):327–335, 2007.

[50] Gert Kwakkel, Robert C Wagenaar, Jos WR Twisk, Gustaaf J Lankhorst, and Johan C Koetsier. Intensity of leg and arm training after primary middle-cerebral-artery stroke: a randomised trial. *The Lancet*, 354(9174):191–196, 1999.

[51] Joachim Liepert, Heike Bauder, Wolfgang HR Miltner, Edward Taub, and Cornelius Weiller. Treatment-induced cortical reorganization after stroke in humans. *Stroke*, 31(6):1210–1216, 2000.

[52] Nadina B Lincoln, D Willis, SA Philips, LC Juby, and P Berman. Comparison of rehabilitation practice on hospital wards for stroke patients. *Stroke*, 27(1):18–23, 1996.

[53] L Ljung. Systems identification: Theory for the user. 1987.

[54] Lennart Ljung and Svante Gunnarsson. Adaptation and tracking in system identification—a survey. *Automatica*, 26(1):7–21, 1990.

[55] Peter S Lum, Charles G Burgar, Machiel Van der Loos, Peggy C Shor, et al. Mime robotic device for upper-limb neurorehabilitation in subacute stroke subjects: A follow-up study. *Journal of rehabilitation research and development*, 43(5):631, 2006.

[56] Judith Mackay, George A Mensah, Shanthi Mendis, and Kurt Greenlund. *The atlas of heart disease and stroke*. World Health Organization, 2004.

[57] Paolo Mantegazza, Emanuele Bianchi, M Angelo, D Beal, and K Yaghmour. Diapm-rtai programming guide 1.0. *Lineo Inc*, 2000.

[58] Stefano Masiero, Mario Armani, Gregorio Ferlini, Giulio Rosati, and Aldo Rossi. Randomized trial of a robotic assistive device for the upper extremity during early inpatient stroke rehabilitation. *Neurorehabilitation and neural repair*, 28(4):377–386, 2014.

[59] Michael M Merzenich, JH Kaas, J Wall, RJ Nelson, M Sur, and D Felleman. Topographic reorganization of somatosensory cortical areas 3b and 1 in adult monkeys following restricted deafferentation. *Neuroscience*, 8(1):33–55, 1983.

[60] J-B Michaud, Réjean Fontaine, and Roger Lecomte. Armax model and recursive least-squares identification for doi measurement in pet. In *Nuclear Science Symposium Conference Record, 2003 IEEE*, volume 4, pages 2386–2390. IEEE, 2003.

[61] Scottish Intercollegiate Guideline Network. Management of patients with stroke or tia: assessment, investigation, immediate management and secondary prevention. *Edinburgh: Scottish Intercollegiate Guidelines Network*, 2008.

[62] A Mohd Nor, C McAllister, SJ Louw, AG Dyker, M Davis, D Jenkinson, and GA Ford. Agreement between ambulance paramedic-and physician-recorded neurological signs with face arm speech test (fast) in acute stroke patients. *Stroke*, 35(6):1355–1359, 2004.

[63] Toshiro Noritsugu and Toshihiro Tanaka. Application of rubber artificial muscle manipulator as a rehabilitation robot. *IEEE/ASME Transactions On Mechatronics*, 2(4):259–267, 1997.

[64] Randolph J Nudo, Birute M Wise, Frank SiFuentes, and Garrett W Milliken. Neural substrates for the effects of rehabilitative training on motor recovery after ischemic infarct. *Science*, 272(5269):1791, 1996.

[65] European Registers of Stroke (EROS) Investigators et al. Incidence of stroke in europe at the beginning of the 21st century. *Stroke*, 40(5):1557–1563, 2009.

[66] World Health Organization. *World report on ageing and health*. World Health Organization, 2015.

[67] Shyamal Patel, Konrad Lorincz, Richard Hughes, Nancy Huggins, John Growdon, David Standaert, Metin Akay, Jennifer Dy, Matt Welsh, and Paolo Bonato. Monitoring motor fluctuations in patients with parkinson's disease using wearable sensors. *IEEE transactions on information technology in biomedicine*, 13(6):864–873, 2009.

[68] Davide Pilastro. *INNOVATIVE CONTROL TECHNIQUES AND STRATEGIES FOR ROBOTICS REHABILITATION*. PhD thesis, University of Padova, 2016.

[69] David J Reinkensmeyer, Leonard E Kahn, Michele Averbuch, Alicia McKenna-Cole, et al. Understanding and treating arm movement impairment after chronic brain injury: progress with the arm guide. *Journal of rehabilitation research and development*, 37(6):653, 2000.

[70] G Rosati, S Masiero, and A Rossi. On the use of cable-driven robots in early inpatient stroke rehabilitation. In *Advances in Italian Mechanism Science*, pages 551–558. Springer, 2017.

[71] Jerome N Sanes and John P Donoghue. Plasticity and primary motor cortex. *Annual review of neuroscience*, 23(1):393–415, 2000.

[72] Henning Schmidt, Cordula Werner, Rolf Bernhardt, Stefan Hesse, and Jörg Krüger. Gait rehabilitation machines based on programmable footplates. *Journal of neuroengineering and rehabilitation*, 4(1):2, 2007.

[73] Riccardo Secoli. Controllo di robot per la riabilitazione dell'arto superiore di pazienti post-stroke. 2010.

[74] L. M. Silverman and H. E. Meadows. Controllability and observability in time-variable linear systems. *SIAM Journal on Control*, 5(1):64–73, 1967.

[75] George W Cochran Snedecor and G William. Statistical methods/george w. snedecor and william g. cochran. Technical report, 1989.

[76] AHA Scientific Statements. Heart disease and stroke statistics—2013 update. *Circulation*, 127(1):e6–e245, 2013.

[77] Katharina Stibrant Sunnerhagen, Ulla Svantesson, Lars Lönn, Marcin Krotkiewski, and Gunnar Grimby. Upper motor neuron lesions: their effect on muscle performance and appearance in stroke patients with minor motor impairment. *Archives of physical medicine and rehabilitation*, 80(2):155–161, 1999.

[78] Keng Peng Tee, Etienne Burdet, Chee-Meng Chew, and Theodore E Milner. A model of force and impedance in human arm movements. *Biological cybernetics*, 90(5):368–375, 2004.

[79] T Truelsen, M Ekman, and G Boysen. Cost of stroke in europe. *European journal of neurology*, 12(s1):78–84, 2005.

[80] Toshio Tsuji and Makoto Kaneko. Estimation and modeling of human hand impedance during isometric muscle contraction. In *Proceedings of the ASME Dynamic Systems and Control Division*, volume 5, pages 575–582, 1996.

[81] Bruce T Volpe, Hermano I Krebs, and Neville Hogan. Is robot-aided sensorimotor training in stroke rehabilitation a realistic option? *Current opinion in neurology*, 14(6):745–752, 2001.

[82] BT Volpe, HI Krebs, N Hogan, L Edelsteinn, CM Diels, and ML Aisen. Robot training enhanced motor outcome in patients with stroke maintained over 3 years. *Neurology*, 53(8):1874–1874, 1999.

[83] Kelly P Westlake and Carolynn Patten. Pilot study of lokomat versus manual-assisted treadmill training for locomotor recovery post-stroke. *Journal of neuroengineering and rehabilitation*, 6(1):18, 2009.

[84] Markus Wirz, David H Zemon, Ruediger Rupp, Anke Scheel, Gery Colombo, Volker Dietz, and T George Hornby. Effectiveness of automated locomotor training in patients with chronic incomplete spinal cord injury: a multicenter trial. *Archives of physical medicine and rehabilitation*, 86(4):672–680, 2005.

[85] Eric T Wolbrecht, Vicky Chan, David J Reinkensmeyer, and James E Bobrow. Optimizing compliant, model-based robotic assistance to promote neurorehabilitation. *IEEE Transactions on Neural Systems and Rehabilitation Engineering*, 16(3):286–297, 2008.

[86] Steven L Wolf, Sarah Blanton, Heather Baer, Jenifer Breshears, and Andrew J Butler. Repetitive task practice: a critical review of constraint-induced movement therapy in stroke. *The neurologist*, 8(6):325, 2002.

[87] Jinchuan Zheng and Minyue Fu. A reset state estimator using an accelerometer for enhanced motion control with sensor quantization. *IEEE Transactions on Control Systems Technology*, 18(1):79–90, 2010.

[88] Huiyu Zhou and Huosheng Hu. Human motion tracking for rehabilitation—a survey. *Biomedical Signal Processing and Control*, 3(1):1–18, 2008.